

**University of Alberta**

**Library Release Form**

**Name of Author:** Muhammad Sajid Iqbal

**Title of Thesis:** Discrete Element Modeling of Cone Penetration Testing in Coarse Grain Soils

**Degree:** Master of Science

**Year of Degree Granted:** 2004

Permission is hereby granted to the University of Alberta Library to reproduce single copies of this thesis and to lend or sell such copies for private, scholarly or scientific research purposes only.

The author reserves all other publication and other rights in association with the copyright in the thesis, and except as herein before provided, neither the thesis nor any substantial portion thereof may be printed or otherwise reproduced in any material form whatever without the author's prior written permission.



115, Block F - 1, Jauhar Town,  
Lahore, PAKISTAN  
Email: [msajid@brain.net.pk](mailto:msajid@brain.net.pk)  
Phone: +92 - 42 -5300237

September 13, 2004

**University of Alberta**

**Discrete Element Modeling of Cone Penetration Testing in Coarse Grain Soils**

by

**Muhammad Sajid Iqbal**

**A thesis submitted to the Faculty of Graduate Studies and Research in partial fulfillment  
of the requirements for the degree of Master of Science**

in

**Geotechnical Engineering**

**Department of Civil and Environmental Engineering**

**Edmonton, Alberta**

**Fall 2004**

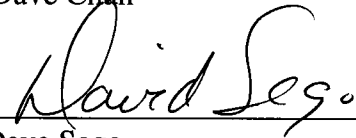
**University of Alberta**

**Faculty of Graduate Studies and Research**

The undersigned certify that they have read, and recommend to the Faculty of Graduate Studies and Research for acceptance, a thesis entitled Discrete Element Modeling of Cone Penetration Testing in Coarse Grain Soils, submitted by Muhammad Sajid Iqbal in partial fulfillment of the requirements for the degree of Master of Science in Geotechnical Engineering.



Dr. Dave Chan



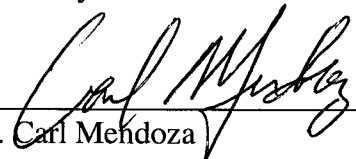
Dr. Dave Sego



Dr. Peter Robertson



Dr. Dwayne Tannant



Dr. Carl Mendoza

Date: Sept. 10, 2004

*A man's reach should exceed his grasp or  
what's a **heaven** for!*

**to my parents**

## ABSTRACT

A discrete element numerical modeling analysis for Cone Penetration Testing (CPT) was carried out to quantify grain size effects on cone penetration tip resistance. Analyses were performed simulating a model chamber using Particle Flow Code in 2 Dimensions (PFC<sup>2D</sup>) employing the Discrete Element Method (DEM) with uniform as well as distributed grain sizes. Analyses were carried out to simulate normally consolidated granular material with vertical / horizontal overburden stress ratio ( $k_0$ ) equal to 0.5 and with varying relative densities. In the numerical analysis, chamber diameter, boundaries and particle diameter were varied to investigate the possible effects on the measured cone tip resistance. Some limitations of the 2-dimensional modeling vs. 3-dimensional field conditions are also discussed.

The results were compared with recent CPT research in terms of chamber diameter and boundary effects. The results are in good agreement. This research has shown that refusal of penetration can be expected when the grain to cone diameter ratio is around 1.0. Also the measured cone tip resistance will start to be influenced by the grain size when the grain to cone diameter ratio reaches about 0.3.

**KEYWORDS:** cone penetration testing, calibration chamber, boundary conditions, grain size effects, sandy gravel, particle flow code, discrete element method, relative density.

## ACKNOWLEDGEMENTS

“Alhamdulillah”; thanks to **ALLAH** almighty, the creator of this Universe, the most merciful and the most gracious, for giving me the strength and knowledge to fulfill my dream,

I would like to thank my parents, brother and sisters for their unwavering support and faith in me,

My sincere gratitude to my supervisors Dr. Dave Sego and Dr. Peter Robertson, who gave me guidance, kind support and helped me in every way throughout this study,

Lastly, but not least, my thanks are extended to all my colleagues both in Pakistan and at the University of Alberta, Canada for the priceless friendship they have given to me during the course of this study.

## TABLE OF CONTENTS

CHAPTER	Page No.
<b>1. INTRODUCTION</b>	<b>1</b>
1.1 General	1
1.2 Objective of the Thesis	2
1.3 Scope and Organization	2
<b>2. CONE PENETRATION TESTING</b>	<b>4</b>
2.1 General Description of Cone Penetration Testing (CPT)	4
2.2 Historical Development	5
2.3 Role of CPT in Site Investigation	8
2.4 CPT Equipment	9
2.5 Cone Penetration Test (CPT) Procedure	10
2.6 Interpretation in Soils by CPT Parameters	11
2.7 Effect of Varying Size of Cone on Interpretation of CPT parameters	13
2.8 Calibration Chamber Testing (CC)	14
<b>3. DISCRETE ELEMENT METHOD (DEM)</b>	<b>28</b>
3.1 Background Information and Developments in DEM	28
3.2 Basic Ideology of DEM	30
3.2.1 Calculation Cycle	33
3.2.2 Force-Displacement Law	34
3.2.3 Law of Motion	38
3.2.4 Damping	39
3.2.5 Boundary Conditions	40
3.2.6 Critical Time-Step Determination	41
3.2.7 Contact Detection	41
3.3 Limitations and Shortcomings of DEM	42
3.3.1 Size of the Time-Step	42
3.3.2 Search Time in the Contact Detection Algorithm	42
3.3.3 Material Calibration	43
<b>4. PARTICLE FLOW CODE IN 2 DIMENSIONS (PFC<sup>2D</sup>)</b>	<b>46</b>
4.1 Introduction	46

## TABLE OF CONTENTS

CHAPTER	Page No.
4.2 Background and Overview	48
4.3 Components of a PFC <sup>2D</sup> Model	51
4.4 General Features	52
4.5 Fields of Application	56
4.6 Mechanics of Using PFC <sup>2D</sup>	56
4.7 Main Working Steps Involved in the Computer Code PFC <sup>2D</sup>	57
4.7.1 Particle Contact Detection	57
4.7.2 Application of Force-Displacement Law	58
4.7.3 Application of Newton's Law of Motion	58
4.7.4 Creation of Graphical Results	58
4.8 Limitations of PFC <sup>2D</sup> Modeling	59
<b>5. SIMULATION OF CONE PENETRATION TESTING</b>	<b>67</b>
5.1 Chamber Size and Characteristics	67
5.2 Constitutive Law for Granular Material	68
5.3 Particle Generation and Application of Initial Field Conditions	69
5.4 Boundary Conditions and <i>In-situ</i> Stresses	72
5.5 Cone Penetration Modeling Mechanism in Granular Material	74
5.6 Interpretation of Results	76
<b>6. RESULTS AND DISCUSSIONS</b>	<b>87</b>
6.1 Implication of Results	94
<b>7. CONCLUSIONS AND RECOMMENDATIONS</b>	<b>106</b>
<b>8. REFERENCES</b>	<b>108</b>
Appendix – A Letter of permission from Itasca Consulting Group, Inc.	116
Appendix – B Random Generated Assemblies in PFC <sup>2D</sup>	118
Appendix – C Trial run results in comparison to Ahmadi (2004) for both BC1 and BC3	122
Appendix – D Photographs of damaged cones that have penetrated gravelly sands (Courtesy of ConeTec Limited).	124
Appendix – E Example CPT profiles (Including sections through gravel). (Courtesy of ConeTec Limited).	127



## LIST OF TABLES

	<b>Page No.</b>
Table 2.1: Major <i>in situ</i> tests and their perceived applicability in various ground conditions (after Lunne et al. 1997)	20
Table 2.2: Various boundary conditions usually applied to calibration chamber testing.	21
Table 4.1: Maximum number of PFC <sup>2D</sup> particles in available RAM	62
Table 5.1: Parameters used in PFC <sup>2D</sup> model.	77

## LIST OF FIGURES

	<b>Page No.</b>
Figure 2.1: Cone penetrometer (modified from Lunne et al. 1997)	22
Figure 2.2: Old type Dutch cone (modified from Sanglerat, 1972)	22
Figure 2.3: Begemann type cone with friction sleeve (from Sanglerat, 1972)	23
Figure 2.4: Soil classification from cone resistance and sleeve friction readings (from Begemann, 1965)	23
Figure 2.5: The Fugro electrical friction cone (after de Ruiter, 1971)	24
Figure 2.6: CPT soil behavior type classification chart by Douglas and Olsen (1981)	24
Figure 2.7: CPT soil behavior type classification chart (Robertson et al., 1986)	25
Figure 2.8: CPT soil behavior type classification chart based on CPTU (Robertson 1990)	25
Figure 2.9: Effects of sand compressibility on $q_c$ , overburden stress and $D_r$ (Robertson and Campanella, 1983b)	26
Figure 2.10: Effect of chamber size and boundary condition on CPT for Hokksund sand (Parkin and Lunne, 1982)	26
Figure 2.11: Effect of chamber size and boundary conditions on cone tip resistance (Ahmadi 2004)	27
Figure 3.1: Calculation cycle in DEM	44
Figure 3.2: A pair of particles in contact (Cundall and Strack, 1979)	44
Figure 3.3: Sign Convention for $F_n$ and $F_s$ (Cundall and Strack, 1979)	45
Figure 3.4: Spring and dashpot model (Cundall and Strack, 1979)	45
Figure 4.1: General solution procedure in PFC <sup>2D</sup> modeling	63
Figure 4.2: Flow chart for updating the contact list	64
Figure 4.3: Flow chart for detecting the new possible contacts	64
Figure 4.4: Flow chart for calculating the contact force	65
Figure 4.5: Flow chart for applying the law of motion	65
Figure 4.6: Graphical output from PFC <sup>2D</sup> . Notice the command window at the bottom	66

## LIST OF FIGURES

	<b>Page No.</b>
Figure 5.1: General layout of the model with symmetrical section along vertical axis having a radius of 1.5 meters	78
Figure 5.2: General layout of the model; Initial Particle Generation Phase along with 6 measurement circles	79
Figure 5.3: Plot of mean unbalanced force versus cycling steps	80
Figure 5.4: Assembly configuration at equilibrium after numerically cycled for 200 steps	81
Figure 5.5: Configuration of the assembly with the raft boundaries in place	82
Figure 5.6: A close-up view of the cone geometry, chamber configuration and the grains composition	83
Figure 5.7: A close-up view of the contact forces developed around the cone during penetration process	84
Figure 5.8: A plot of the vertical force exerted by the particles on the cone tip during penetration process versus penetration depth	85
Figure 5.9: Full scale view of the chamber / numerical model with the location of the various cone tips at an arbitrary depth	86
Figure 6.1: Plot of cone tip resistance versus the grain to cone diameter ratio at varying porosity values	97
Figure 6.2: Plot of cone tip resistance versus chamber / cone diameter ratio. Trial run results	98
Figure 6.3: Plot of average cone tip resistance versus chamber to cone diameter ratio. Extended for chamber / cone diameter ratio up to 600 (cone diameter = 5 mm)	99
Figure 6.4: Plot showing the vertical force versus depth for a grain / cone diameter ratio of 0.05	100
Figure 6.5: Plot showing the vertical force versus depth for a grain / cone diameter ratio of 2.0	101

## LIST OF FIGURES

	<b>Page No.</b>
Figure 6.6: Plot showing the maximum, average and minimum cone tip resistance versus the chamber / cone diameter ratio and grain /cone diameter ratio	102
Figure 6.7: Plot for maximum cone tip resistance versus grain / cone diameter ratio	103
Figure 6.8: Configuration of a well graded and a uniformly graded assembly	104
Figure 6.9: Plot for maximum cone tip resistance versus mean grain / cone diameter ratio (well & uniformly graded assemblies).	105
Figure B.1: Example of random generated assembly configuration.	119
Figure B.2: Example of random generated assembly configuration.	120
Figure B.3: Example of random generated assembly configuration.	121
Figure C.1: Plot of cone tip resistance versus chamber / cone diameter ratio. Trial run results.	123
Figure D.1: A damaged cone with a broken tip.	125
Figure D.2: A damaged cone with prominent scratch marks.	125
Figure D.3: A damaged cone with prominent scratch marks.	126
Figure D.4: A damaged cone with prominent scratch marks.	126
Figure E.1: CPT Profile at CP Rail Poco location. Site: 04 – 156; CPT04 - 02.	128
Figure E.2: CPT Profile at CP Rail Poco location. Site: 04 – 156; CPT04 - 04.	129
Figure E.3: CPT Profile at Richter/Sutherland location. Site: 03 – 111; CPT - 02.	130
Figure E.4: CPT Profile at Telegraph Tower location. Site: CPT04 - 22.	131
Figure E.5: CPT Profile at 19855 98 Ave. location. Site: CPT04 - 26.	132
Figure E.6: CPT Profile at Katzie Slough location. Site: CPT04 - 48.	133
Figure E.7: CPT Profile at Jager Site location. Site: CPT03 - 19.	134
Figure E.8: CPT Profile at Jager Site location. Site: CPT03 - 09.	135
Figure E.9: CPT Profile at Section 1 location. Site: CPT04 - 03.	136

## **1. INTRODUCTION:**

### **1.1 General:**

The Cone Penetration Test (CPT) has gained wide acceptance as an important in-situ test for the characterization of soils where penetration into the ground is possible. The CPT provides excellent near continuous profiles to determine soil type, detailed stratigraphy, and mechanical properties of the ground. Cone penetration testing has been in use for over 75 years and has justifiably acquired its place as one of the most promising in-situ subsurface investigation tools. The standard cone is 35.7 mm in diameter.

Traditionally CPT has been used in fine grained soils due primarily to the fact that coarser grained soils, such as gravels, usually give “Refusal” to the standard cone. Coarser grained soils are often difficult to sample at depth especially coarse sand and gravels (CANLEX, 1998). Even if possible at shallow depths, it is also expensive to do so. Hence in-situ testing is important for assessing the properties of coarser grained non-cohesive soils.

Although some references are available on the use of the CPT in coarse grained soils, such as residual soils, there are few references available on the use of CPT in gravels. Brand and Phillipson (1985) and Chang (1998) have reported that cone penetration can be difficult in residual soils due to frequent hard core stones of the weathered rock. Sowers (1985) reports the successful use of a non-standard 73 mm diameter simple cone in gravels in the United States. Peuchen et al. (1995) reported some experience with the CPT in harsh environment (coarse soils), in which a 20 tonnes truck and a standard 35.7 mm cone was used.

Almost all research conducted on the CPT using Calibration Chamber Testing (CC) has also been limited to fine grained soils such as sands, silts and clays. Hence the need to understand the behavior of coarser grained soils such as sandy gravel and gravel

is ever important. The mechanism of reaching “Refusal” during a CPT needs to be better understood.

## **1.2 Objective of the thesis:**

The main objective of this research is to develop some understanding of the effect of grain size on the penetration resistance of the cone using a discontinuum approach. This was achieved by modeling granular material using the Discrete Element Method (DEM). The following were explored in this thesis research:

- How well can penetration of a cone in a granular soil be modeled using DEM?
- What is the maximum particle size of a uniform granular soil that can be penetrated with a standard cone?
- When does particle size start affecting the results of the cone tip resistance measurements in uniform granular soils?
- Why and when is refusal encountered during penetration of a cone into coarse granular soils?

A discontinuum approach to simulate cone penetration into a granular material is studied in this research. The governing mechanism (discrete element method) in the simulation of granular flow as well as the application of boundary conditions is explored. The effects of chamber size, particle size and cone size on the measured tip resistance are evaluated. The limitations of each parameter and the simulation techniques are discussed. Finally, in order to demonstrate the relevance of the results, field examples are provided (via photographs and field data).

## **1.3 Scope and Organization:**

Chapter 2 presents a review of the existing literature on related topics. This includes the description and developments in Cone Penetration Testing (CPT) and Calibration Chamber Testing (CC).

Chapter 3 contains the background information and descriptions of the theoretical basis for the simulation of granular material movement, including the explanation of computer coding for DEM. Discussions about the limitations and shortcomings of the method are also outlined.

Chapter 4 gives an introduction to the capabilities and applications of Particle Flow Code in 2 Dimensions (PFC<sup>2D</sup>). It encompasses the developments and salient features of this computer programming code.

Chapter 5 contains the explanation of the approach used in this research for numerical modeling / simulation of granular material movement. This chapter also includes the limitations and shortcomings of the approach used.

Chapter 6 presents the results and discussion of the numerical simulation using DEM.

Chapter 7 presents the conclusions drawn from this research and any areas of research are also highlighted.

## 2. CONE PENETRATION TESTING:

In the words of Michele Jamiolkowski, President of the International Society of Soil Mechanics and Geotechnical Engineering (ISSMGE) and Suzanne Lacasse, Director, Norwegian Geotechnical Institute (NGI) (Lunne et al. 1997);

“The static cone penetrometer (CPT) represents the most versatile tool currently available for *in situ* soil exploration”.

### 2.1 General Description of Cone Penetration Testing (CPT):

In a Cone Penetration Test (CPT), a cone on the end of a series of rods is pushed into the ground at a constant rate and continuous or intermittent measurements are made of the cone resistance to penetration. Measurements can be made either of the combined tip resistance and sleeve resistance or the resistance of a sleeve only. Figure 2.1 illustrates the main terminology regarding a cone.

The total force acting on the cone,  $Q_c$ , divided by the projected area of the cone,  $A_c$ , produces the cone tip resistance,  $q_c$ . The total force acting on the friction sleeve,  $F_s$ , divided by the surface area of the friction sleeve,  $A_s$ , produces the sleeve friction,  $f_s$ .

In a piezocone penetrometer, pore pressure is measured typically at one, two or three separate locations as shown in Figure 2.1. These pore pressures are known as: on the cone ( $u_1$ ), behind the cone ( $u_2$ ) and behind the friction sleeve ( $u_3$ ).

Existing CPT systems can be divided into three main groups; mechanical cone penetrometer, electric cone penetrometer and piezocone penetrometer.

A cone penetrometer with a diameter of 35.7 mm, 10 cm<sup>2</sup> base area cone and an apex angle of 60 degrees is accepted as the reference and has been specified in the International Reference Test Procedure (ISSMFE, 1989).



## **2.2 Historical Development:**

A detailed review of the history of penetration testing can be found in Sanglerat (1972) and Broms and Foldin (1988). A short summary is provided below for quick reference.

### **(a) Mechanical cone penetrometers**

The first Dutch cone penetrometer tests were used in 1932 by P. Barentsen in Holland. A gas pipe of 19 mm inner diameter was used; inside this a 15 mm steel rod could move freely up and down. A cone tip of 35 mm diameter, 10 cm<sup>2</sup> base area and 60° apex angle was attached to the steel rod (Figure 2.2).

Downward force was applied by hand. 10 – 12 m of penetration depth was achieved in soft soils and resistance was read on a manometer. Subsequently, Delft Soil Mechanics Laboratory designed the first manually operated 10 tonnes cone penetration rig and tests were carried out in 1935 (de Graaf and Vermeiden, 1988). Improvements to prevent soil from entering the gap between the cone and rods were achieved by adding a conical shape part just above the cone, Vermeiden (1948) and Plantema (1948).

The skin friction measurement was first introduced by Begemann (1953, 1969) with the addition of an “adhesion jacket” behind the cone (Figure 2.3). Begemann (1965) was also the first to propose that the friction ratio (sleeve friction / cone resistance) could be used to classify various soil layers in terms of soil type (Figure 2.4).

Sanglerat (1972) reported on the development of the first hydraulic cone in 1966 by The Centre Experimental du Batiment et des Travaux Publics (CEBTP) in France. According to Sanglerat, CEBTP also developed a static-dynamic penetrometer.

Mechanical cone penetrometers are still used in some countries, although electric penetrometers are now more commonly used.

### **(b) Electrical cone penetrometers**

Broms and Foldin (1988) noted that the first electric cone penetrometer was probably developed at the Deutsche Forschungsgesellschaft für Bodenmechanik (Degebo) in Berlin during the Second World War. Muhs (1978) reviewed the main improvements of the new penetrometer relative to mechanical penetrometers, namely:

1. The elimination of possible erroneous interpretation of test results due to friction between inner rods and the outer tubes.
2. Continuous testing with a constant rate of penetration without the need for alternative movements of different parts of penetrometer tip and no possibility of undesirable soil movements influencing the cone resistance.
3. The simpler and more reliable electrical measurements of the cone resistance with the possibility for continuous readings and ease of recording the results.

Also, sensitive load cells can be used in electrical cone penetrometers and thereby more accurate readings can be obtained in very soft soils.

The Rotterdam cone was the first electrical cone penetrometer in Holland and it was developed and patented in 1948 by municipal engineer Bakker. Delft Soil Mechanics Laboratory (DSML) have worked with electric cone penetrometers since 1949 and developed in 1957 the first electrical cone penetrometer on which the local side friction could also be measured separately from the tip resistance (Vlasblom, 1985).

DSML carried out a series of comparative experiments to exploit all the previous experience with mechanical cone penetrometers. The geometry was also altered in order to assess comparison of results obtained by mechanical cone penetrometers (Heijnen, 1973; Vlasblom 1985).

In 1965 an electric cone was developed by Fugro in co-operation with the Dutch State Research Institute (TNO) (de Ruiter, 1971) (Figure 2.5). This cone later became the basis for the International Reference Test Procedure (ISSMFE, 1977, 1989).

de Ruiter (1971) also reported the use of an electrical inclinometer which enabled deviations of the cone from vertical to be monitored during a test.

### **(c) The piezocone (CPTU)**

Schmertmann (1974) recognized the importance of pore water pressure measurement for the interpretation of CPT data. Both Janbu and Senneset (1974) and Schmertmann (1974) showed the results of the changes in pore pressures during a pause in the penetration. Hence almost immediately Torstensson (1975) in Sweden and Wissa et al. (1975) in the USA developed electric piezometer probes with the special purpose of measuring pore water pressures during penetration and pauses in the penetration.

Many researchers have worked on piezocones and presented papers at the ASCE National Convention in 1981. Among those were de Ruiter (1981); Muromachi (1981); Baligh et al. (1981); Jones et al. (1981); Tumay et al. (1981) and Campanella and Robertson (1981).

A large number of piezocones (CPTU) have been developed in recent years. For practical purposes pore pressures are measured in fine grained soils only, usually at one location; most frequently behind the cone ( $u_2$ ). For coarse grained soils, measurement of pore pressure is generally of less importance, as dissipation takes place as soon as penetration is achieved, except if the fines content is high. Bayne and Tjelta (1987) and Zuidberg et al. (1987) reported the development of the triple element piezocones. For research purposes piezocones with two or three filter positions have also been developed.

### **2.3 Role of CPT in Site Investigation:**

Usually an ideal site investigation program should include a mix of field and laboratory tests. Field tests may include drilling, sampling, in situ testing, full scale testing and geophysical tests. Table 2.1 presents a partial list of the major in situ tests and their perceived applicability for use in different ground conditions. Qualitative evaluation grades have been assigned for each method based on experience (Lunne et al. 1997). The table is only a guide and the applicabilities are only approximation of perception based on soil and equipment type and details.

Most of the main in situ tests are applicable to soils with an average grain size finer than gravel size (i.e.  $< 2$  mm). Only a small number of tests can be carried out in hard ground conditions, such as sandy gravels, gravels, glacial tills, soft and hard rocks. Pre-boring or non-destructive seismic techniques are generally required in such soil types. However, recent use of high capacity CPT equipment has increased the range of applicable ground conditions.

From Table 2.1, it is evident that CPT has the highest applicability for soils. The CPT also provides a near continuous profile and is generally more cost-efficient.

The CPT has three main applications in the site investigation process:

- to determine sub-surface stratigraphy and identify materials present,
- to estimate geotechnical parameters, and,
- to provide results for use in direct geotechnical design.

In soft soils, cone penetration from ground level to depths in excess of 100 metres may be achieved provided verticality is maintained. Gravel layers and boulders, heavily cemented zones and dense sand layers can resist the penetration severely and damage the cones.

The CPT has three main advantages over the conventional combination of borings, samplings and other testing.

1. continuous or near continuous data
2. repeatable and reliable penetration data
3. efficient; thus cost effective.

## 2.4 CPT Equipment:

The CPT equipment consists of a cone penetrometer, pushing equipment and data acquisition systems. International Reference Test Procedure (IRTP) issued by the International Society of Soil Mechanics and Foundation Engineering (ISSMFE, 1989) is generally considered the standard test procedure.

- a) Cone:** The reference test equipment consists of a 60° cone, base area of 10 cm<sup>2</sup> and a 150 cm<sup>2</sup> friction sleeve located above the cone. The preferred filter location as suggested by IRTP is  $u_2$  for measurement of pore water pressure (Figure 2.1).
- b) Pushing Equipment:** The pushing equipment consists of a reaction system, a thrust mechanism and push rods. Usually hydraulically jacked or reaction system rigs are used to push the penetrometer. Traditionally, CPT has been used in finer soils (clays, silts and sands), where maximum thrust capacity up to 20 tonnes (200 MPa on cone tip) is needed to push the cones. Thrust capacity greater than this has generally been considered “Refusal”. Hence, the current maximum allowable thrust on the standard 35.7 mm diameter high-tensile steel push rods is about 20 tonnes (200 MPa), (Lunne et al. 1997). Exceeding that load can result in damage and /or buckling of the test rods, either in the rig or in the soft upper layers of the soil. Typically the standard cone rods are 1 m in length and are pushed in 1 m strokes also. Systems also exist which push the rods into the ground without any pause to reset the system (i.e. continuous push).

IRTP also requires a friction reducer be placed at least 1 m behind the cone for reducing the friction between the push rods and the soils.

- c) **Data Acquisition systems:** Modern electric cone penetrometers produce continuous signals that require relatively complex data collection and processing. Most data acquisition systems include analogue to digital converters so that the analogue signals can be directly converted to digital form for real time data logging. Modern equipment also allows amplification and digitization of the data in the cone to reduce the signal-to-noise ratio, thus improving the quality of data obtained for processing. Once data has been digitized, real time graphical output can be obtained for on-site evaluation of the results.

Usually the ideal space for the data acquisition systems is the enclosure of the truck. With climate control features the personnel can have added comfort and equipment can be preserved from harsh weather or other factors.

## **2.5 Cone Penetration Test (CPT) Procedure:**

The test procedure for CPT has been best described in IRTP by ISSMFE (1989). To obtain good results from CPT in the field, the first and foremost thing is to have well-qualified operators and good technical back-up facilities for calibration and maintenance of the equipment.

Sometimes when testing in hard soils or coarse material / fills, some sort of pre-drilling may be necessary in order to avoid damage to cone penetrometer. Casing may be used in some cases to support the upper part of the hole from caving. The verticality of the initial thrust is controlled by setting up the thrust machine as near as possible to vertical position. A maximum deviation of  $2^0$  is allowed by IRTP. The axis of the push rods should also coincide with the thrust direction. The pushing rods should be checked for straightness as per IRTP. Modern electric cone penetrometers come equipped with a slope sensor to measure the non-verticality of the sounding. Experience suggests that

once the penetrometer is deflected, it continues along a path with a relative consistent radius of curvature. Hence for sounding greater than 15 m, it is advisable to record inclinations on a continuous basis to allow for correction to be made to the depth of penetration.

The rate of penetration for a CPT, as outlined in the IRTP, should be  $20 \text{ mm/s} \pm 5 \text{ mm/s}$ . According to IRTP the depth interval between readings shall in no case be more than 200 mm. However, modern electric cone penetrometers produce continuous analogue data which can be converted to digital form at any desired interval. The output is much better if the interval of readings is kept as close as possible. IRTP requires that the depth of penetration of the cone be determined with an accuracy of  $\pm 100 \text{ mm}$ , relative to the ground surface or other fixed reference point, with a resolution of better than 10 mm. This is usually achieved by either a depth wheel concept or a cable drive system method.

## **2.6 Interpretation in Soils by CPT Parameters:**

Douglas and Olsen (1981) presented some of the most comprehensive work on soil classification using electric CPT data from areas in western USA (Figure 2.6). Their work confirmed earlier observations by Begemann (1965) (Figure 2.4), that sandy soils tend to produce high cone resistance and low friction ratio, whereas soft clay soils tend to produce low cone resistance and high friction ratio. Douglas and Olsen emphasized the fact that CPT classification charts cannot be expected to provide soil type based on grain size distribution, rather they provide a guide to the approximate soil behavior type (SBT). Olsen and Farr, 1986 and Robertson et al., 1986, presented improved soil classification charts (Figure 2.7) based on an expanded database. Lunne et al., 1986; Gillespie, 1990, have shown that even with careful procedures and corrections applied, the measurement of the sleeve friction ( $f_s$ ) is often less accurate and less reliable than the cone resistance ( $q_c$ ). A modified soil behavior type classification chart (Figure 2.8) has been proposed by Robertson (1990) on the basis of linear normalization of cone resistance,  $Q_t$ , to account for changes in overburden stress.

Using basic CPT data where only  $q_c$  and  $f_s$  are available, the chart shown in Figure 2.8 can be used to classify soils in various soil behavior types (SBT). Granular soils such as gravely sands exist in the upper left corner of the charts which confirms the higher cone resistance and small friction ratio values obtained by CPT in these soils.

Generally speaking CPT in granular soils such as gravels or sandy gravels is considered a drained penetration. No significant pore water pressure is build up when the cone penetrates into such soils as the hydraulic conductivity of these soils is very high.

Generally, soils that fall in zones 6 and 7 (Figure 2.8) represent approximately drained penetration. Robertson (1990) suggested that the chart (Figure 2.8) is global in nature and should be used as a guide to define soil behavior type. Factors such as stress history, *in-situ* stresses, sensitivity, macrofabric, mineralogy and void ratio will also influence classification.

- **Fine grained soils:** In fine grained soils, cone penetration is generally undrained and requires measurement of pore pressure. Several soil design, strength and deformation parameters can be interpreted using the cone resistance, sleeve friction and pore pressure measurements. These include but are not limited to, soil unit weight, overconsolidation ratio (OCR), undrained shear strength, soil sensitivity, constrained modulus, undrained Young's modulus, small strain shear modulus, coefficient of consolidation and hydraulic conductivity.
- **Coarse grained soils:** In coarse grained soils, the cone penetration testing is generally drained. Under drained conditions there should be no significant excess pore pressures generated as a result of cone penetration, that is, the *in-situ* static pore pressure is usually measured. Hence in coarse grained soils under fully drained conditions, only measured cone resistance and sleeve friction are used in the interpretation. In the case of gravely sands, the sleeve friction is usually less than



1 % of  $Q_t$  (Figure 2.8), hence cone resistance alone can be used for interpretation of coarse grained soils (coarser than 2 mm).

Several soil design, strength and deformation parameters can be interpreted, including, but are not limited to, relative density ( $D_r$ ), state parameter  $\psi$ , overconsolidation ratio (OCR), constrained modulus, drained Young's modulus, small strain shear modulus and hydraulic conductivity.

## **2.7 Effect of Varying Size of Cone on Interpretation of CPT Parameters:**

Cone penetrometers with diameters differing from the standard 35.7 mm are becoming more common. Examples are:

- 15 cm<sup>2</sup> cones (dia. = 43.7 mm) used in offshore investigations (Lunne and Powell, 1992).
- 15 cm<sup>2</sup> cone penetrometers with 10 cm<sup>2</sup> push rods are being used extensively in Great Britain (Powell et al. 1995) and North America.
- 5 cm<sup>2</sup> and smaller cone penetrometers have been used in laboratory calibration chambers and in centrifuge tests (Parkin and Lunne, 1982; Baldi et al., 1985).
- 1 cm<sup>2</sup> minicone has been used in offshore applications in favourable grounds (Power and Geise, 1995).

Several researchers, including Lunne et al. (1986), Powell and Quartermann (1988) and de Lima and Tumay (1991) have studied scale effects. de Lima and Tumay (1991) carried out a systematic program using cone penetrometers with cross-sectional areas 1.27 cm<sup>2</sup>, 10 cm<sup>2</sup> and 15 cm<sup>2</sup> in five sites in Louisiana, USA. They found that *cone resistance from the 1.27 cm<sup>2</sup> cone penetrometer was consistently larger than the reference 10 cm<sup>2</sup> penetrometer*. Although there were many factors involved in this conclusion, it showed a clear trend of higher cone resistance measurement for smaller area cone penetrometers.

Lunne et al. (1997) suggest that in practice cone penetrometers ranging in cross-section from 5 cm<sup>2</sup> (25 mm diameter) to 15 cm<sup>2</sup> (43.7 mm diameter) will give similar cone resistance values in most uniform soils. For dimensions outside this range, further study is needed, which is one of the main objectives for this research program.

## **2.8 Calibration Chamber Testing (CC):**

Most of the empirical correlations to estimate parameters from the CPT in granular soils (primarily sands) are based on interpretation methods derived from large scale calibration chamber tests, (Schmertmann, 1975; Veismanis, 1975; Bellotti et al., 1982; Parkin and Lunne, 1982; Baldi et al. 1986; Ghionna and Jamiolkowski, 1992).

Calibration chamber testing of the CPT in sands, by organizations around the world, have had an important impact on our ability to interpret CPT results in terms of engineering parameters. The purpose of calibration chamber testing has been to study the response of the CPT under well defined and well controlled soil conditions in terms of relative density, stress state and stress history. The results of these tests have provided empirical relationships between the significant parameters affecting the cone penetration resistance in sands, namely relative density and stress state.

The Country Road Board (CRB) in Australia developed the first advanced calibration chamber, where boundary stresses and strains could be measured. The original CRB chamber housed a sample 760 mm diameter and 910 mm high (Holden, 1971).

Subsequently, Dr Jim Holden designed calibration chambers at the University of Florida, Monash University, NGI and ENEL (Holden 1992). The first engineering correlations based on CC tests were developed by Schmertmann (1971, 1976, 1978) at the University of Florida. These guidelines were used for interpreting CPT results in sand in terms of relative density, friction angle and deformation parameters.

After that, Lunne and Christopherson (1983), Robertson and Campanella (1983, 1986) and Baldi et al. (1986) gave numerous correlations which are used extensively in practice.

The large calibration chamber tests that have formed the basis for these correlations were carried out on a relatively narrow range of uniform sands. The main aim was to correlate penetration resistance to relative density corresponding to depths larger than 5 m below ground level. The correlations are therefore only strictly applicable for unaged, predominantly quartz, non-cemented and uniform fine to medium sands. However, most natural sands are aged to some extent and often have some degree of cementation. The effect of cementation on the strength-deformation behavior of sands is often neglected in design since cementation improves strength. However, neglecting cementation in the interpretation of CPT data may result in an overestimate of the strength of the deposit since most available correlations are based on uncemented soils. This is one of the major limitations of correlations obtained from calibration chamber (CC) testing.

Most of the engineering correlations (based on CC tests) in use today are based on tests on Ticino and / or Hokksund sands. Both these sands are uniform fine to medium sands with 30 to 35 % quartz. Usually from the calibration tests the following parameters can be extracted:

- Relative density from preparation of samples
- Constrained modulus from consolidation of samples
- In situ stress state before and during a cone penetration test, and,
- $q_c$  and  $f_s$  from a CPT in the CC.

Recent research has shown repeatedly that the stress-strain and strength behavior of granular soils is too complicated to be represented by relative density alone. Yet relative density is still commonly used by many practicing engineers.

Relative density is defined by;

$$D_r = \{(e_{\max} - e) / (e_{\max} - e_{\min})\} \quad (2.1)$$

where  $e_{\max}$  and  $e_{\min}$  are the maximum and minimum void ratios determined in the laboratory using appropriate standard methods.  $e$  is the *in-situ* void ratio of the soil formation.

Calibration testing has shown that cone resistance in sands is controlled by relative density, *in-situ* vertical and horizontal effective stress and sand skeleton compressibility.

- Cone tip resistance is higher for higher density and vice versa.
- Cone tip resistance is higher for higher vertical and horizontal stress and vice versa.
- Cone tip resistance is higher for lower compressibility and vice versa.

These facts were shown by Robertson and Campanella (1983b) in Figure 2.9.

Calibration chambers have finite dimensions, and stress as well as strain (deformation) conditions at the chamber boundaries need to be imposed. The boundaries imposed by the calibration chamber may not represent the real field situation. In order to simulate the semi-infinite soil mass in the field, the required boundary conditions are between two extreme limits of constant stress and zero displacement on both the horizontal and vertical boundaries. This discrepancy may influence the cone tip resistance measured in calibration chambers. It is a well-know fact that the measured values of  $q_c$  and  $f_s$  are influenced by the chamber boundary conditions and the chamber / cone diameter ratio. Yet, the grain / cone diameter ratio effects have not been investigated to date. This is the main area of research of this study.

Depending on whether stresses are kept constant or displacements are zero at the top, bottom and lateral sample boundaries, four different types of boundary conditions can be applied in this type of calibration chamber testing (Lunne et al., 1997). These are listed in Table 2.2.

None of these four different boundary conditions simulate the field condition perfectly. The larger the chamber size, the less significant is the difference between results obtained in the chamber and the results obtained in the field. This means that the boundary conditions in the chamber can influence the results of penetration resistance if the chamber size is small relative to the size of the cone.

Thus in order to be applicable to field conditions, the measured values should be corrected for the following factors:

- Boundary condition used
- Chamber / cone diameter ratio
- Sand density ( $D_r$ )
- Sand compressibility

Calibration chamber testing also has additional limitations. Been et al. (1987) and Ghionna and Jamiolkowski (1992) have indicated that the following factors should be considered as limitations to CC testing:

- Sample age
- Types of sand tested
- Sample size and boundary effects

The biggest limitation is the physical dimensions one can handle for testing. Most CC tests have been carried out in chambers less than 3 m in diameter. Parkin and Lunne (1982) carried out CC tests on Hokksund sand where chamber to cone diameter ratio varied between 21 and 50 (Figure 2.10). Lunne and Christopherson (1983), based on

chamber test results on Hokksund sand, suggested that for a chamber to cone diameter ratio of 50, the difference in tip resistance obtained in the chamber and the field should be small. Ghionna and Jamiolkowski (1992) showed that for less compressible sands like the Toyura sand, chamber/cone diameter ratio and boundary conditions are very important. From these tests, it was concluded that for loose sands, typical chamber size and boundary conditions do not have significant effect on the cone resistance but for *dense sands these effects can be considerable*.

This conclusion was also confirmed by Ahmadi (2000, 2002 and 2004) in his research on granular material by finite difference method using continuum approach with computer software (FLAC). Ahmadi (2004) carried out a series of numerical simulation with  $k_0=0.5$ , three different relative densities 50%, 70% and 90%, varying vertical effective stresses and the boundary conditions listed in Table 2.2. The chamber to cone diameter ratio was varied from 20 to 120. Figure 2.11 shows the results reported by Ahmadi (2004). The numerical analysis indicates that a chamber to cone diameter ratios of 112, 67 and 33.6 are required for dense, medium-dense and loose sands, respectively, to eliminate any boundary effects. This analysis also indicates that boundary condition BC3 (i.e. zero horizontal strain plus constant vertical stress) appears to represent the best boundary condition with the least affect on the measured cone resistance.

As mentioned earlier the inability to physically model larger chambers and the inability to actually view the behavior of granular soils in the vicinity of the penetrating cone have led to some interesting new research recently.

Although some references are available on the use of the CPT in coarse grained soils such as residual soils, there are few references available on the use of CPT in gravels. Brand and Phillipson (1985) and Chang (1998) have reported that cone penetration can be difficult in residual soils due to frequent hard core stones of the weathered rock. Sowers (1985), reports the successful use of a non-standard 73 mm diameter simple cone in gravels in the United States. Peuchen et al. (1996) reported some experience with the CPT in harsh environment (coarse soils), in which a 20 tonnes truck

and a standard 35.7 mm cone was used. The selected refusal/termination criteria by Peuchen et al. (1996) were one or more of the following:

Overloading of the cone tip load sensor (100 kN)

Maximum thrust 20 tonnes (200 kN)

Maximum penetrometer inclination (usually  $15^0$ )

Rapid increase in penetrometer inclination.

These criteria served well to minimize loss of penetrometers and thrust rods when testing in coarse grained soils.

In this research the effect of grain size on the cone tip resistance was investigated. The analyses were carried out for dense and loose coarse granular material. Calibration chambers were modeled using different boundary conditions. The analyses were performed for varying grain to cone diameter ratios from 0.05 to 2.0 and chamber to cone diameter ratios from 15 to 600. The discrete element method based computer program PFC<sup>2D</sup> (2002) was used for all the analysis involved in this research.

Soil Parameters															Ground Type							
Group	Device	Soil type	Profile	u	$\phi'$	$s_u$	$I_D$	$m_v$	$c_v$	k	$G_o$	$\sigma_h$	OCR	$\sigma - \epsilon$	Hard		Soft					
															rock	$\epsilon$	rock	silt	clay	peat		
Penetrometers	Dynamic	C	B	-	C	C	C	-	-	-	C	-	C	-	-	C	B	A	B	B	B	B
	Mechanical	B	A/B	-	C	C	B	C	-	-	C	C	C	-	-	C	C	A	A	A	A	A
	Electric (CPT)	B	A	-	C	B	A/B	C	-	-	B	B/C	B	-	-	C	C	A	A	A	A	A
	Piezcone (CPTU)	A	A	A	B	B	A/B	B	A/B	B	B	B/C	B	C	-	-	-	A	A	A	A	A
	Seismic (SPT/SCPTU)	A	A	A	B	A/B	A/B	B	A/B	B	A	B	B	B	-	C	-	A	A	A	A	A
	Flat dilatometer (DMT)	B	A	C	B	B	C	B	-	-	B	B	B	C	C	C	-	A	A	A	A	A
	Standard penetration test (SPT)	A	B	-	C	C	B	-	-	-	C	-	C	-	-	-	C	B	A	A	A	A
Pressuremeters	Resistivity probe	B	B	-	B	C	A	C	-	-	-	-	-	-	-	-	-	A	A	A	A	A
	Pre-bored (PBP)	B	B	-	C	B	C	B	C	-	B	C	C	C	C	A	B	B	B	A	B	B
	Self boring (SBP)	B	B	A <sup>1</sup>	B	B	B	B	A <sup>1</sup>	B	A <sup>2</sup>	A/B	B	A/B <sup>2</sup>	-	-	-	B	B	A	B	B
	Full displacement (FDP)	B	B	-	C	B	C	C	C	-	A <sup>2</sup>	C	C	C	C	-	-	-	B	B	A	A
Others	Vane	B	C	-	-	A	-	-	-	-	-	-	B/C	B	-	-	-	-	-	A	B	B
	Plate load	C	-	-	C	B	B	B	C	C	A	C	B	B	B	B	B	A	A	A	A	A
	Screw plate	C	C	-	C	B	B	B	C	C	A	C	B	-	-	-	-	A	A	A	A	A
	Borehole permeability	C	-	A	-	-	-	-	B	A	-	-	-	-	-	A	A	A	A	A	B	B
	Hydraulic fracture	-	-	B	-	-	-	-	C	C	-	B	-	-	-	B	B	-	C	A	C	C
	Crosshole/downhole/ surface seismic	C	C	-	-	-	-	-	-	-	A	-	B	-	-	A	A	A	A	A	A	A

Applicability: A = high; B = moderate; C = low; - = none.

$\phi'$  = Will depend on soil type; <sup>1</sup> = Only when pore pressure sensor fitted; <sup>2</sup> = Only when displacement sensor fitted.

Soil parameter definitions:  $\nu$  = *in situ* static pore pressure;  $\phi'$  = effective internal friction angle;  $s_u$  = undrained shear strength;  $m_v$  = constrained modulus;  $c_v$  = coefficient of consolidation;  $k$  = coefficient of permeability;  $G_o$  = shear modulus at small strains; OCR = overconsolidation ratio;  $\sigma - \epsilon$  = stress-strain relationship;  $I_D$  = density index.

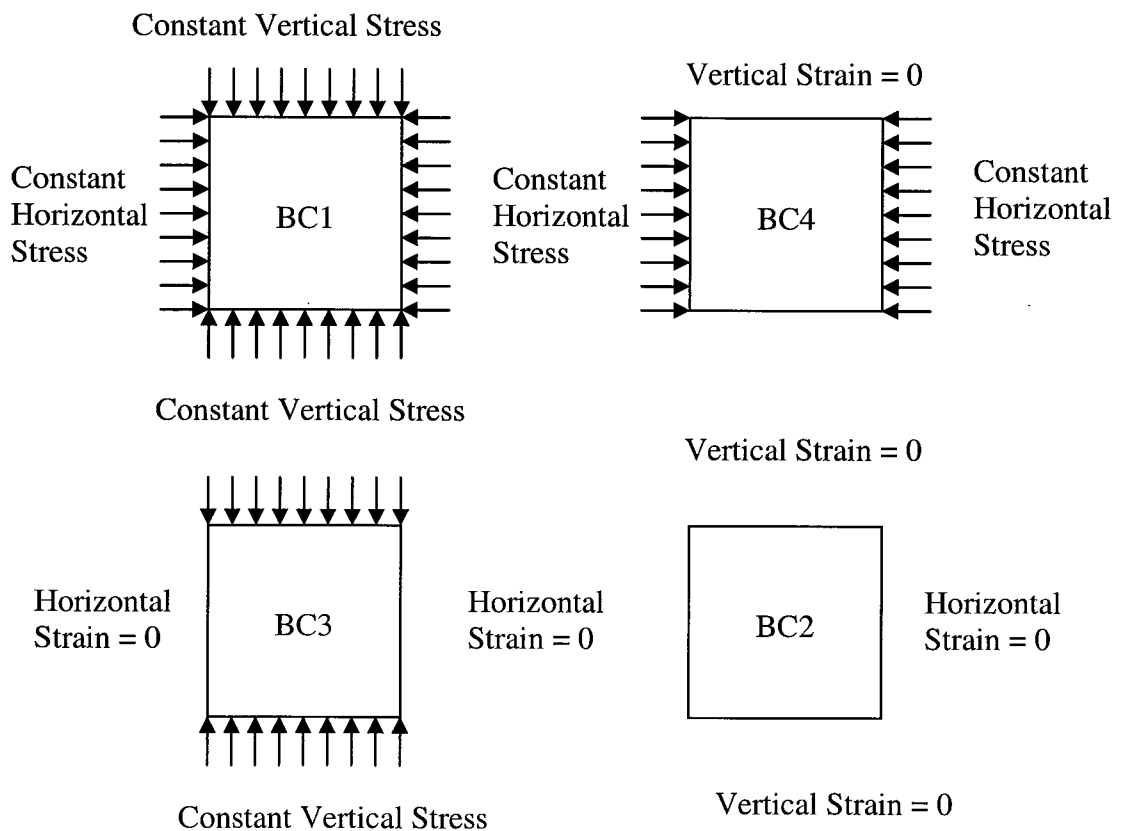
Table 2.1: Major *in situ* tests and their perceived applicability in various ground conditions (after Lunne et al. 1997).



Type of boundary condition	Lateral and bottom boundary condition
BC1	Horizontal stress = Constant Vertical stress = Constant
BC2	Horizontal strain = 0 Vertical strain = 0
BC3	Horizontal strain = 0 Vertical stress = Constant
BC4	Horizontal stress = Constant Vertical strain = 0

Table 2.2: Various boundary conditions usually applied to calibration chamber testing.

A graphical illustration is provided below.



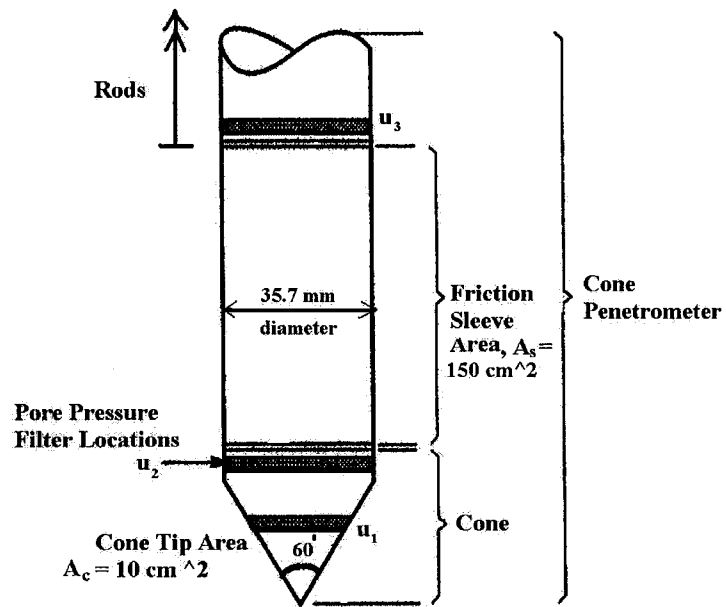


Figure 2.1: Cone penetrometer (modified from Lunne et al. 1997).

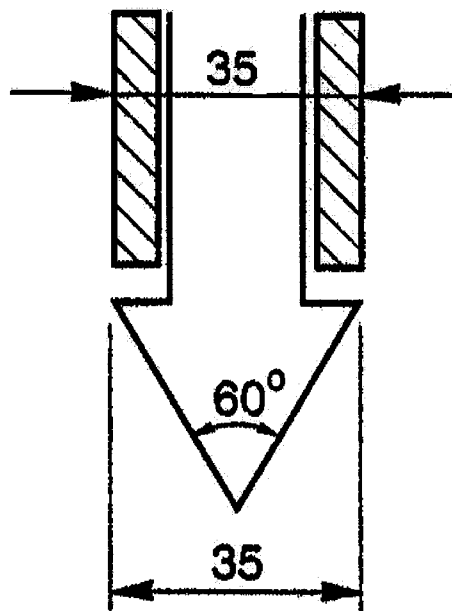


Figure 2.2: Old type Dutch cone (modified from Sanglerat, 1972).

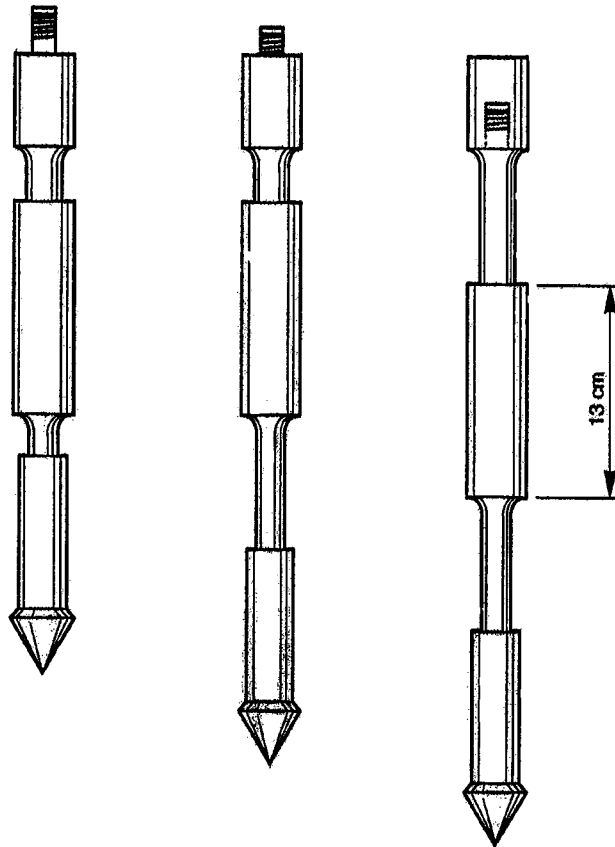


Figure 2.3: Begemann type cone with friction sleeve (from Sanglerat, 1972).

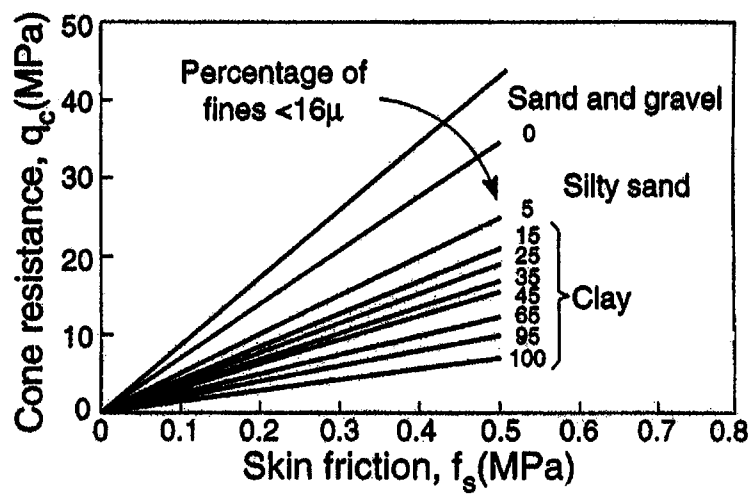


Figure 2.4: Soil classification from cone resistance and sleeve friction readings (from Begemann, 1965).

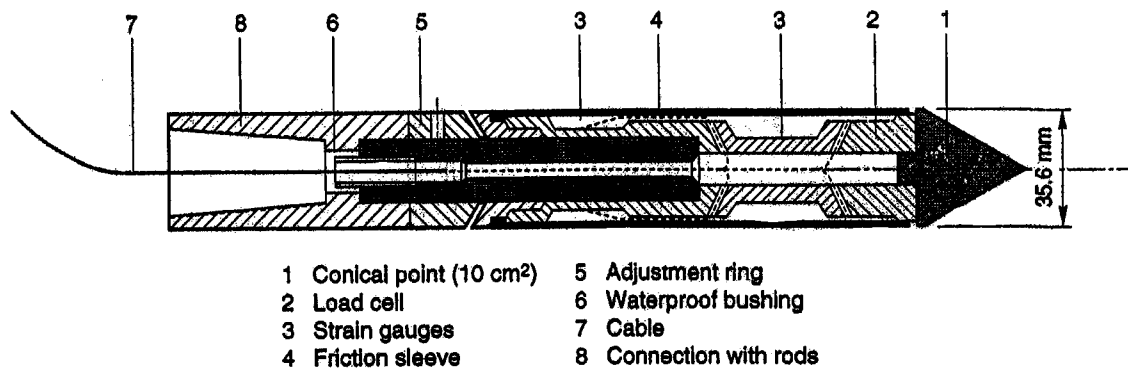


Figure 2.5: The Fugro electrical friction cone (after de Ruiter, 1971).

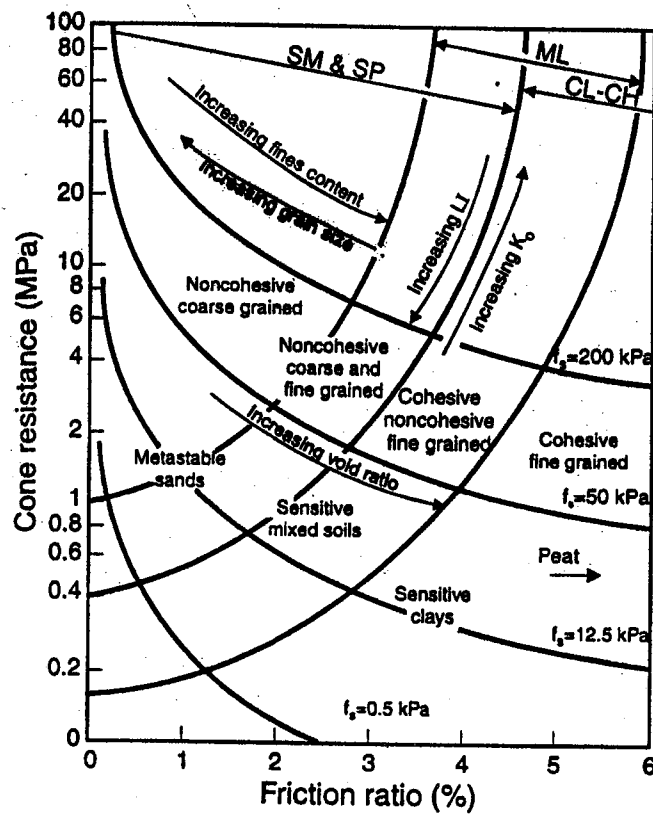
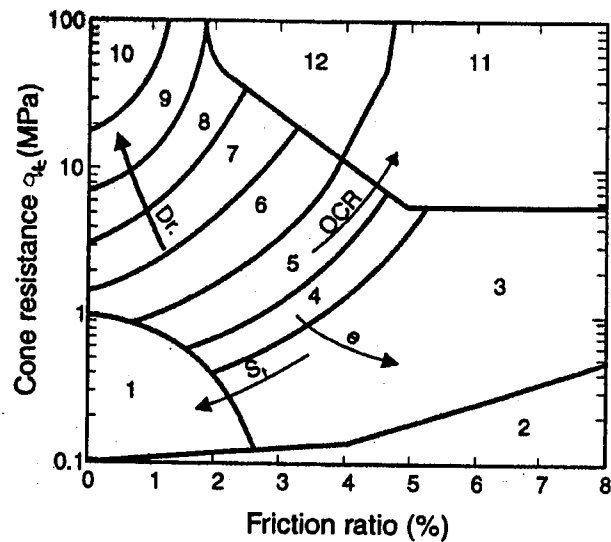


Figure 2.6: CPT soil behavior type classification chart by Douglas and Olsen (1981).



**Zone: Soil Behaviour Type:**

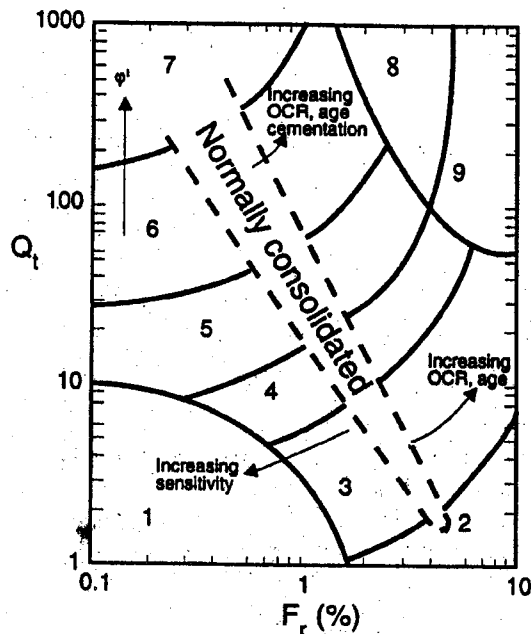
- 1. Sensitive fine grained
- 2. Organic material
- 3. Clay
- 4. Silty clay to clay

- 5. Clayey silt to silty clay
- 6. Sandy silt to clayey silt
- 7. Silty sand to sandy silt
- 8. Sand to silty sand

- 9. Sand
- 10. Gravelly sand to sand
- 11. Very stiff fine grained\*
- 12. Sand to clayey sand\*

\* Overconsolidated or cemented.

Figure 2.7: CPT soil behavior type classification chart (Robertson et al., 1986).



**Zone Soil behaviour type**

- 1. Sensitive, fine grained;
- 2. Organic soils-peats;
- 3. Clays-clay to silty clay;

**Zone Soil behaviour type**

- 4. Silt mixtures clayey silt to silty clay
- 5. Sand mixtures; silty sand to sand silty
- 6. Sands; clean sands to silty sands

**Zone Soil behaviour type**

- 7. Gravelly sand to sand;
- 8. Very stiff sand to clayey sand
- 9. Very stiff fine grained

Figure 2.8: CPT soil behavior type classification chart based on CPTU (Robertson 1990).

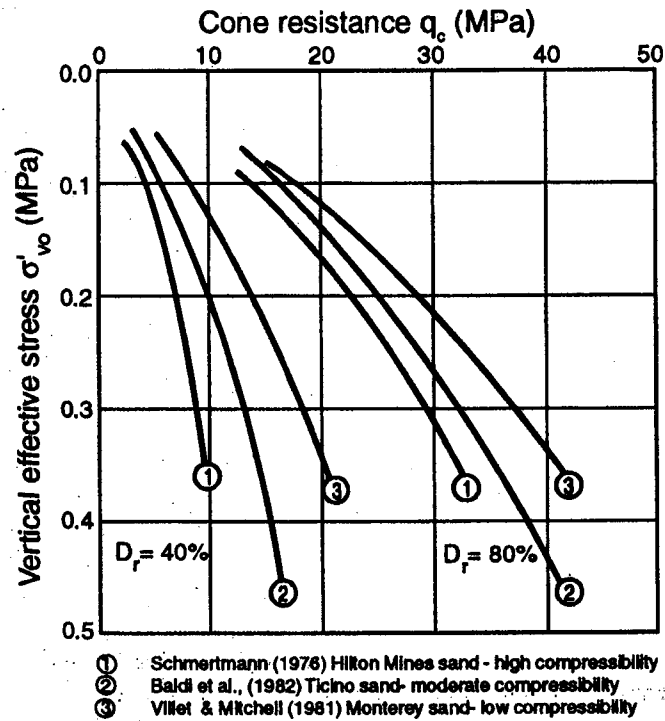


Figure 2.9: Effects of sand compressibility on  $q_c$ , overburden stress and  $D_r$  (Robertson and Campanella, 1983b).

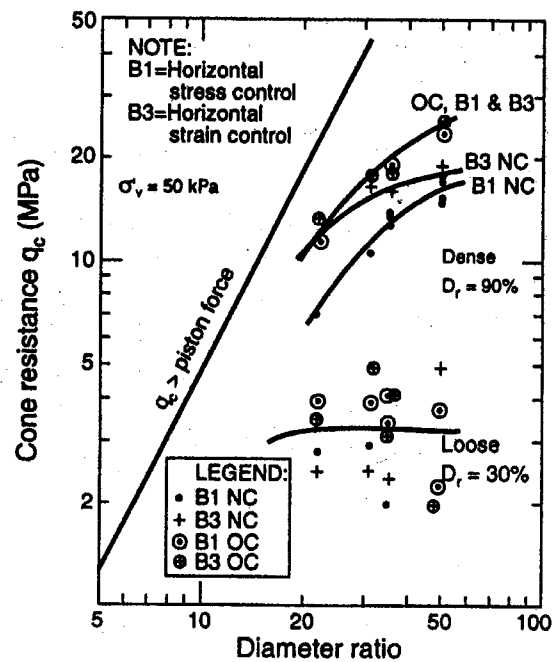


Figure 2.10: Effect of chamber size and boundary condition on CPT for Høksund sand (Parkin and Lunne, 1982).

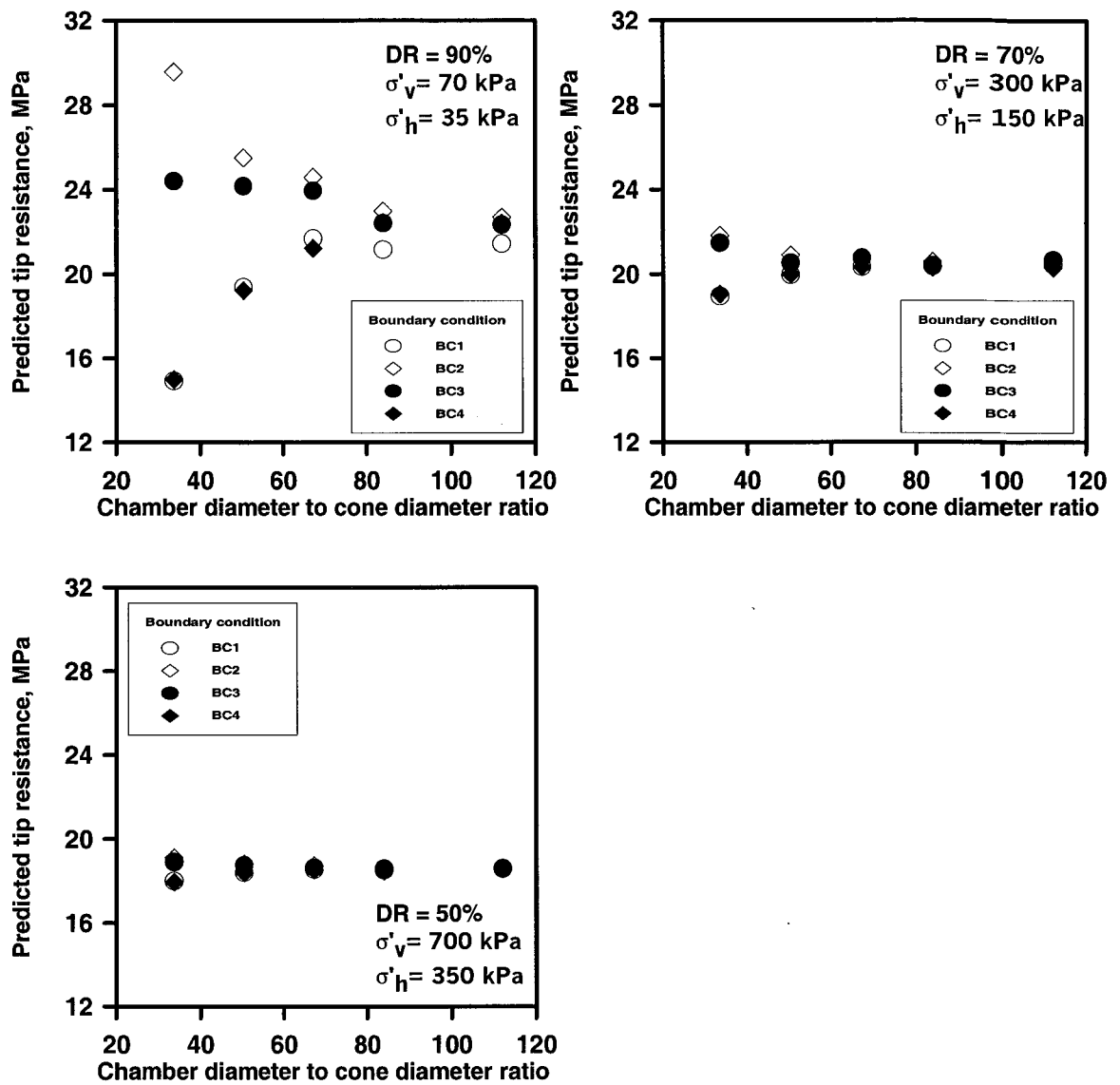


Figure 2.11: Effect of chamber size and boundary conditions on cone tip resistance (Ahmadi 2004).

### **3. DISCRETE ELEMENT METHOD (DEM)**

Several numerical methods, including the finite difference and finite element methods, consider soils to be continuous media. However, it is difficult to manage the problem of large deformation, such as fracture and flow, using continuum approaches. Discrete Element Method or DEM, which is based on discontinuum modeling, is a numerical procedure for simulating the mechanical behavior of a system of discrete, interacting particles and is not as restricted as the continuum approaches.

This chapter contains the general description and theoretical concepts of discrete element method for the simulation of granular material movement. This chapter is divided into three sections. Section 3.1 gives the background information and developments of DEM. Section 3.2 gives the descriptions of the theoretical basis of the DEM. Theoretical formulations as well as the main concepts regarding the calculation cycle, general descriptions of the boundary conditions, the implementation scheme and contact detection algorithm are explained. Section 3.3 discusses the limitations and shortcomings of the granular material simulation.

#### **3.1 Background Information and Developments in DEM**

Cundall (1971), proposed the Discrete Element Method (DEM). It was initially used to analyze the stability of jointed rock slopes by employing plane polygonal-shaped particles as elements. DEM was later extended to cover applications in soils by Cundall and Strack (1979) who defined it as follows:

*“The granular material is idealized as an assemblage of circular-shaped rigid disks or three-dimensional spherical elements”.*

A thorough description of the method is given in the two-part paper of Cundall (1988) and Hart et al. (1988), which was later enhanced enabling it to deal with three-dimensional problems by Cundall and Hart (1992). Although the simulation of circular-



shaped particles has the advantage of being very simple in routine calculations, it could not represent the real behavior of materials such as sand and gravel (granular material) due to the excessive rolling or rotation of the round particles (Ting et al., 1995). With the aim of emulating the natural media more closely, other complex shapes of particles have been proposed, such as arbitrary polygonal-shaped elements Hopkins (1992), or the elliptical-shaped elements Rothenburg and Bathurst (1991). These more complex-shaped elements are able to account for particles shapes, but the expense is the need for more complicated computational algorithms.

DEM has also been advanced in other areas related to its implementation scheme, i.e. contact detection. Vinogradov (1992, 1993 and 1997), Gavrilov and Vinogradov (1997) and Vinogradov and Sun (1997) suggested algorithms to increase the computational efficiency and accuracy in the simulation of particle clusters.

Path matrix was the basis of the proposed algorithms in these works, which is used to describe how particles are located in the assembly. These improved algorithms for the implementation scheme have resulted in increased computational efficiency and decreased search time during a calculation cycle. Furthermore, the extensions of the DEM to couple it with various mechanics (e.g. fluid and fracture) have been developed. DEM coupling with fracture mechanics is dominantly used in solving rock mechanics problems. Taylor and Preece (1992) modified a DEM code to model rock motion associated with conventional blasting. Trent and Margolin (1994) conducted numerical analysis based on DEM to model fracture in cemented granular materials. Potyondy et al. (1996) as well as Minchinton and Lynch (1996) made the simulation of crack generation in explosive rock by the DEM to study the importance of induced stresses and gas flow.

It is obvious that DEM has expanded into many applications. One useful advantage of the DEM is the ability to provide insight on how microscopic properties can impact macroscopic responses. Chang and Misra (1989) used numerical simulation based on the DEM to compare the results with the micro-structural continuum model. Potyondy et al. (1996) described a computational methodology to simulate certain kinds of material

testing using bonded assemblies of circular-shaped particles, similar to the work by Potyondy and Cundall (1998). Cleary et al. (1998) used DEM to study mixing processes. Ng (1999) applied DEM to revise the microscopic properties in granular materials. Antony (2000) also utilized DEM to analyze the normal contact force distribution and studied the effect of microstructure and contact fabric on stresses in granular media. The understanding of how the micro-properties affect the macro material responses can lead to more insight into the constitutive behavior of the material. Additionally, DEM has been applied in the field of powder technology and as well as in physical animation for computer graphics.

### 3.2 Basic Ideology of DEM<sup>1</sup>

---

*1. Most of the theories described here are excerpts of the work by Cundall and Strack (1979) and the PFC<sup>2D</sup> manual, Itasca Consulting (2002).*

A general particle-flow model simulates the mechanical behavior of a system comprised of a collection of arbitrarily-shaped particles. DEM treats the granular material as an assembly of discrete and interacting particles i.e. a granular assembly is idealized by a collection of circular-shaped particles (commonly called disks) for 2-D problems. The interaction of particles in the interaction pair is only at the contact point. Each particle will displace independently i.e. the displacement of particles is independent of each other. This assumption greatly helps in defining the location of the resultant contact forces. The particles that comprise the granular assembly are often considered rigid and the behavior at the contacts is characterized using a soft-contact approach. The choice of using either hard or soft contacts is given by Cundall and Hart (1992).

The contacts occur over a vanishingly small area, i.e. at a point, relative to the particle sizes. A finite normal stiffness is taken to represent the measurable normal stiffness that exists at a contact. At the contact point, each particle in the interaction pair are allowed to overlap each other to a magnitude that is proportional to the contact normal force. The force-displacement law (force = stiffness  $\times$  displacement) governs the

relationship between the magnitude of the particle overlap and contact force. Then, all acting forces are summed for each individual granular particle, and each particle movement can be found. Newton's laws of motion (force = mass  $\times$  acceleration) provide the fundamental relationship between particle motion and forces causing that motion. The force system may be in static equilibrium, in which case there is no motion or it may be such as to cause the particles to flow. The mechanical behavior of the granular material is described in terms of the movement of each particle and inter-particle forces acting at each contact point (Cundall and Strack, 1979).

Six basic **assumptions** are usually considered for particle-flow model:

1. Particles comprising the granular assembly are treated as rigid bodies.
2. Behavior at the contacts uses a soft-contact approach wherein the rigid particles are allowed to overlap one another at contact points.
3. The contacts occur over a vanishingly small area (i.e., at a point).
4. The magnitude of the particle overlap is related to the contact force via the force-displacement relationship and all overlaps are small in relation to particle sizes.
5. Bonds can exist at contacts between particles.
6. All particles are circular; however, the clump logic supports the creation of super-particles of arbitrary shape. Each clump consists of a set of overlapping particles that act as a rigid body with a deformable boundary.

The assumption of particle rigidity is a good one when most of the deformation in a physical system is accounted for by movements along interfaces. The deformation of a packed-particle assembly or a granular assembly such as sand and gravel, as a whole is described well by this assumption, since the deformation results primarily from the sliding and rotation of the particles as rigid bodies and the opening and interlocking at interfaces and not from individual particle deformation. Precise modeling of particle deformation is not necessary to obtain a good approximation of the mechanical behavior for such systems.

The contacts are described by three constitutive models; a stiffness model, a slip model and a bonding model. The stiffness model provides an elastic relationship between the contact force and the relative displacement. The contact forces consist of normal and shear components. The slip model enforces the relationship between shear and normal contact forces such that two contact particles may slip relative to each other. The Mohr-Coulomb criterion is generally used,  $F_{\max}^s \leq \mu |F_i^n|$ , where  $F_{\max}^s$  is the maximum shear force,  $\mu$  is the frictional coefficient and  $F_i^n$  is the normal force. The bonding model is applied to the more complex behavior. The particles are bonded together at their contact points to form a clump of particles. The interparticle contacts may be modeled with an elastic spring and a dashpot.

The interaction between contact particles is treated as a dynamic process in which the movements of the particles are the results of the propagation through the particle system of disturbances originating from the boundaries, with states of equilibrium developing whenever the internal forces balance. The calculation alternates between the application of the force-displacement law and Newton's second law to keep track of the movement history of all individual particles in the assembly. The contact forces and displacements of a stressed assembly of particles are found by tracing the movements of the individual particles. Movements result from the propagation through the particle system of disturbances caused by specified wall(s) (cone in the case of this research) and particle motion and/or body forces. This is a dynamic process in which the speed of propagation depends on the physical properties of the discrete system.

Initially, the positions of all granular particles are known. Any two particles in contact are detected and the contact list is being updated at the same time. By using the force-displacement law, the interaction forces between contact particles can be found from the magnitude of the particle overlap. Newton's second law of motion is then applied to find the particle movement resulted from the summation of all forces acting on a particle. It is assumed that the positions, velocities and accelerations of the particles are constant over a single time-step.

The dynamic behavior is represented numerically by an explicit time-stepping algorithm, using a central-difference scheme to integrate accelerations and velocities. The solution scheme is identical to the one that is used in the explicit finite-difference method for continuum analysis. The use of an explicit, as opposed to an implicit, numerical scheme makes it possible for the scheme to simulate the non-linear interaction of a large number of particles without excessive memory requirements or the need for an iterative procedure. The DEM is based upon the idea that the timestep chosen may be so small that, during a single timestep, disturbances cannot propagate from any particle further than its immediate neighbors. Otherwise the scheme is numerically unstable. Then, at all times, the forces acting on any particle are determined exclusively by its interaction with the particles with which it is in contact. Since the speed at which a disturbance can propagate is a function of the physical properties of the discrete system, the critical timestep can be chosen to satisfy the above constraint. Further explanation is provided in Sections 3.2.6 and 3.3.1.

In addition, the damping concept (Section 3.2.4) may be taken into account for increasing the systematic energy dissipation, rather than from frictional sliding only, and that induces the motion of the particle system to reach steady-state in a reasonable amount of time.

### **3.2.1 Calculation Cycle**

The calculation cycle in the discrete element method is a time-stepping algorithm that consists of the repeated application of the law of motion to each particle, a force-displacement law to each contact, and a constant updating of wall positions (PFC<sup>2D</sup> manual, Itasca Consulting, 2002). Contacts, which may exist between two balls (particles) or between a ball and a wall, are formed and broken automatically during the course of a simulation. Newton's second law of motion gives the movement of a particle resulting from the action forces and moments, while the force-displacement law is used to find the contact forces that are induced by the relative motion between the contact particles.

At the start of each timestep, the set of contacts is updated from the known particle and wall positions in an assembly. The force-displacement law is then applied to each contact to update the contact forces based on the relative motion between the two entities (the particle overlap) at the contact and the contact constitutive model. Next, the law of motion is applied to each particle to update its velocity and position based on the resultant force and moment arising from the contact forces and any body forces acting on the particle. Also, the wall positions are updated based on the specified wall velocities. The calculation cycle based on these two physical governing laws is shown in Figure 3.1. This allows the DEM to track the movement history of each individual particle in the granular assembly.

The calculations performed within each of the two boxes of Figure 3.1 are performed, conceptually, in parallel (because the set of input data to each box remains fixed during the execution within a given box).

### 3.2.2 Force-Displacement Law<sup>2</sup>

---

*2. All of the proofs in this section are referred to the work by Cundall and Strack (1979).*

The force-displacement law derives the contact force acting on two entities in contact to the relative displacement between the entities. The contact force arises for both ball-ball and ball-wall contacts from contact occurring at a point (modeled using the soft-contact approach). For ball-ball contact, an additional force and moment arising from the deformation of the cementitious material represented by a parallel bond can also act on each particle.

Contact force is divided into two components: a normal component acting normal to the contact surface and a shear component acting in the tangential direction. Figure 3.2 illustrates the case of two particles (balls) A and B being in contact.

The coordinates of the centers of particles A and B according to a Cartesian coordinate system are  $(\chi_{A1}, \chi_{A2})$  and  $(\chi_{B1}, \chi_{B2})$ , respectively. The velocities of the particles are  $(\chi'_{z1}, \chi'_{z2})$ , in which the subscript letter is used to designate the particle and the subscript number refers to the axis. The angular velocities are also presented in Figure 3.2 as  $\theta_A$  for particle A and  $\theta_B$  for particle B. Particles A and B have radii  $R_A$  and  $R_B$  and masses  $m_A$  and  $m_B$  respectively. Points  $P_A$  and  $P_B$  in Figure 3.2 are defined as the points of the intersection of the line connecting between two particle centres with the boundaries of particles A and B, respectively.

Two particles will be in contact, if the distance  $D$  between their centres is less than the summation of their radii; i.e. if

$$D < R_A + R_B \quad (3.1)$$

The unit vector  $e = (\cos\theta, \sin\theta)$  in Figure 3.2 points from the center of particle A to the centre of particle B, i.e.

$$e = \cos\theta \, i + \sin\theta \, j \quad (3.2)$$

$$= e_1 i + e_2 j$$

where  $e_1 = \cos\theta$ , and  $e_2 = \sin\theta$ .  $i$  and  $j$  are unit vectors.

And the unit vector  $t$  is obtained by a clockwise rotation of  $e$  through  $90^\circ$ , i.e.

$$t = \sin\theta \, i - \cos\theta \, j \quad (3.3)$$

$$= e_2 i - e_1 j$$

If the coordinate of point  $P_A$  is given by

$$x_{PAi} = x_{Ai} + R_A e_i \quad (3.4)$$

The velocity of point P<sub>A</sub> will be:

$$x'_{PAi} = x'_{Ai} + R_A e'_i \quad (3.5)$$

$$= x'_{Ai} - R_A \theta_A t_i$$

Similarly, velocity of point P<sub>B</sub> will be given by the same expression except that the angle  $\theta$  in the equation (3.5) is replaced by  $180 + 0$  degrees;

$$x'_{PBi} = x'_{Bi} + R_B \theta_B t_i \quad (3.6)$$

The relative velocity of point P<sub>A</sub> with respect to point P<sub>B</sub> may be expressed as:

$$\begin{aligned} X'_i &= x'_{PAi} - x'_{PBi} \\ &= (x'_{Ai} - x'_{Bi}) - (R_A \theta_A + R_B \theta_B) t_i \end{aligned} \quad (3.7)$$

Normal (n) and shear (s) components of the relative velocities are the projections of  $X'_i$  onto  $e$  and  $t$  respectively:

$$n'_i = (x'_{Ai} - x'_{Bi}) e_i \quad (3.8)$$

and

$$s'_i = (x'_{Ai} - x'_{Bi}) t_i - (R_A \theta_A + R_B \theta_B) \quad (3.9)$$

To give the components  $\Delta n$  and  $\Delta s$  of the relative displacement increment, the relative velocity components are integrated with respect to time:

$$\Delta n = (n'_i) \Delta t = \{(x'_{Ai} - x'_{Bi}) e_i\} \Delta t \quad (3.10)$$



$$\text{and} \quad \Delta s = (s'_i) \Delta t = \{(x'_{Ai} - x'_{Bi}) t_i - (R_A \theta_A + R_B \theta_B)\} \Delta t \quad (3.11)$$

These increments of the relative displacements are used with the force-displacement law to calculate the increments of the normal and shear forces,  $\Delta F_n$  and  $\Delta F_s$ .

$$\Delta F_n = k_n \Delta n = k_n \{(x'_{Ai} - x'_{Bi}) e_i\} \Delta t \quad (3.12)$$

$$\text{and} \quad \Delta F_s = k_s \Delta s = k_s \{(x'_{Ai} - x'_{Bi}) t_i - (R_A \theta_A + R_B \theta_B)\} \Delta t \quad (3.13)$$

where  $k_n$  and  $k_s$  represent the normal and shear stiffnesses, respectively.

Finally, at each time-step the force increments  $\Delta F_n$  and  $\Delta F_s$  are added into the summation of all force increments,  $F_n$  and  $F_s$ , determined for previous time-steps:

$$(F_n)_N = (F_n)_{N-1} + \Delta F_n ; (F_s)_N = (F_s)_{N-1} + \Delta F_s \quad (3.14)$$

where the indices  $N$  and  $N-1$  refer to times  $t_N$  and  $t_{N-1}$  such that  $t_N - t_{N-1} = \Delta t$ . Sign convention for the normal and shear forces acting on a particle viz.  $Z$  is indicated in Figure 3.3.  $F_n$  and  $F_s$  are taken as positive in the directions opposite to  $e$  and  $t$ .

A Coulomb friction law is incorporated as follows. The magnitude of the shear force  $F_s$  found from the equation (3.14) is checked against the maximum possible value  $(F_s)_{\max}$  defined as:

$$(F_s)_{\max} = F_n \tan \Phi + c \quad (3.15)$$

where  $\Phi$  is the inter-particle friction angles and  $c$  is the cohesion. If the absolute value of  $(F_s)_N$  in equation (3.14) is larger than  $(F_s)_{\max}$ , the magnitude of  $(F_s)_N$  is set equal to  $(F_s)_{\max}$ , preserving the sign obtained from equation (3.14).

Once the normal and shear forces have been determined for each contact of a particle, they are resolved into two components according to the directions in the Cartesian coordinate system. Summation of all force components acting at the particle gives the resultant forces  $\Sigma F_{zi}$ . Resultant moment on a particle,  $\Sigma M_z$ , is positive if acting in the counter-clockwise direction, and is determined from  $\Sigma M_z = \Sigma F_s R_z$ , where the summation is taken over all forces acting on particle Z in the tangential direction.

The resultant forces and moments acting on the granular particle are used with Newton's second law of motion to determine the movement of the particle.

### 3.2.3 Law of Motion<sup>3</sup>

---

3. All of the proofs in this section are referred to the work by Cundall and Strack (1979).

The motion of a single rigid particle, determined by the resultant forces and moments acting upon it, can be described in terms of the translational motion of a point in the particle and the rotational motion of the particle. Translational motion of the particle mass center includes the particle position  $x_i$ , velocity  $x'_i$ , and acceleration  $x''_i$ , while the rotational motion of the particle includes the angular velocity  $\theta'_z$  and angular acceleration  $\theta''_z$ . Newton's second law is applied to the particle Z as:

$$m_z x''_{zi} = \Sigma F_{zi} \quad (3.16)$$

$$\text{and} \quad I_z \theta''_z = \Sigma M_z \quad (3.17)$$

where  $m_z$  and  $I_z$  represent the mass and moment of inertia of particle Z.

Assume that the time interval  $\Delta t$  is so small that the translational and angular acceleration,  $x_i$  and  $\theta_z$ , are constant over the interval. Equations (3.16) and (3.17) lead to the following expressions for the translational and angular velocities at the next time-step:

$$(x'_{zi})_{N+1} = (x'_{zi})_N + (\Sigma F_{zi} / m_z)_N \Delta t \quad (3.18)$$

$$\text{and} \quad (\theta'_z)_{N+1} = (\theta'_z)_N + (\Sigma M_z / I_z)_N \Delta t \quad (3.19)$$

where  $\Sigma F_{zi}$  is the term for the summation of all forces acting on the particle Z, including contact forces, as well as other forces such as body forces, drag forces and buoyant forces.

Finally, the new values for velocities are used to update the positions and rotations of the particles by a further numerical integration.

$$(x_{zi})_{N+1} = (x_{zi})_N + (x'_{zi})_N \Delta t \quad (3.20)$$

$$\text{and} \quad (\theta_z)_{N+1} = (\theta_z)_N + (\theta'_z)_N \Delta t \quad (3.21)$$

### 3.2.4 Damping

The contact model between particles in both normal and tangential direction may be conceived as a spring and a dashpot as shown in Figure 3.4.

The spring in the model is taken into account as the stiffness in the force-displacement law, while the dashpot is set to provide some sort of damping for dissipation of the system energy. The use of damping other than by friction alone is necessary in order that the assemblies reach a state of equilibrium for all conditions.

Damping forces are calculated based on the relative velocities at the contact. Formulations to calculate the damping forces are separated into two components:

Normal damping:

$$D_n = c_n \dot{n} \quad (3.22)$$

$$= c_n (\dot{x}'_{Ai} - \dot{x}'_{Bi}) e_i$$

Shear damping:

$$D_s = c_s s \quad (3.23)$$

$$= c_s \{ (x'_{Ai} - x'_{Bi}) t_i - (R_A \theta'_A + R_B \theta'_B) \}$$

where  $c_n$  is the damping coefficient in the normal direction and  $c_s$  is the damping coefficient in the tangential direction. Note that if the shear force is greater than the maximum possible shear force, there will be no shear damping applied.

Damping forces  $D_n$  and  $D_s$ , found from the equations (3.22) and (3.23), are included in the total forces acting on a particle. It is assumed that the damping coefficients in the normal and tangential directions are taken to be proportional to the normal and shear stiffnesses  $k_n$  and  $k_s$ , respectively, with proportionality constant  $\beta$  (in this simulation, 0.01). Damping coefficients are (Cundall and Strack, 1979):

$$C_n = \beta k_n ; C_s = \beta k_s \quad (3.24)$$

### 3.2.5 Boundary Conditions

In general, a particle can move freely according to the resultant forces and governed by Newton's second law of motion, except when it moves and faces the boundary condition. Boundary conditions in this simulation refer to the boundaries of the chamber such as the side, top or the bottom walls. Interaction of boundaries to a particle is similar to the interaction of particles in contact with each other. Therefore, granular particles will not be able to move across these boundaries. However, the particle can move along the boundaries, resulting in energy loss in the granular system due to the friction between the particle and the boundary. If the friction coefficient value assigned to the walls is zero (as a penetrating cone in the case of this study), then no energy loss will take place. A particle will slip along the boundary, if the tangential force acting on the particle is greater than the maximum possible value of the shear force.

### 3.2.6 Critical Time-Step Determination

As a consequence of the explicit numerical scheme employed in the discrete element method, a time-step must be selected which is small enough that the numerical simulation is stable or, during a single time-step, disturbances cannot propagate from any particle further than its immediate neighbors. This is the major disadvantage of the explicit numerical scheme. The scheme is only conditionally stable. In the work by Thallak et al. (1990), the value of a critical time-step  $\Delta t_c$  is estimated by the natural period of a one-dimensional mass-spring system; i.e., from a single degree-of-freedom mass spring model with the lowest mass and the highest stiffness in the simulation, according to:

$$\Delta t_c = 2 \sqrt{(m_{\min} / K_n)} \quad (3.25)$$

where  $m_{\min}$  represents the mass of the smallest particle in the assembly and  $K_n$  the highest normal contact stiffness.

### 3.2.7 Contact Detection

From the positions of all particles in the assembly, the approach is to identify all pairs of particles that are in contact before calculating the contact forces. The algorithm for contact detection incorporated into this simulation is very simple. The position of one particle is checked against the position of every other particle to determine if contact will occur. Since circular-shaped particles are used in the simulation, this avoids the ambiguities that usually occur in contact detection for other particle shapes. For instance, if the polygonal-shaped particles are used, it is necessary to determine whether the contact is an edge-edge type contact, edge-corner type contact or corner-corner type contact. But for the circular-shaped particle, the program needs only to compare the distance between the particles with the sum of the radii (refer to Equation 3.1).

This approach is acceptable when the number of particles is not too high. The computation time of this approach is proportional to the square of the particle number in

the assembly or  $n^2$ , where  $n$  is the total number of particles within the granular assembly. However, modern computing machines with high computing power have solved this problem to a great extent and this approach can now be used for quite large number of particles depending on the available RAM capacity.

### **3.3 Limitations and Shortcomings of DEM**

#### **3.3.1 Size of the Time-Step**

As a result of the explicit numerical scheme employed in the discrete element method, the simulation will be stable if the time-step  $\Delta t$  is taken as a fraction or less than one of the critical time-step. The critical time-step is estimated on the basis of a single degree-of-freedom system of a mass  $m$  connected to the ground by a spring with stiffness  $k$ . The critical time-step for this case is equal to  $2\sqrt{m/k}$ . Therefore, the critical time-step is a function of the physical properties of the discrete system. By the nature of the explicit numerical scheme, the concept is very simple but it suffers from the limitations that the time-step must be small. Therefore, a simulation will require a higher number of computation steps than the implicit scheme.

#### **3.3.2 Search Time in the Contact Detection Algorithm**

Although the approach of the contact detection used in this simulation is very simple and does not need a highly sophisticated organization of the data structure, it requires a large amount of searching time especially when the number of particles reaches several thousands. Therefore, to maintain the computational time in a reasonable range, the number of particles in any simulation should be limited.

In recent research, there are a number of developments in the contact detection algorithm. By using good organization of data structure and a unique data management approach, the overall search time can be improved. An example for reducing search time is to do one exhaustive search at the start of the simulation, and then maintain a list of

neighbors for each body. Subsequent searches will be restricted to the local area around each body instead of searching over the entire domain, so that search time will be proportional to the number of particles in the assembly (or  $n$ ). Complete details can be found in the work by Munjiza and Andrews (1998), as well as, by Perkins and Williams (2001).

### 3.3.3 Material Calibration

Discrete element method describes the overall macro-mechanical material behavior in terms of the micro-mechanisms. The input properties of the DEM model are in the microscopic level, and are not usually known. In order to reproduce a material that behaves in the same way as the intended macro responses, the micro properties must be selected appropriately. Since there is no direct formulation that relates the micro parameters with the macro-responses, a calibration process to match the micro-scale properties with the relevant macro-responses may be required. In addition, it should be realized that the term "particle" used in the discrete element method differs from its more general definition. By the common sense in the field of mechanics, the term "particle" means to a body whose dimensions are negligible and thus occupies only a single point in space. In the DEM, the term "particle" denotes a body that occupies a finite volume of space. *Thus, particle size does not correspond directly with the actual grain size of the granular material.* Size of the particles must be chosen such that it is smaller than the smallest interesting features in the simulation. Therefore particles can be viewed as a collection of grains, especially when the grains of the material are very small, such as silt and fine sands. In this study, the particle size corresponds to a relative size between a penetrating cone and a sand and/or gravel grain. Consequently, other causes related to the particle size such as particle shape, fabric and packing arrangement can also affect the behavior of the DEM model.

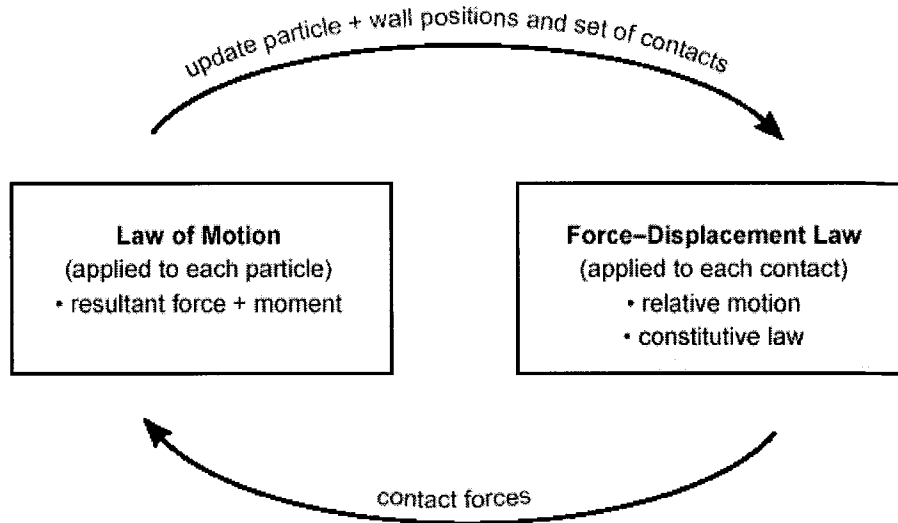


Figure 3.1: Calculation cycle in DEM.

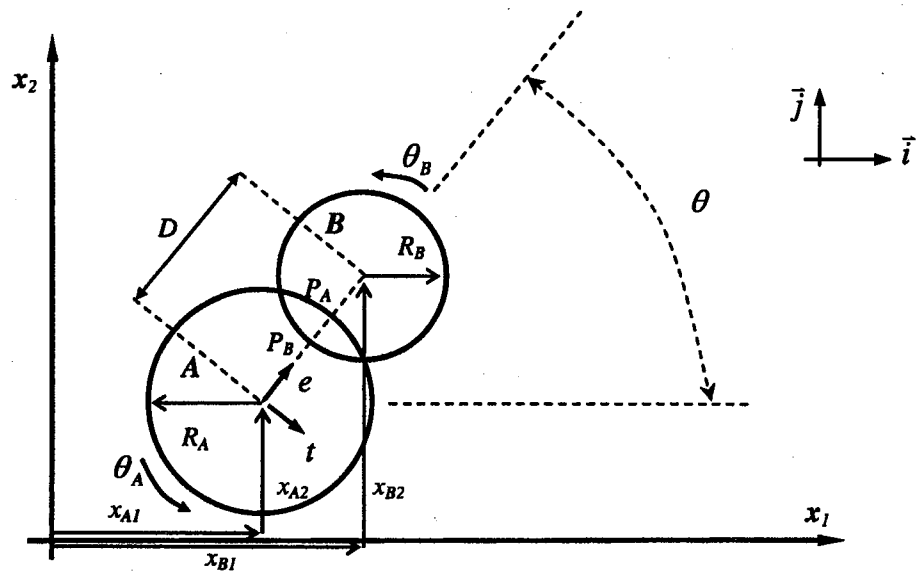


Figure 3.2: A pair of particles in contact (Cundall and Strack, 1979).



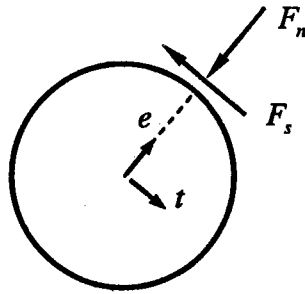


Figure 3.3: Sign Convention for  $F_n$  and  $F_s$  (Cundall and Strack, 1979).

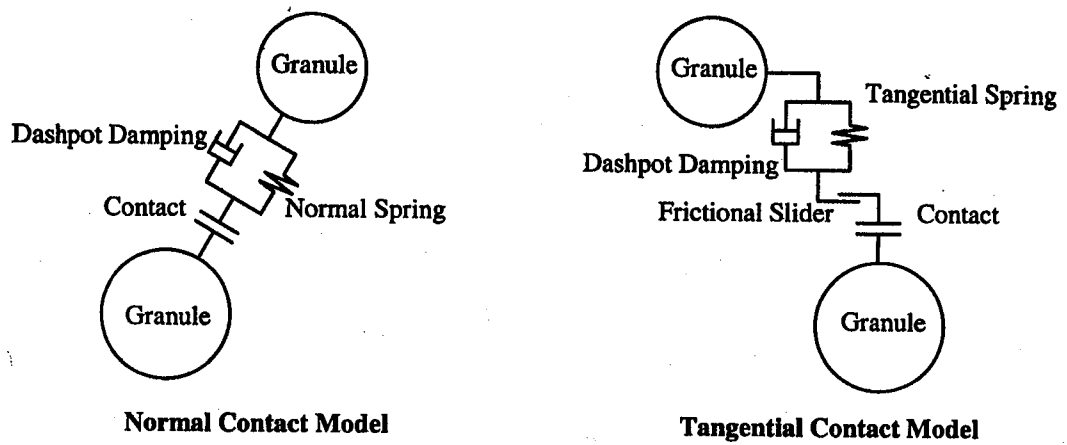


Figure 3.4: Spring and dashpot model (Cundall and Strack, 1979).

## 4. PARTICLE FLOW CODE IN 2 DIMENSIONS (PFC<sup>2D</sup>)<sup>1</sup>

---

1. The discussions in this chapter are attributed to PFC<sup>2D</sup> manual, Itasca Consulting (2002).  
A letter of permission from M/s. ITASCA is enclosed in **Appendix –A**.

### 4.1 Introduction

“Particle Flow Code in 2 Dimensions (PFC<sup>2D</sup>) is classified as a discrete element code based on the definition in the review of Cundall and Hart (1992) since it allows finite displacements and rotations of discrete bodies, including complete detachment, and recognizes new contacts automatically as the calculation progresses. PFC<sup>2D</sup> can be viewed as a simplified implementation of the DEM because of the restriction to rigid circular particles”, PFC<sup>2D</sup> Manual 2002.

In other words, PFC<sup>2D</sup> is a program for modeling the movement and interaction of assemblies of arbitrarily-sized circular (2D) particles. The particles are rigid but deform locally at contact points using a soft contact approach, in which finite normal and shear stiffnesses are taken to represent measurable contact stiffnesses.

The particles may represent individual grains in a *granular material* or they may be bonded together to represent a *solid material*, in which case, fracturing occurs via progressive inter particle bond breakage. Solutions using the discrete element method allow dynamic stress waves to propagate through the particle assembly, which may exhibit slip or separation, with unlimited displacement, under the action of the applied loading. Bonded assemblies can exhibit complex macroscopic behaviors such as strain softening, dilation, and fracture that arise from extensive micro cracking at the contacts.

PFC<sup>2D</sup> is an ideal research tool, because it provides a powerful and flexible simulation environment within which one can create instances of different synthetic materials, subject them to general loadings, and observe their behavior. In addition to modeling bulk flow and mixing of materials, the codes are also well-suited to support

fundamental studies of micro- and macro cracking in solid bodies including damage accumulation leading to fracture, dynamic breakage and seismic response.

Some of the salient features of PFC<sup>2D</sup> are as follows:

- A model consisting of any number of particles may be simulated on a computer with the appropriate amount of RAM by using PFC<sup>2D</sup>
- Built-in programming language (*FISH*) provides full access to internal state variables and allows one to customize analyses
- Explicit solution scheme provides a stable solution for unstable physical processes and makes it possible to simulate the non-linear interaction of a large number of particles without excessive memory requirements or the need for an iterative procedure
- Built-in damping for optimal static convergence; damping can be adjusted for dynamic simulations
- Linear or nonlinear contact model with frictional sliding in both models
- Two forms of bonding at contacts; bonds have finite strengths in tension and shear
- Particle generator can be coded to produce specified distribution of radii (uniform or well graded) within generation region
- Walls, composed of multiple linear segments (2D) can be used to impose velocity boundary conditions upon the particles

- Measurements of average stress, strain rate and porosity can be made over any number of specified circular regions

## 4.2 Background And Overview

PFC<sup>2D</sup> models the movement and interaction of circular particles by the discrete element method (DEM), as described by Cundall and Strack (1979). The original application of this method was as a tool to perform research into the behavior of granular material; representative elements containing several hundred particles were tested numerically. The particle model was used to understand element behavior (in which conditions are “uniform”), and a continuum method was used to solve real problems that involve complicated deformation patterns (with the element behavior derived from the particle-model tests). Two factors have brought about a change in this approach. First, the task of deriving general constitutive laws from test results on particle assemblies is difficult. Second, with the spectacular increase in power of small computers, it is now possible to model entire problems with particles; the constitutive behavior is built into the model automatically. PFC<sup>2D</sup> is designed to be an efficient tool to model complicated problems in *solid mechanics* and *granular flow of “particles”*.

A physical problem that is concerned with the movement and interaction of circular particles may be modeled directly by PFC<sup>2D</sup>. It is also possible to create particles of arbitrary shape by attaching two or more particles together, such that each group of particles acts as an autonomous object using the clump logic. PFC<sup>2D</sup> is also able to model a brittle solid, by bonding every particle to its neighbor; the resulting assembly can be regarded as a “solid” that has elastic properties and is capable of “fracturing” when bonds break in a progressive manner. PFC<sup>2D</sup> contains extensive logic to facilitate the modeling of solids as close packed assemblies of bonded particles, much of this logic has been implemented in the Augmented FishTank, a set of functions written in FISH, the PFC<sup>2D</sup> embedded language. The solid may be homogeneous, or it may be divided into a number of discrete regions or blocks.

PFC<sup>2D</sup> has three main advantages over other programming codes. First, it is potentially more efficient, since contact detection between circular objects is much simpler than contact detection between angular objects; second, there is essentially no limit to the magnitude of displacement that can be modeled; and third, it is possible for the blocks to break since they are composed of bonded particles. The drawback to modeling a blocky system with PFC<sup>2D</sup> is that block boundaries are not planar; in exchange for the advantages offered by PFC<sup>2D</sup>, the user must accept “bumpy” boundaries.

The specification of the geometry, properties and solution conditions is not so straightforward in PFC<sup>2D</sup> as in programs such as FLAC and UDEC (Itasca, 2002). For example, with a continuum program, a grid is created, initial stresses installed, and boundaries set as fixed or free.

Whereas, in a particle code such as PFC<sup>2D</sup>, *a compacted state cannot be pre-specified in general, since there is no unique way to pack a number of particles within a given volume*. A process analogous to physical compaction must be followed until the required porosity is obtained. The initial stress state cannot be specified independently of the initial packing since contact forces arise from the relative positions of particles. Finally, the setting of boundary conditions is more complicated than for a continuum program because the boundary does not consist of planar surfaces. Apart from all these shortcomings, there are practical procedures which can be used for making realistic models.

A further difficulty arises when it is required to match the behavior of a simulated material with a real material tested in the laboratory. To some extent, *this is a trial-and-error process, because there is no complete theory that can predict macroscopic behavior from microscopic properties and geometry*. However, guidelines are given that should help in the matching process (e.g., which factors influence some aspect of behavior and which do not). It should be realized that such modeling is difficult because it is exercising the limits of current knowledge; however, *by performing tests with*

*PFC<sup>2D</sup>, we stand to gain some fundamental understanding in granular material mechanics.*

The calculation method (DEM) is a time-stepping, explicit scheme, which is described in more detail in Section 3.2.1. There are several advantages to such a scheme. Systems that exhibit physical instability may be modeled without numerical difficulty. Large populations of particles require only modest sizes of computer memory, since matrices are never stored. PFC<sup>2D</sup> may be used to model static or dynamic problems, but the full dynamic equations of motion are solved even when static solutions are required. This is done in order to follow such phenomena as failure and “flow” of material in a realistic manner; it is not necessary to invoke some nonphysical algorithm, as done in some implicit methods. Modeling with PFC<sup>2D</sup> involves the execution of many thousands of time-steps. At each step, Newton’s second law (force = mass × acceleration) is integrated twice for each particle to provide updated velocities and new positions, given a set of contact forces acting on the particle. Based on these new particle positions, contact forces are derived from the relative displacements of pairs of particles; a linear or nonlinear force/displacement law at contacts may be used.

The current version of PFC<sup>2D</sup> operates on most computers running Windows and other operating systems. Table 4.1 summarizes the approximate number of particles that can be created for different sizes of Random Access Memory (RAM). Note that this is approximately a linear relation. However, *more RAM is required when contacts are formed between particles.*

A parallel-processing option is available, whereby a simulation may be split between several processors, connected by a network. PFC<sup>2D</sup> operates, by default, in a command-driven mode; a graphical, menu-driven mode also exists for file-handling, plotting and print redirection. In either mode, there are graphics facilities in PFC<sup>2D</sup> that allow high-resolution, color-rendered plots to be generated rapidly. The graphics displays allow the user to view the model during creation or at any stage during a run. The model can be translated and magnified on the screen for optimum viewing. Plots may be made

of the particles, walls, contacts, forces, displacements, velocities and other quantities. All plotted output can be directed to a black-and-white or color output device, to the Windows clipboard, or to a file (in PostScript and various bitmap formats).

### **4.3 Components of a PFC<sup>2D</sup> Model**

A PFC<sup>2D</sup> model is constructed of circular particles (or balls). The smallest possible model that can be analyzed with PFC<sup>2D</sup> consists of only one particle. Most problems, however, are defined by assemblies of hundreds or thousands of particles and often involve the compaction of these assemblies to a closely packed state.

If two balls are moved together so that they touch, then a point contact will be formed. Each ball in a PFC<sup>2D</sup> model can touch several other balls, and the number of contacts that form can change dynamically during a model calculation as the balls move.

Walls are used in PFC<sup>2D</sup> both to define boundaries of a model and assist with the generation and compaction of balls. Walls can be positioned to generate clusters of balls in different regions of the model and then be deleted after the generation phase is complete. Wall velocities can also be specified. The balls and walls interact with one another via the forces that arise at contacts. The equations of motion are satisfied for each ball; however, the equations of motion are not satisfied for each wall i.e., forces acting on a wall do not influence its motion. Instead, its motion is specified by the user and remains constant regardless of the contact forces acting upon it. Also, contacts may not form between two walls; thus, contacts are either ball-ball or ball-wall.

Balls are generated within a region of space defined by global coordinates. All ball centroids and contact points are located by their (x, y) position vector. Walls are defined by the global coordinates of the line segments that comprise the wall. Each ball and wall is also identified by an identification (ID) number.

## 4.4 General Features

PFC<sup>2D</sup> models the dynamic behavior of assemblies of arbitrarily-sized circular particles. A particle generator allows the statistical generation of specified distributions of particles to be done automatically. Particle radii may distribute uniformly or according to a Gaussian distribution. Typically, initial porosity is high, but dense packing may be achieved by a controlled expansion of particle radii or, if the radius is to be kept constant, by a self readjusting algorithm which determines the number of particles required to achieve a certain porosity value. Radii may be changed by any factor at any stage, so that it is possible to achieve a compacted state of prescribed porosity without much trial and error. Properties are associated with individual particles or contacts, rather than with “type numbers.” Hence, continuous gradations in properties and radii may be prescribed. A “joint generator” is provided that modifies the properties of contacts that lie along the track of a prescribed set of lines, which are assumed to be superimposed on the particle assembly. In this way, the model may be traversed by sets of weak planes (corresponding, for example, to rock joints). The plotted color of a particle is also regarded as a property, so various marking schemes may be specified by the user. To ensure long-term freedom from numerical drift in PFC<sup>2D</sup> model’s coordinates and radii are stored in double precision. Relative displacements at contacts are computed directly from coordinates, not from incremental displacements. The contact physics consists of the following elements:

- linear springs, or simplified Hertz-Mindlin law;
- Coulomb sliding; and
- optional bonding. (Bonded contacts may carry tension, and the bonds have finite strengths in tension and shear. Two types of bonds, a contact bond and a parallel bond, may be installed at particle-particle contacts. These two types of bonds correspond to two physical possibilities: (1) contact bonds reproduce the effect of adhesion acting over the vanishingly small area of the contact point, thus the name contact bond; and (2) parallel bonds reproduce the effect of additional material (e.g., cementation) deposited after the balls are in contact.



The effective stiffness of this additional material acts in parallel with the contact point stiffness, thus the name parallel bond.)

The generality of the code has been enhanced by the clump logic, which supports the creation of groups of slaved particles or clumps. Particles within a clump may overlap to any extent, and each clump behaves as a rigid body with deformable boundaries and, thus, can serve as a super-particle of general shape. The assembly is loaded by prescribing wall velocities, a mixture of particle velocities and applied external forces, and/or gravity. The Augmented FishTank provides functions to install a specified stress field within the assembly, or apply stress boundary conditions to the assembly.

The timestep calculation is automatic and includes the effects of changing stiffnesses due to the Hertz contact model. The timestep also changes during a simulation according to the number of contacts around each particle and the instantaneous stiffness values. There is a cell-mapping scheme that uses an optimum number of cells, based on estimated particle count; it automatically adjusts the outer size of the cell space to accommodate escaping particles and/or new entities as they are specified. The cell-mapping scheme supports the contact-detection algorithm to ensure that solution time increases linearly with number of particles, rather than quadratically.

Any number of arbitrarily-oriented line segments may be specified as walls, each with its own set of contact properties. Special contact conditions are enforced at wall corners that are convex with respect to the wall's active side to maintain a single value of contact force as a particle rolls across such a peak. Wall velocities (both translational and rotational) may be specified and resultant forces and moments acting upon each wall can be monitored.

Particles and walls may be created or deleted (and their properties may be modified) at any time during a simulation.

Local non-viscous damping is provided (similar to that in FLAC). This form of damping has the following advantages:

- body forces approach zero for steady motion (only accelerating motion is damped);
- the damping constant is non-dimensional; and
- regions of the assembly with different natural periods are damped equally, using the same damping constant, since damping is frequency-independent.

Density scaling may be used to increase the timestep and to optimize solution efficiency. Gravity forces are unaffected by density scaling.

Energy tracing may be activated. The following energy terms are traced:

- body work (total accumulated work done by all body forces on the assembly);
- bond energy (total strain energy of the assembly stored in parallel bonds);
- boundary work (total accumulated work done by all walls on the assembly);
- frictional work (total energy dissipated by frictional sliding at all contacts);
- kinetic energy (total kinetic energy of all particles); and
- strain energy (total strain energy of the entire assembly stored at all contacts).

The facility exists to measure the following quantities over any number of arbitrary circular areas within the particle assembly:

- all components of the average stress and average strain-rate tensor
- the porosity
- the coordination number (average number of contacts per particle)
- the fraction of contacts that are sliding.

Any quantity may be tracked with time and stored as a history. Stored histories may be plotted, dumped to the screen, or sent to a file in a form that can be processed by other programs (such as spreadsheets).

PFC<sup>2D</sup> may be operated in quasi-static mode (ensuring rapid convergence to a steady-state solution) or in fully dynamic mode.

PFC<sup>2D</sup> has a save/restore facility; all data are saved, including accumulated histories.

PFC<sup>2D</sup> contains the powerful built-in programming language FISH, which enables the user to define new variables and functions. FISH offers a unique capability to users who wish to tailor analyses to suit their specific needs. For example, FISH functions can be created to perform the following operations:

- specify user-prescribed property variations in the model (e.g., nonlinear variation in contact stiffness across a model);
- plot and print user-defined variables (i.e., custom-designed plots);
- servo-control numerical tests;
- specify unusual boundary conditions;
- automate parameter studies;
- create or delete particles according to some user-defined algorithm;
- create groups of particles that are packed in some desired way; and
- write and read files either (a) in ASCII (to permit data exchange with non-Itasca codes), or (b) in binary (to exchange data with other Itasca codes that also contain FISH).

PFC<sup>2D</sup> has been compiled as a native Windows executable program using the WIN32 API to support execution under Windows and other operating systems. The program has the look and feel of a typical Windows program. However, most modeling operations are performed in the command-driven mode, while the graphical user interface

supports file-handling, model and response visualization (plotting), and printing (using the standard Windows file-handling and printing facilities).

#### **4.5 Fields of Application**

Some possible uses of PFC<sup>2D</sup> are noted below. These applications exploit the ability of the program to model the interaction of many discrete objects, the large-strain capability (actually unlimited motion and/or separation), or the ability to treat the process of fracturing as the progressive breaking of discrete bonds:

- bulk flow of material in chutes, pipes, bins and silos
- mine caving: fracture, collapse, fragmentation and flow of rock blocks
- compaction of powder in molds
- impact of objects composed of bonded particles: dynamic breakage
- seismic response and collapse of structures composed of beams represented by arrays of bonded particles
- *fundamental studies of granular materials: yield, flow, volume changes, etc.*
- fundamental studies of solids, represented by bonded assemblies of particles: damage accumulation, fracture and acoustic emission

#### **4.6 Mechanics of Using PFC<sup>2D</sup>**

PFC<sup>2D</sup> utilizes a command-driven format. Word commands control the operation of the program. In order to set up a model to run a simulation with PFC<sup>2D</sup>, three fundamental components of a problem must be specified:

- (1) an assembly of particles;
- (2) contact behavior and material properties; and
- (3) boundary and initial conditions.

The particle assembly consists of the locations and size distribution of particles. The contact behavior and associated material properties dictate the type of response the model will display upon disturbance (e.g., deformation response due to penetration of cone). Boundary and initial conditions define the in-situ state (i.e., the condition before a change or disturbance in problem state is introduced).

After these conditions are defined in PFC<sup>2D</sup>, the initial equilibrium state is calculated for the model. An alteration is then made (e.g., change the rate of penetration of cone or change boundary conditions), and the resulting response of the model is calculated. The actual solution of the problem is different for an explicit discrete element program like PFC<sup>2D</sup> than it is for conventional implicit-solution programs. PFC<sup>2D</sup> uses an explicit time-marching method to solve the algebraic equations. The solution is reached after a series of computational steps. In PFC<sup>2D</sup>, the number of steps required to reach a solution can be controlled automatically by the code or manually by the user. However, the user ultimately must determine if the number of steps is sufficient to reach the solved state. The general solution procedure, illustrated in Figure 4.1, is convenient because it represents the sequence of processes that occurs in the physical environment.

#### **4.7 Main Working Steps Involved in the Computer Code (PFC<sup>2D</sup>):**

Discrete element method programs like PFC<sup>2D</sup> generally do three major tasks. The first task is to determine particle contacts. The other two tasks are to perform the calculation cycle based on the application of two basic governing equations: the force-displacement law to each contact and Newton's second law to particles. After these calculations, the information (including location, displacement, velocities, etc.) for each particle is revised, forces calculated and thus the computer can display graphical results.

##### **4.7.1 Particle Contact Detection:**

The algorithm for contact detection used by PFC<sup>2D</sup> is very simple. It updates contacts that are already in the contact list from the previous time-step. If the contact does

not occur at the current time-step, it simply deletes the contact information from the contact list. Then, it detects the new contact that can initially occur at the current time-step. The position of one particle is checked against the position of every other particle in the assembly. If it finds that there is a contact and it is not in the contact list yet, it creates the new record for this new contact. The contact information is stored to be used later. Flow charts for these steps are shown in the Figures 4.2 and 4.3.

#### **4.7.2 Application of Force-Displacement Law:**

A flow chart for calculating the contact forces is shown in Figure 4.4. After PFC<sup>2D</sup> has updated the contact list, it can calculate the contact force. The force-displacement law is applied to each contact including contact damping and, the Coulomb frictional law.

#### **4.7.3 Application of Newton's Law of Motion:**

All resultant forces and moments acting on the particle are summed, and then the movement of the particle can be found by the application of Newton's second law of motion. Figure 4.5 shows the flow chart of applying the law of motion. Acceleration, velocity, and position of all particles are initially computed by the law of motion, as well as angular acceleration, and angular velocity. However, if the particle is in contact with the boundary, the friction force will be considered. This friction will be acting against the motion of the particle, changing its velocity. Again, Coulomb frictional law is used to calculate the friction force on the boundary. If the tangential force acting on the particle is greater than the maximum possible value of shear force; the particle will then slip along the boundary under a slip condition.

#### **4.7.4 Creation of Graphical Results**

At the end of every calculation cycle, the discrete element method will give the solution in terms of the movement of the granular particles and the inter-particle forces

acting at the contacts. The main focus of this simulation is the estimation of total vertical force acted on the penetrating cone by the particles in contact. Each particle in the assembly is located by the position of its center. Based on this information, PFC<sup>2D</sup> can plot each particle as the circular- shaped object and the cone as a solid line and show it on the monitor. Figure 4.6 shows one of the graphical results obtained from PFC<sup>2D</sup>.

#### 4.8 Limitations of PFC<sup>2D</sup> Modeling

There are certain limitations inherent in using a two-dimensional code like PFC<sup>2D</sup> to model physical phenomena which are three dimensional in nature. These limitations must be kept in mind when formulating PFC<sup>2D</sup> models and interpreting results.

A PFC<sup>2D</sup> model consists of a two-dimensional collection of circular particles. The PFC<sup>2D</sup> “world” is two dimensional in nature.

Hence, only two **force** components and one **moment** component exist in a PFC<sup>2D</sup> model, as opposed to the three force components and three moment components that exist in a three-dimensional particle assembly). The out-of-plane force component and the two in-plane moment components are not considered in any way in the equations of motion or in the force-displacement laws.

Therefore, the question of exactly what, in a three-dimensional sense, is being simulated in a PFC<sup>2D</sup> model is a matter of interpretation. For example, we might consider the PFC<sup>2D</sup> model to be simulating a collection of variable-radius cylinders or, alternatively, we might consider the PFC<sup>2D</sup> model to be simulating a collection of variable-radius spheres whose centroids all lie in the same plane. The choice affects the mass and inertial properties of all balls.

**Stress and strain**, as continuous variables, do not exist at each point in a particle assembly, because the medium is discontinuous. Therefore, an averaging procedure is employed to compute average stress and strain-rate tensors within a user-defined

measurement circle. The averaging procedure for stress relates the two in-plane force components acting on each particle in the measurement circle to a force per unit length of particle boundary which must then be divided by a thickness value in order to obtain a stress quantity.

By default, the reported stress values utilize a **thickness of unity**, such that the values can easily be scaled if a different thickness is desired. For example, scaling the stress values by the average particle diameter of the assembly allows us to interpret the stresses as those belonging to a collection of variable-radius spheres. The averaging procedure for strain rate involves no assumptions about out-of-plane thickness.

Most two-dimensional continuum-based codes determine three-dimensional elastic response by enforcing a condition of either plane stress or plane strain through the constitutive relations between stress and strain. A PFC<sup>2D</sup> model, however, enforces neither of these conditions. As mentioned above, the out-of-plane force component and stresses and strains are simply not considered in the equations of motion or in the force-displacement laws. Thus, the out-of-plane constraint necessary to enforce a state of plane strain is not present.

The **porosity** (relative density for soils in the real world) computed by PFC<sup>2D</sup> is an area-based calculation (ratio of total void area to total area), as opposed to the volume-based calculation (ratio of total void volume to total volume) used to define three-dimensional porosity. There is no clear relation between a two-dimensional porosity value and a three-dimensional porosity value for arbitrary assemblies of spherical particles. However, since porosity is a measure of particle packing, the following information about particle packing in 2D and 3D highlights and explains some of the differences.

Deresiewicz (1958) showed that the closest of all regular packings of uniform spheres in 3D has a porosity of 0.2595, while the closest of all regular packings of uniform circles in 2D has a porosity of 0.0931. In the absence of compressive forces



acting on the assembly, these are the theoretical lowest values of porosity obtainable without particle interpenetration. In general, there is more void space remaining in a 3D assembly than in a 2D assembly.

**In a real material, the porosities will be higher**, because the particles will have “locked-up” before reaching this optimal packing. If particle arching is known to occur in a real material, there are many more opportunities for arches to form in a 3D assembly than in a 2D assembly. Also, the PFC<sup>2D</sup> model assumes that the centroids of all particles are aligned on a single plane, an unlikely occurrence in a 3D assembly. Another difference between 2D and 3D assemblies relates to percolation. Small particles can easily percolate through a 3D assembly comprised of larger particles, but they can never percolate through a PFC<sup>2D</sup> model, regardless of relative particle sizes.

For situations in which particle packing has a significant influence upon behavior, it may be necessary to perform a small number of 3D simulations using the PFC<sup>3D</sup> code in order to establish the relevant parameters needed to obtain measured physical responses, and then use these parameters while performing a larger number of parameter studies using the PFC<sup>2D</sup> code.

The **mass** of each particle is determined by considering the particle to be either a sphere or a disk. The mass is assigned based on the density, radius, and disk thickness. The particle masses affect both the motion calculation (since the inertial properties differ for a disk and a sphere) and the gravity force applied to each particle.

There is one important distinction that should be recognized when applying PFC<sup>2D</sup>, as opposed to a continuum code, to a modeling situation. The fundamental element in PFC<sup>2D</sup> is a circular particle. If the physical problem is concerned with the movement and interaction of circular particles, then PFC<sup>2D</sup> may be applied directly.

In summary, if enough data of a high quality regarding material property are available, PFC<sup>2D</sup> can give good predictions.

Sr. No.	Available RAM (MB)	Approx. maximum number of particles*
1	10	10,000
2	48	50,000
3	98	100,000

Table 4.1: Maximum number of PFC<sup>2D</sup> particles in available RAM  
*\*Compacted state, assuming a reasonable packing density.  
 (Contacts require more memory than balls)*

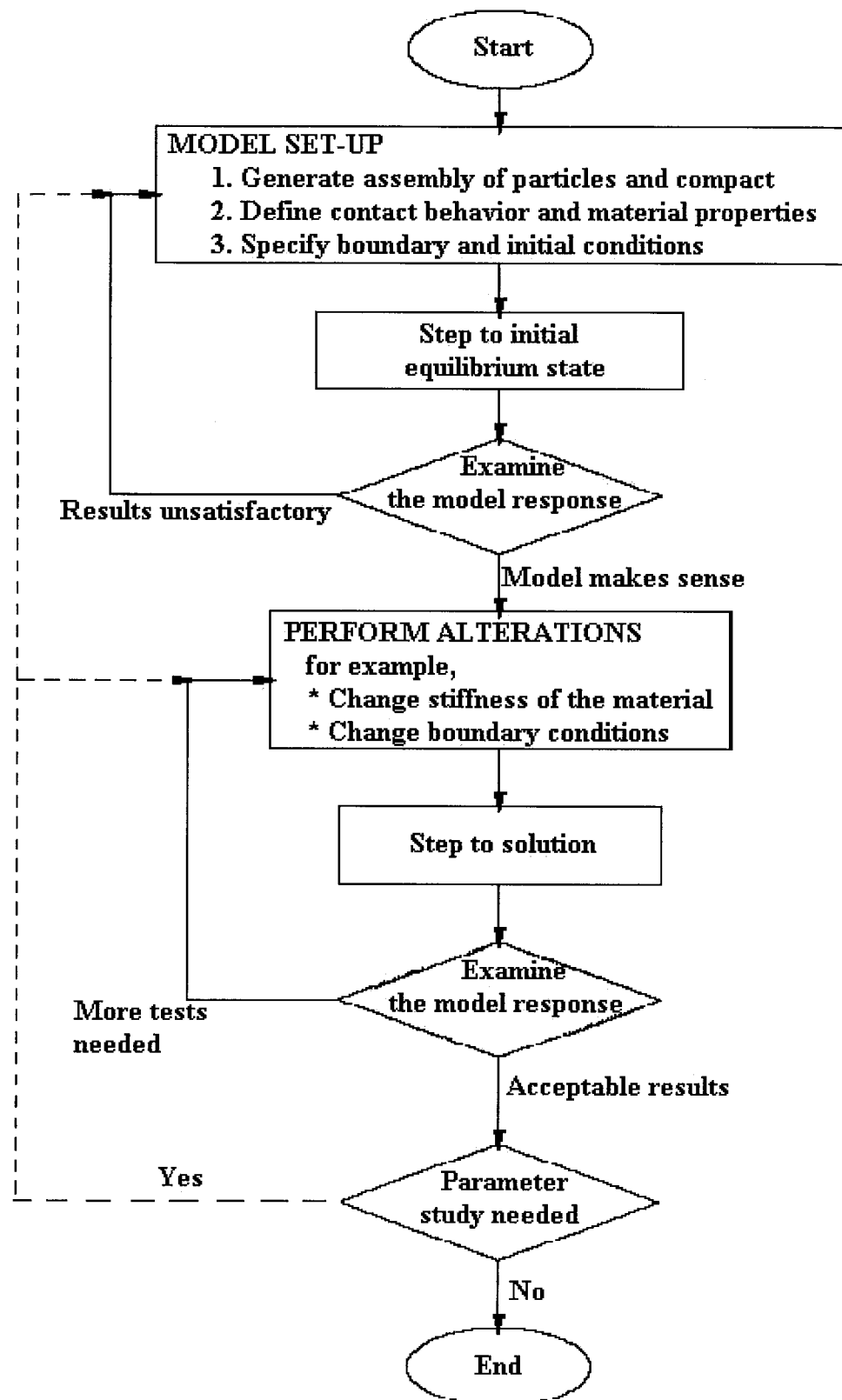


Figure 4.1: General solution procedure in PFC<sup>2D</sup> modeling.

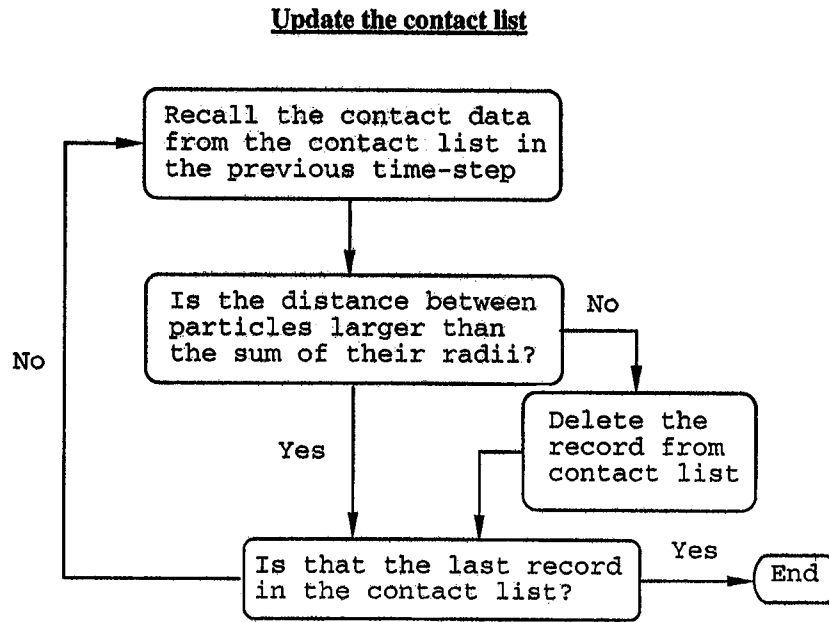


Figure 4.2: Flow chart for updating the contact list.

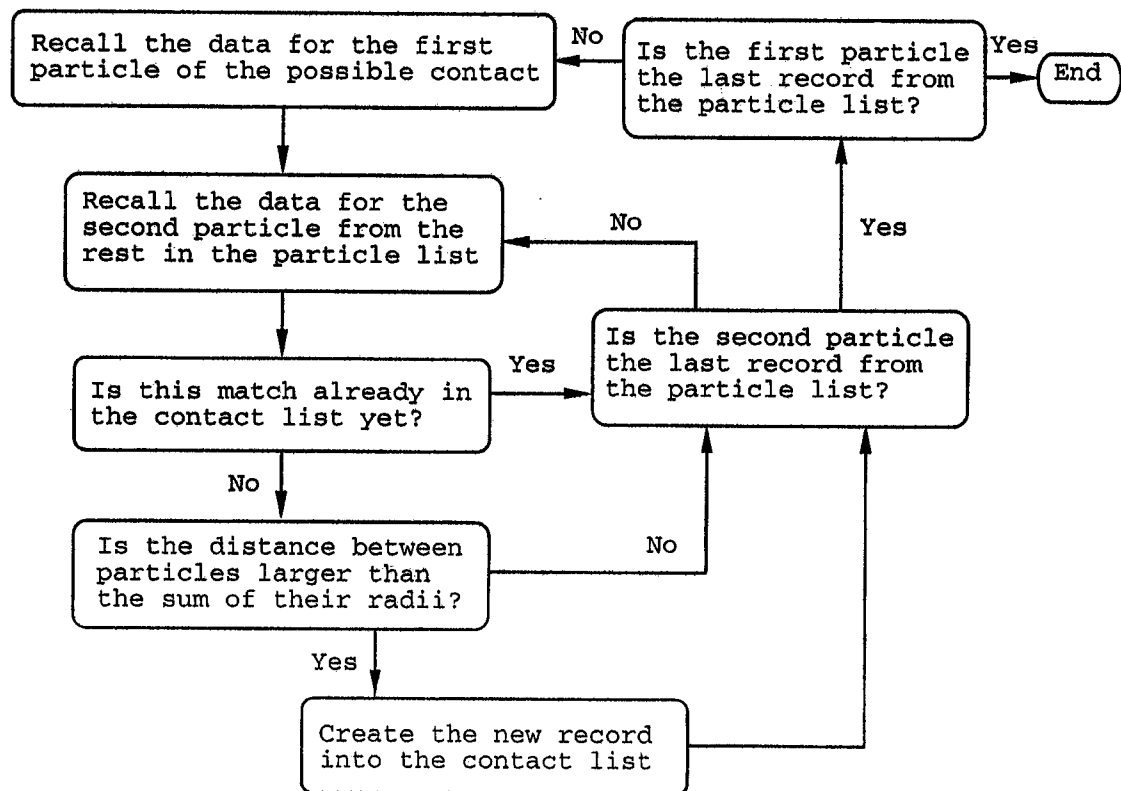


Figure 4.3: Flow chart for detecting the new possible contacts.

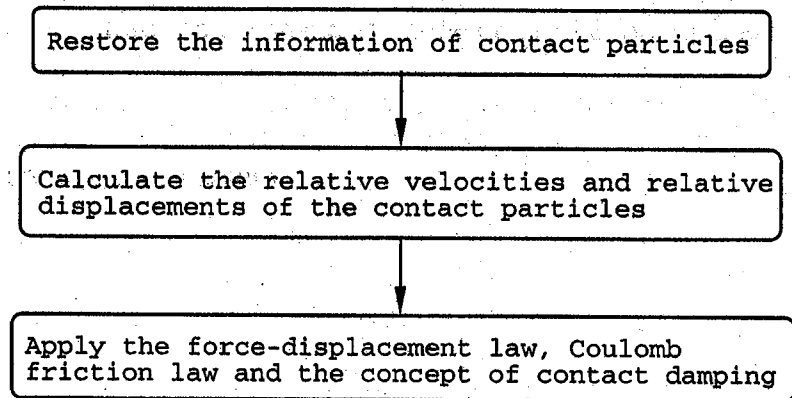


Figure 4.4: Flow chart for calculating the contact force.

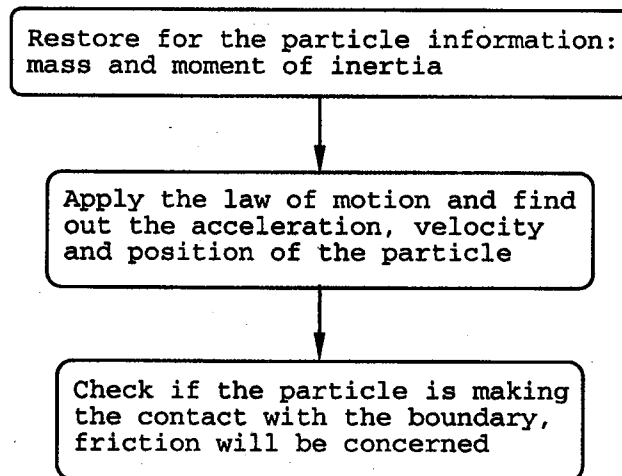


Figure 4.5: Flow chart for applying the law of motion.

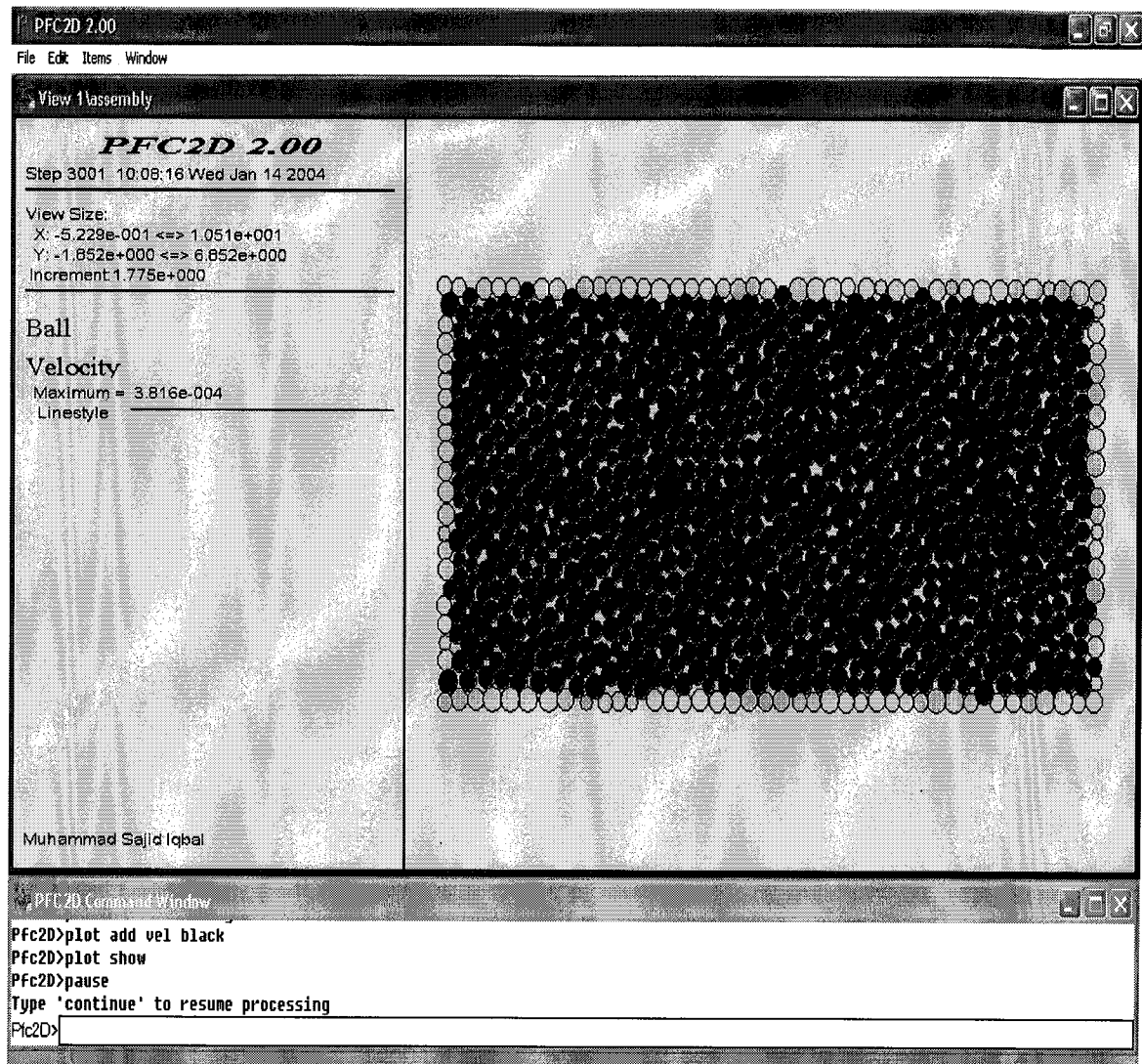


Figure 4.6: Graphical output from PFC<sup>2D</sup>. Notice the command window at the bottom.

## **5. SIMULATION OF CONE PENETRATION TESTING**

This chapter describes the methodology used to simulate cone penetration in granular material. The chamber / model characteristics are described first. Then the constitutive laws used for granular material i.e. the material properties are explained. Particle generation, stress field application, boundary conditions application and the cone penetration mechanism are then presented.

The discrete element modeling (DEM) software PFC<sup>2D</sup> version 3.0, Itasca Consulting (2002) was used for all the analysis involved in this study. As mentioned in Section 4.2, due to limitation of computer RAM capacity, the number of granular particles that could be considered had to be limited to so that the overall time required for numerical simulation run was not excessively long and that the system remains stable.

In general, the following steps were followed in this simulation study:

- Walls and particle generation
- Choice of contact model and material properties
- Boundary and initial stresses
- Loading, solution and sequential modeling
- Interpretation of results

### **5.1 Chamber Size and Characteristics**

Chamber size for this simulation model was considered in light of the discussion in Section 2.8. The larger chamber size relative to particle size will require more particles therefore the physical limits were restricted to 3.0 m in diameter and 1.5 m in height. The height of the model chosen for this study was kept at 1.5 m so as to avoid any effect on the measured cone tip resistance from either top or the bottom boundaries. The problem was evaluated as being symmetrical along the vertical y-axis; hence, the chamber size to be actually modeled was reduced to 1.5 m in radius and 1.5 m in height. Due to symmetry

in-plane about the vertical axis and considering unit width out-of-plane for the depth in the 3<sup>rd</sup> dimension, the symmetrical model and no stress and / or strain transfer condition in the 3<sup>rd</sup> dimension was used in order to reduce the number of particles. This assumption helped greatly in also reducing the run-time required for model simulations.

Figure 5.1 shows the general layout of the chamber / numerical model being modeled with the in-plane symmetrical section having a radius of 1.5 metres.

## **5.2 Constitutive Law for Granular Material:**

In the model analysis it was assumed that the granular material properties are the same as the average properties for a silica sand. Parameters required for analysis using DEM include the individual grain size of the particles,  $D_{100}$  (in this study, due to uniformly graded particles); density,  $\rho$ ; porosity,  $\eta$  (relative density in 3-D world); friction coefficient,  $\mu$ ; normal stiffness,  $k_n$  and shear stiffness  $k_s$ .

The parameters adopted in this model study have been referred to the parameters previously agreed upon by other researchers (Jenson and Bosscher, 1999; Potyondy, Cundall and Lee, 1996; Gourves, 1997; Lorig and Gibson, 1995) for discrete numerical (discontinuum) modeling of granular particles. The force, length and time units used in this study are Newton, metre and second, respectively. Therefore, the following units apply: particle size [mm], density [ $\text{kg/m}^3$ ], particle stiffness [N/m], parallel-bond strength [ $\text{N/m}^2$ ], parallel-bond stiffness [ $\text{N/m}^3$ ].

In the initial phase of the model study, several different grain diameters with uniform grading ( $D_{100}$ ) were considered ranging from 2 mm to 10 mm in size. Yet, as the study progressed and results were analyzed, a single grain size with 10 mm diameter was adopted for the remaining simulations. The main reason was that this larger particle size enabled the simulations to be carried out in less time and with less RAM capacity.



Table 5.1 summarizes the parameters used in this model study. Drained conditions have been assumed in this simulation study; so no pore pressure generation is considered. The density of the particles was taken at  $2000 \text{ kg/m}^3$ . Several desired values of two dimensional porosity (0.20, 0.18, 0.16, 0.12 and 0.10) were used in this model study to cover a wide range of three dimensional relative density (0.20 corresponding to relative density ( $D_r$ )  $\sim 50\%$  being the loosest possible state and 0.10 corresponding to  $D_r \sim 90\%$  being the most compact state). The particle friction coefficient was set at 0.5 which corresponds to a friction angle of  $30^\circ$ . In PFC<sup>2D</sup>, the normal components are related via secant stiffness, while the shear components are related via a tangent stiffness. A sensitivity analysis was carried out for the normal and shear stiffness values to be used. Values ranged from  $10^4$  to  $10^6 \text{ N/m}$ . The analysis showed lower contact forces generated for lower stiffness value but the difference was insignificant. Hence, the normal and shear stiffnesses of the granular assembly were considered to be  $10^6 \text{ N/m}$  which correspond to the stiffness values for a moderate compressible silica sand. The linear stiffness model: *“the forces and relative displacements are linearly related by the constant contact stiffness, which is a function of the intrinsic stiffnesses of the two contacting entities”* was used in this simulation study (PFC<sup>2D</sup> manual, Itasca Consulting, 2002).

### 5.3 Particle Generation and Application of Initial Field Conditions:

After configuring the chamber, the model was filled with granular particles by first generating individual grains of specified radius. Particle generation was achieved using a random generation algorithm which defines the initial location (local coordinates) of particles within the model boundaries. Ten trial runs were carried out to check whether there is any significant difference in the initial distribution scheme of generated particles. Only very small differences were recorded and the overall distribution of generated particles was considered essentially identical. Three sample graphical results for these trial runs showing generated assembly of particles are shown in the Appendix – B.

PFC<sup>2D</sup> treats relative density in terms of porosity (refer to Section 4.8). In the two dimensional PFC modeling, porosity is defined as the ratio of area occupied by voids to

the area of the model. Hence the smaller the value of porosity, the higher will be the relative density of the equivalent soil. Depending on the porosity value to be achieved, a specified number of particles in the given volume were generated by the algorithm. Measurement circles were drawn in the assembly to measure the average porosity over the entire assembly. It is important to note that *“the porosity measured within a measurement circle will differ from the target porosity because the porosity varies within the sample, and the target porosity includes voids near the walls, which are not accounted for by a measurement circle”* (PFC<sup>2D</sup> manual, Itasca Consulting, 2002). Figure 5.2 shows the configuration of generated particles in the model along with the measurement circles and the values of porosity obtained during the initial particle generation stage. Note that at this point PFC<sup>2D</sup> has assigned coordinates to each particle which will be used to compute contact and shear forces generated by the application of stresses (refer to Section 3.2.1).

Log files were generated during simulations to record the value of porosities obtained. These files were useful in providing a record of the PFC<sup>2D</sup> work session and also provided documentation for quality-assurance purposes.

After generation of the particles, numerical cycling was applied to the assembly so that the model can be brought to the desired state. Generally the following four steps were involved in the numerical cycling:

- First.** No contact friction – approximately 200 numerical cycles to achieve uniform particle arrangement.
- Second.** Apply contact friction and gravity loading – approximately 200 numerical cycles to achieve equilibrium in terms of mean unbalanced force.
- Third.** Apply boundary stresses – approximately 200 numerical cycles to achieve uniform stress state.
- Fourth.** Cone penetration mechanism – approximately 600 to 700 cycles (0.6 to 0.7 m of penetration) to achieve desired cone penetration.

In the first step, numerical cycling was applied to the model without any contact friction present, in order to achieve a uniform particle arrangement.

In the second step, contact friction was added and gravity loading (acceleration due to gravity,  $9.81 \text{ m/sec}^2$ ) is turned on and applied to the assembly so as to simulate the real field conditions. Contact forces develop between particles due to the application of contact friction and gravity loading. At this stage these forces may fluctuate wildly from point to point in the particle assembly. PFC<sup>2D</sup> determines the mean of all these contact unbalanced forces within the particle assembly and terms it as mean unbalanced force. In order to achieve equilibrium within the assembly, numerical cycling was applied. To check whether the system has reached equilibrium, mean unbalanced force was tracked. Figure 5.3 shows the plot of mean unbalanced force verses numerical cycling steps. The mean unbalanced force rapidly dropped in the first 100 numerical cycles and the asymptotic nature after 100 numerical cycles confirmed that the system under consideration was brought to equilibrium in about 200 numerical cycles. Figure 5.4 shows the assembly configuration at equilibrium after it has been cycled for 200 numerical steps. The compact state achieved corresponds to the minimum possible porosity value of 0.1 in PFC<sup>2D</sup> (Section 4.8). This porosity is the minimum possible achieved in this study. Hence it was considered equivalent to about 90 % relative density.

The *in-situ* stress is applied to the assembly in the third step. The overburden (boundary) stresses are applied to the model and numerical cycling is applied until the stress field inside the assembly reaches the *in-situ* stress level. The application of overburden stress is explained in the next section. The application of the stress field is an approximation only as in PFC<sup>2D</sup>, *unlike continuum codes; the concept of stress in discontinuum medium is different with no meaning to the term “stress at a point”, because forces may fluctuate wildly from point to point. In other words, the particle generation, boundary conditions and initial stress condition are all interrelated in discontinuum codes like PFC<sup>2D</sup>.* Even a slight change in one of these can change the entire configuration of the model. Hence this is a trial and error procedure at the best

(PFC<sup>2D</sup>). Measurement circles were drawn and average stress was measured to check the in-situ stress level during the simulations.

#### **5.4 Boundary Conditions and *In-situ* Stresses:**

The boundary stresses were applied on the top, bottom and one side of the chamber. The chamber consisted of four wall elements each having a contact stiffness of  $10^{12}$  N/m. The high stiffness assigned to the wall elements ensured that when particles come in contact with the wall, the wall acts as a rigid element that will not deform and therefore maintains the contact forces generated.

As discussed in Section 2.8 and Table 2.2, four different types of boundary conditions have been applied in calibration chamber studies and the numerical work by Ahmadi (2000, 2002 and 2004). The experimental observations as well as numerical analysis indicated that chamber to cone diameter ratios of about 112, 67 and 33.6 are required for dense, medium-dense and loose sands, respectively, to eliminate any possible boundary effects. Salgado et al. (1998) refers to boundary condition BC1 (i.e. constant vertical and horizontal stresses) as the one most suitable to be simulated using numerical models, for investigating chamber size effects based on his calibration chamber studies. Ahmadi (2004) refers to boundary condition BC3 (i.e. zero horizontal strain plus constant vertical stress) as the best boundary condition with the least affect on the measured cone resistance based on his numerical work and calibration chamber test results.

In this study only boundary conditions BC1 and BC3 (refer to Table 2.2) were studied and results compared with the work reported by Ahmadi (2004). The chamber / numerical model was considered under constant vertical and horizontal stresses in BC1 and constant vertical stress with zero horizontal strain in BC3. The top boundary stress represented the overburden stress at a given depth. The model was assumed to be at a depth of 5 to 10 m from the ground surface thus giving rise to approximately 100 kPa of effective overburden stress with the following assumption:

If soil is dry;	depth = 5 m;	effective stress = 100 kPa
If soil is saturated;	depth = 10 m;	effective stress = 100 kPa

Keeping a unit thickness of the model in the 3<sup>rd</sup> dimension (in to the paper) in mind and the model height is small compared to overall real field scenario, top and bottom overburden stresses were considered similar. The side boundary that simulated the centerline of the model (Figure 5.1) was considered having zero horizontal strain in both BC1 and BC3. The other side boundary either had constant horizontal stresses acting as far field stresses (BC1) or zero horizontal strain (BC3) depending on the boundary condition under consideration. Keeping  $k_0 = 0.50$ , (i.e. horizontal stress is half of vertical stress), a uniform average stress of 50 kPa was applied on the side boundary for the BC1 boundary condition.

For application of stresses in PFC<sup>2D</sup>, *it is not possible to apply forces directly on a wall*. Hence, rafts of balls having the same diameter as the granular particles in the assembly but with higher stiffness were created to simulate the presence of artificial boundaries at the top, bottom and/or side of chamber. The main purpose of the generation of these rafts was to apply forces to the balls that make up these rafts to simulate boundary stresses to the assembly. Balls in these rafts have a normal stiffness of  $10^{10}$  N/m, four orders of magnitude more than the granular material and with high parallel bond stiffness so as to act as a rigid entity and do not bend.

In the case of BC3, the top and bottom boundaries were simulated with these rafts. Top and bottom walls of the chamber were deleted after the generation of these raft boundaries and 100 kPa of overburden stress was simulated with the application of forces on the balls in these rafts. Due to the two dimensional limitation of the simulation, stresses were computed using a unit depth of the chamber. The force on the top and bottom raft boundaries came out to be 2000 N / ball. The side boundaries were simulated with zero horizontal strain by keeping the walls in place.

In the case of BC1, the top, bottom and one of the side boundaries were simulated with these rafts. Top, bottom and outer side walls of the chamber were deleted after the generation of these raft boundaries. On the top and bottom rafts, 100 kPa of overburden stress was simulated with the application of forces on the balls. Again, due to the two dimensional limitation of the simulation, stresses were computed using a unit depth of the chamber. The force on the top and bottom raft boundaries came out to be 2000 N / ball. The centerline side boundary was simulated with zero horizontal strain by keeping the wall in place. The other side boundary was simulated with 50 kPa of horizontal far field stress ( $k_o = 0.50$ ) with the application of forces on the balls. The forces on the side raft boundary came out to be 1000 N / ball. Figure 5.5 shows the configuration of the assembly with the raft boundaries in place. A close up view of the stress distribution from top as well as the side raft boundary to the assembly is also included.

## **5.5 Cone Penetration Modeling Mechanism in Granular Material:**

In this section a brief explanation of the numerical procedure used to model the cone penetration mechanism is discussed.

In order to simulate the penetration mechanism, the granular material was assumed to be isotropic, uniformly graded, and a single sized particulate. The cone was represented by two rigid walls (symmetrical along vertical axis) having very high stiffness value  $10^{12}$  N/m (6 orders of magnitude more than the granular material used). The cone tip was represented with a wall at  $30^\circ$  angle from vertical and the sleeve and the rods with a vertical wall (Figure 5.6). The contact friction coefficient between cone (wall) and particle was considered zero. The cone walls were then applied the desired penetration velocity in terms of metres per numerical cycling steps in the downward direction. The penetration velocity was simulated keeping in mind that the critical time step required should be small enough so that the disturbance is local and the system remains stable. The velocity simulated to the cone was such that the cone at least attains 0.6 m to 0.8 m total penetration into the assembly so as to eliminate any possible effects due to the top and bottom boundary. Generally the critical time step was kept at 0.0001

seconds based on the minimum mass (10 mm particle) and highest normal stiffness value in the assembly (Sections 3.2.6 and 3.3.1).

The penetration of a cone into the granular material is tracked to determine the vertical and horizontal forces being applied by the granular material to the cone tip wall. The granular material located along the cone path is pushed away in a quasi-static manner that starts from the top of the model and continue to a desired depth into the material. This process simulates the penetration mechanism as the cone penetrates downward in the ground pushing the soil particles to the side horizontally as well as vertically. Figure 5.6 shows a close-up view of the cone geometry at an arbitrary depth along with the chamber configuration and the composition of the grains.

During penetration, the magnitude of stresses around the cone tip can become much greater than those far from the cone tip. Figure 5.7 shows a close up view of the contact forces developed around the cone during the penetration process. The thickness of the lines representing the contact forces is proportional to the magnitude of contact forces around and far from the cone tip. Although the response of sand is stress dependent and model parameters should be different in the near field and far field, but due to simplicity, the model parameters for the whole field were considered the same in this study. The vertical force (N) on the cone face is then converted to the cone tip resistance ( $\text{N/m}^2$ ) (considering unit thickness for the depth of the chamber) by dividing by the cone tip area ( $\text{m}^2$ ). Figure 5.8 shows a plot of the vertical force exerted by the particles on the cone tip during the penetration process versus penetration depth.

This modeling process mimics the penetration process in a realistic way. The penetration modeling starts at the top of the chamber and progresses into the assembly, and can end at any desired depth, meaning that the modeling process is simulating the cone moving downward and penetrating the soil. Figure 5.9 shows the full scale view of the chamber / numerical model with the location of the cone tip at an arbitrary depth. This figure also shows the various cone sizes used in this simulation study. In this study a grain size of 10 mm, chamber diameter of 3.0 m and cone diameters ranging from 200

mm to 5 mm were modeled. This gave a chamber / cone diameter ratio of 15 to 600 and a grain / cone diameter ratio of 0.05 to 2. The simulations were done with a constant chamber / grain diameter ratio of 300.

## **5.6 Interpretation of results:**

Because PFC<sup>2D</sup> models a nonlinear system of discrete particles as it evolves in time, the interpretation of results may be more difficult than with a conventional numerical code that produces a “**solution**” at the end of its calculation phase. Hence the results obtained by PFC<sup>2D</sup> should be interpreted carefully keeping all the limitations and assumptions in mind. Equilibrium in the assembly being modeled should be checked regularly by tracking the history of the mean unbalanced force. Also measurement circles are helpful in keeping track of the desired porosity and average stress tensors in the assembly. The velocity field should be checked regularly during simulation. A random velocity field of low magnitude is a good indicator of equilibrium in the assembly. Chapter 6 presents the results obtained from this study.



Sr. No.	Parameter description	Parameter value(s)
1	Material Type	Average Silica Sand
2	Density of Particles	2000 kg/m <sup>3</sup>
3	Porosity (2 Dimensional)	0.2, 0.18, 0.16, 0.12 and 0.10
4	Particle-Particle Contact Friction Coefficient	0.5
5	Particle-Cone (Wall) Contact Friction Coefficient	0.0
6	Particle Normal Stiffness	10 <sup>6</sup> N/m
7	Particle Shear Stiffness	10 <sup>6</sup> N/m
8	Parallel Bond Stiffness	10 <sup>10</sup> N/m <sup>3</sup>
9	Pore Pressure	No
10	Wall element stiffness	10 <sup>12</sup> N/m
11	Particle Size <ul style="list-style-type: none"> <li>• Uniformly graded (100 %)</li> <li>• Well graded (25 %)</li> <li>• Well graded (50 %)</li> <li>• Well graded (25 %)</li> </ul>	2 to 10 mm 10 to 15 mm 10 mm 5 to 10 mm

Table 5.1: Parameters used in PFC<sup>2D</sup> model.

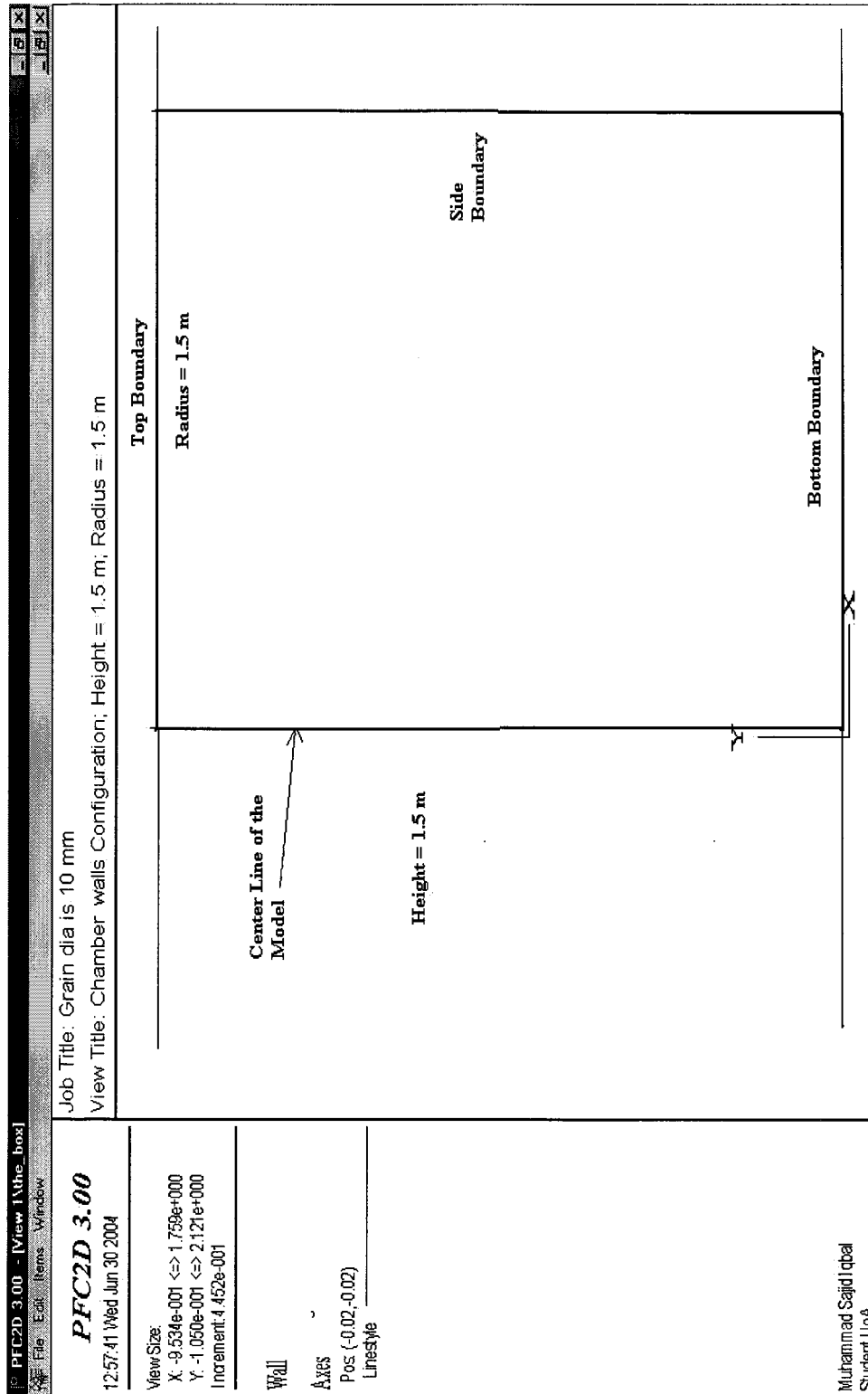


Figure 5.1: General layout of the model with symmetrical section along vertical axis having a radius of 1.5 metres.

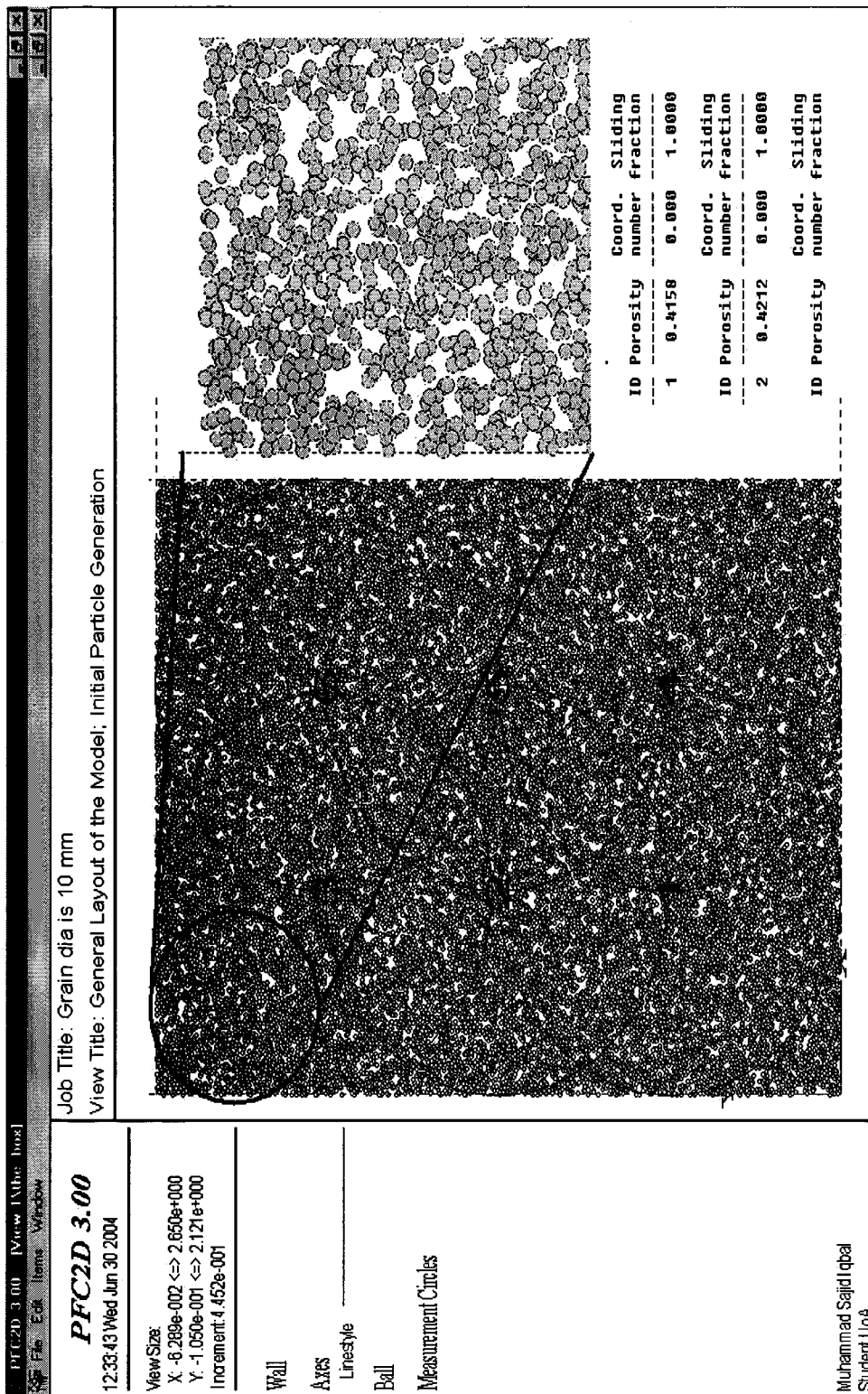


Figure 5.2: General layout of the model; Initial Particle Generation Phase along with 6 measurement circles.  
 Inset: A blown up view of generated particles in the initial stage. Initial measured porosity values by PFC<sup>2D</sup>.

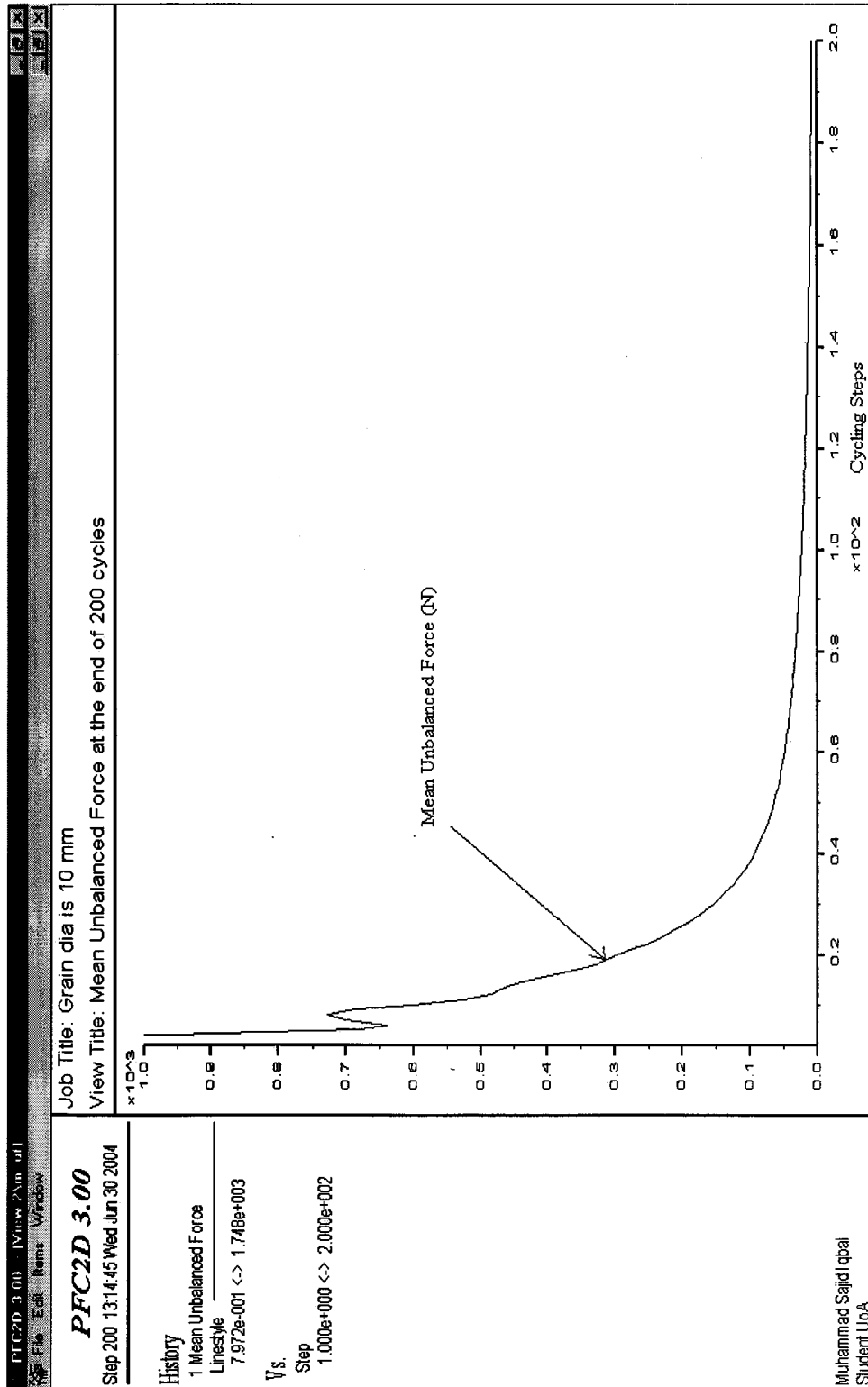


Figure 5.3: plot of mean unbalanced force versus cycling steps.

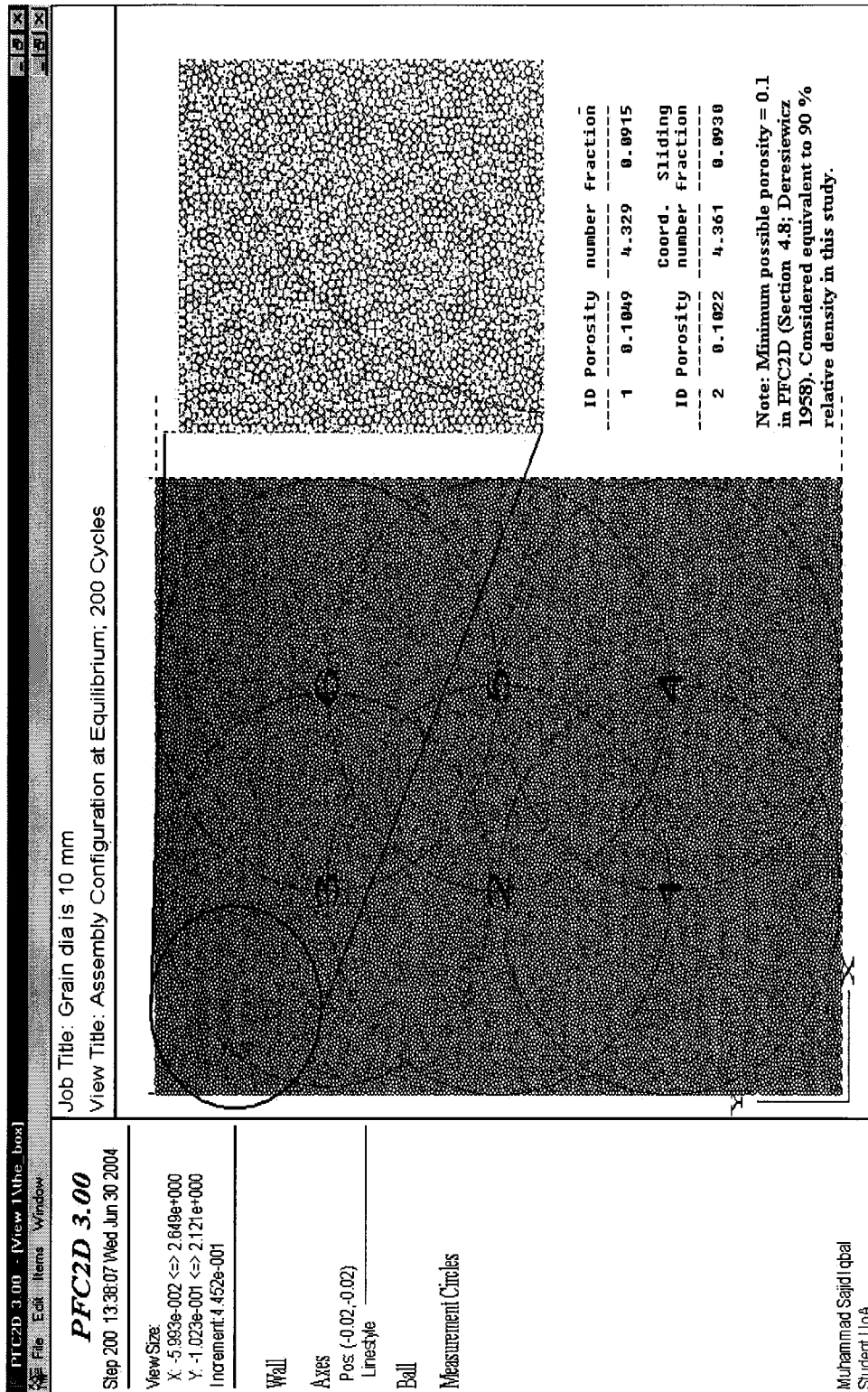


Figure 5.4: Assembly configuration at equilibrium after numerically cycled for 200 steps.

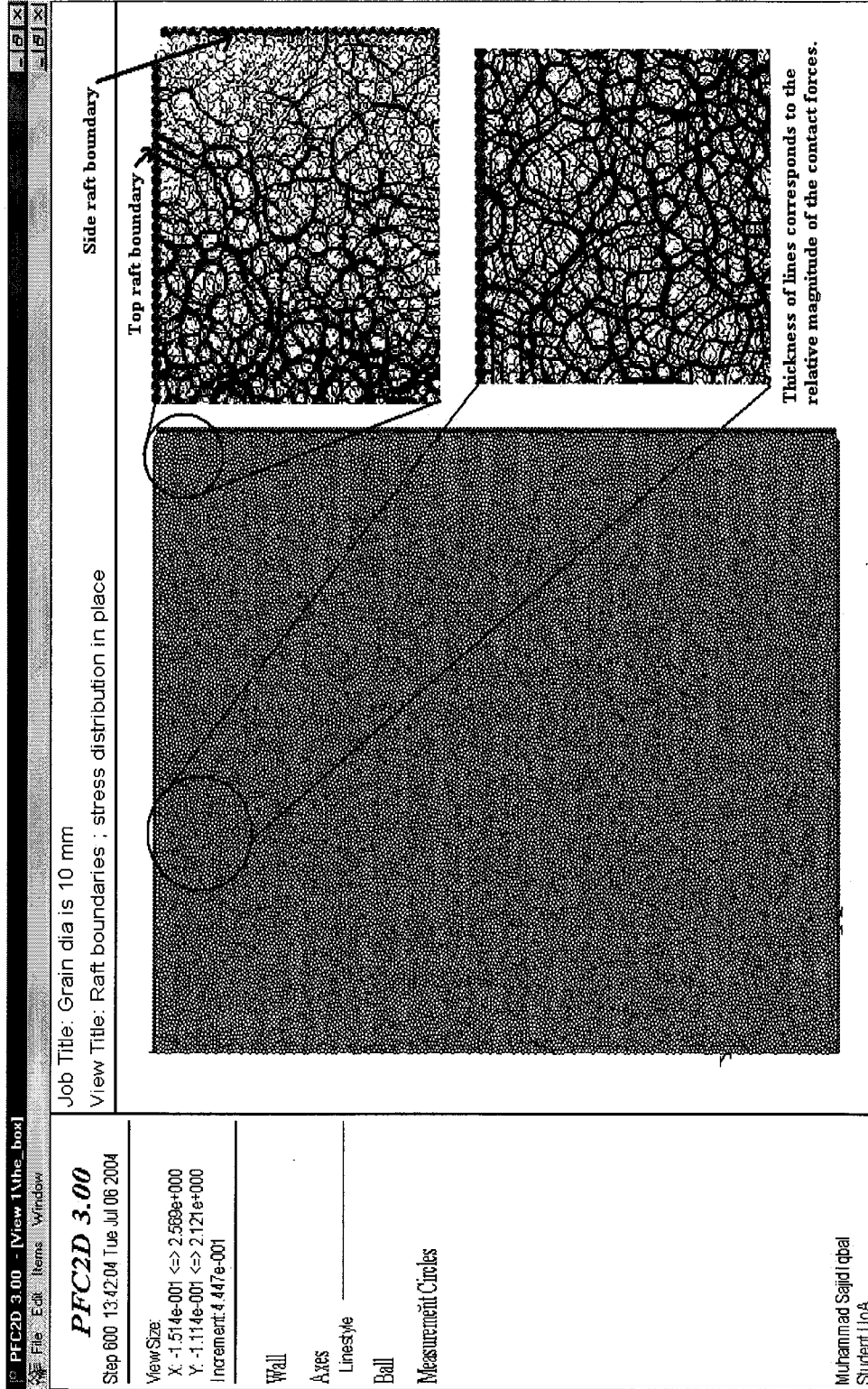


Figure 5.5: Configuration of the assembly with the raft boundaries in place. Close up views of the stress distribution from side raft and the top raft boundaries to the assembly are also included. Force was applied on each ball of the raft.

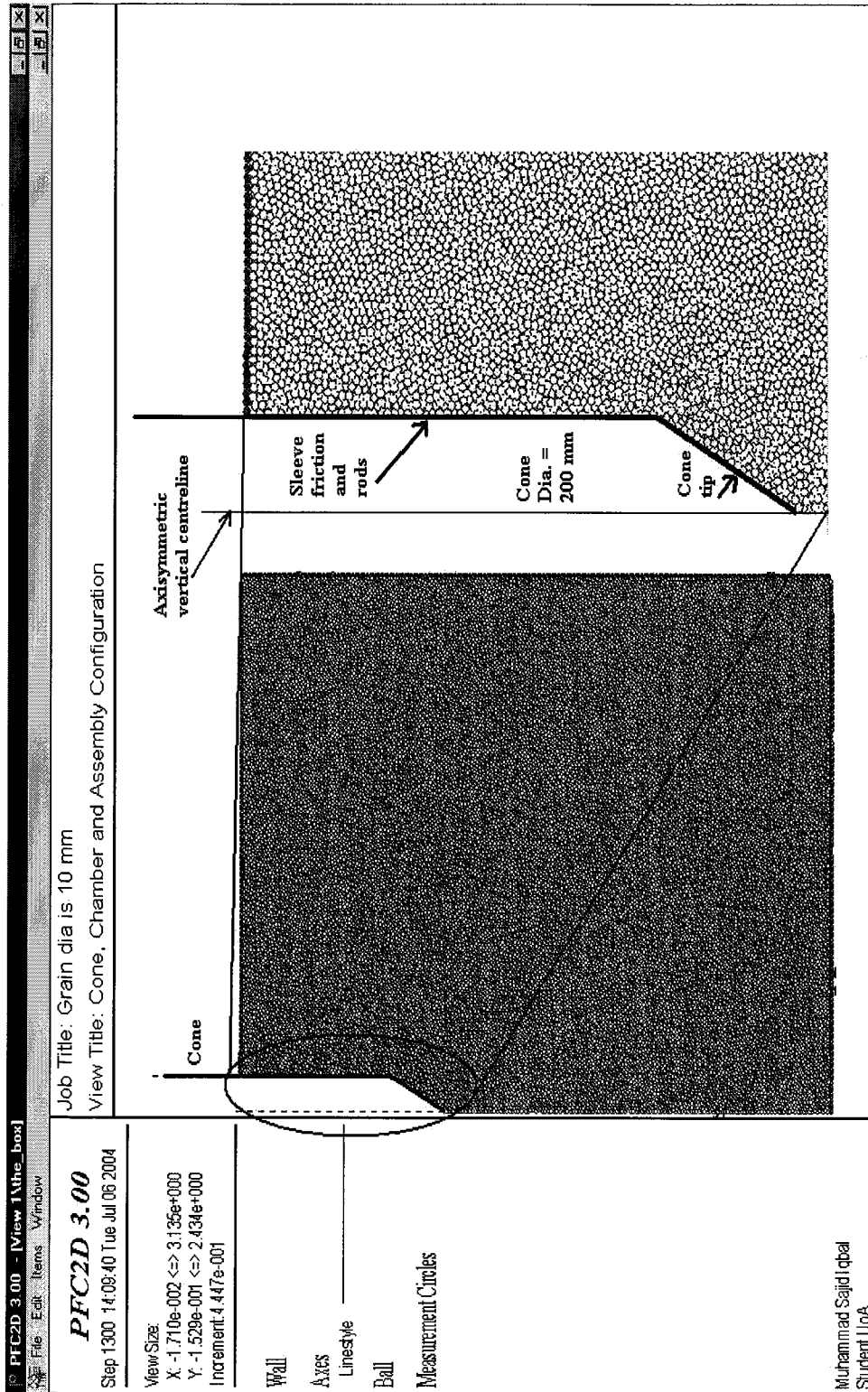


Figure 5.6: A close-up view of the cone geometry, chamber configuration and the grains composition.

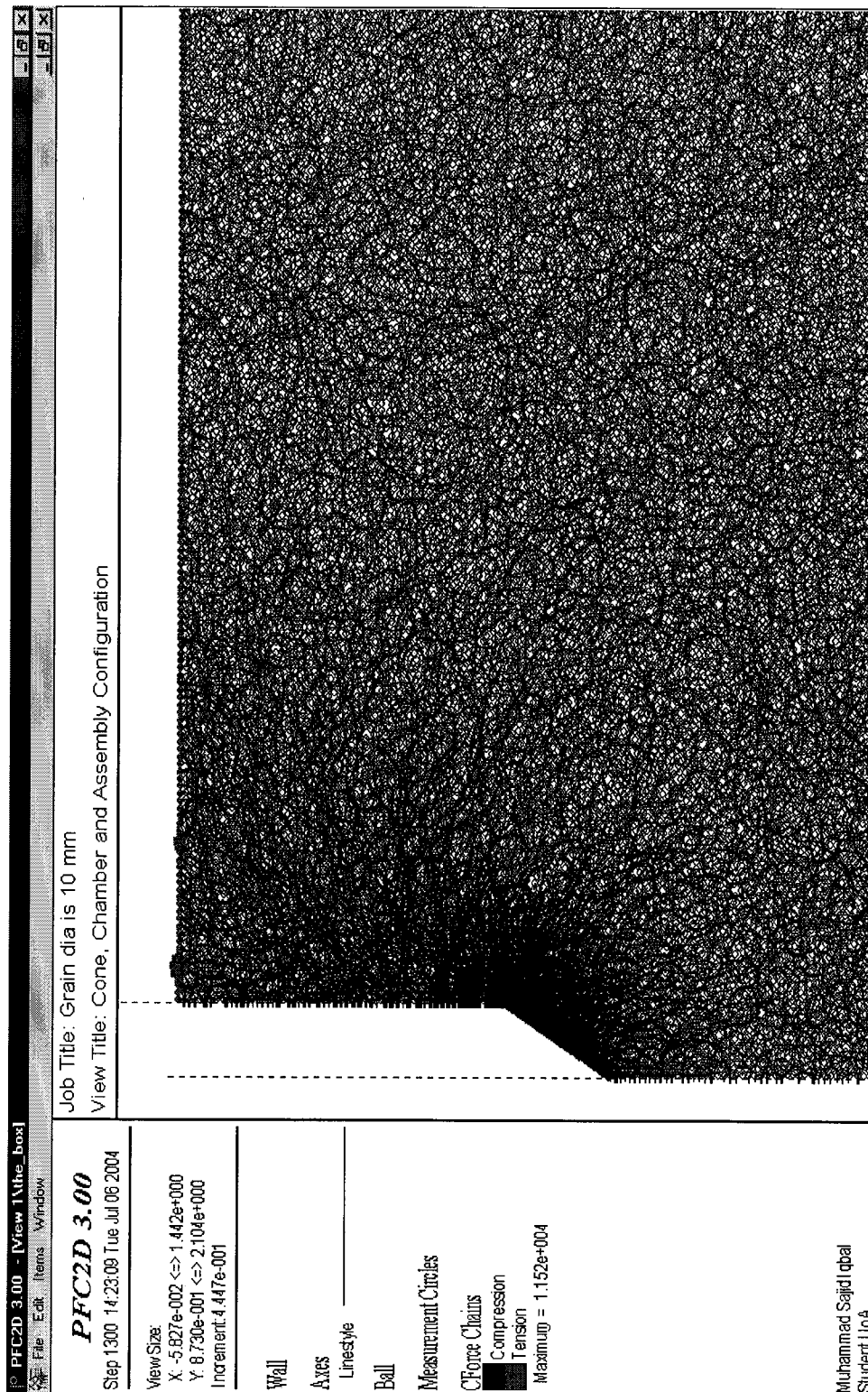


Figure 5.7: A close-up view of the contact forces developed around the cone during penetration process.



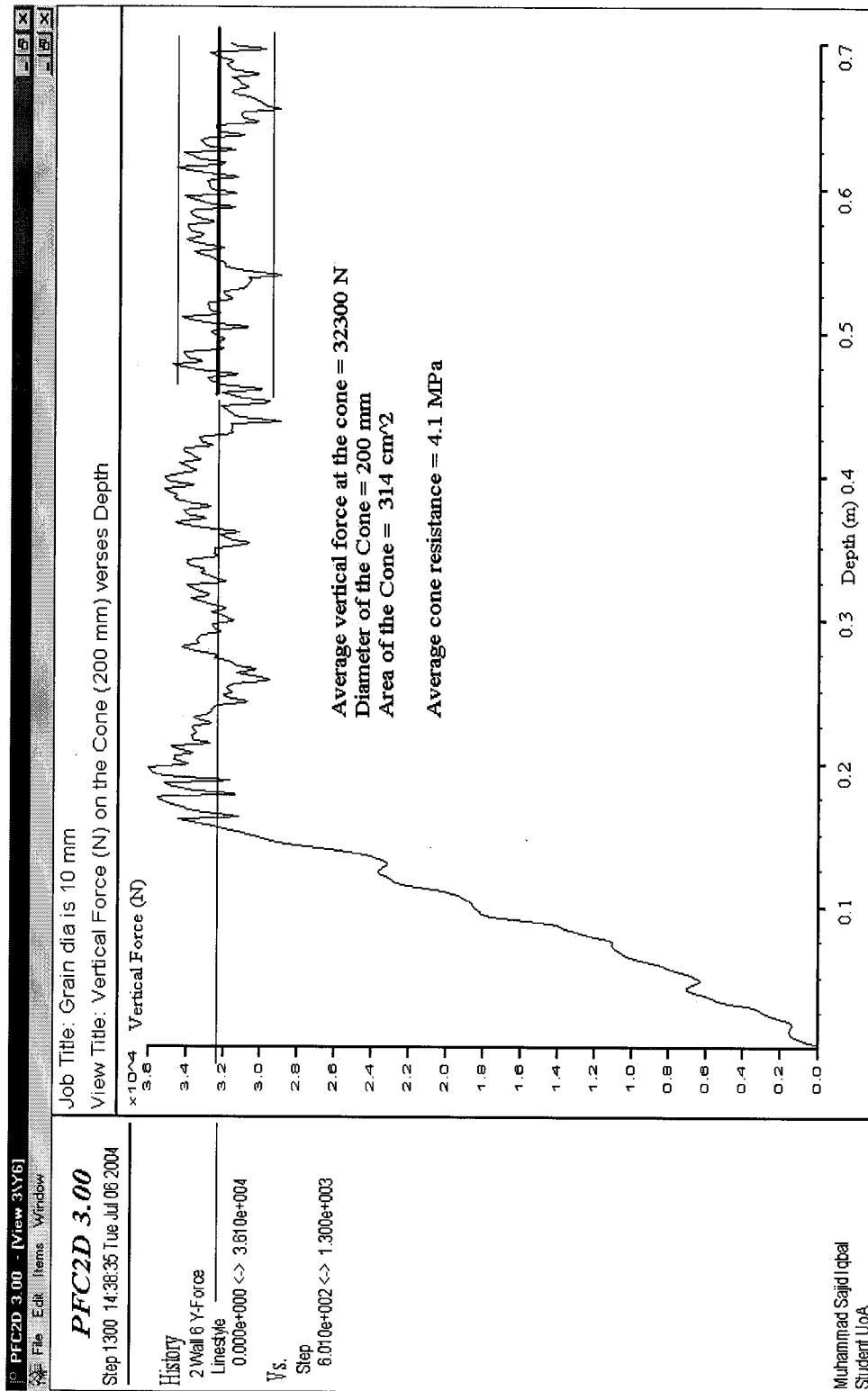


Figure 5.8: A plot of the vertical force exerted by the particles on the cone tip during penetration process versus penetration depth.

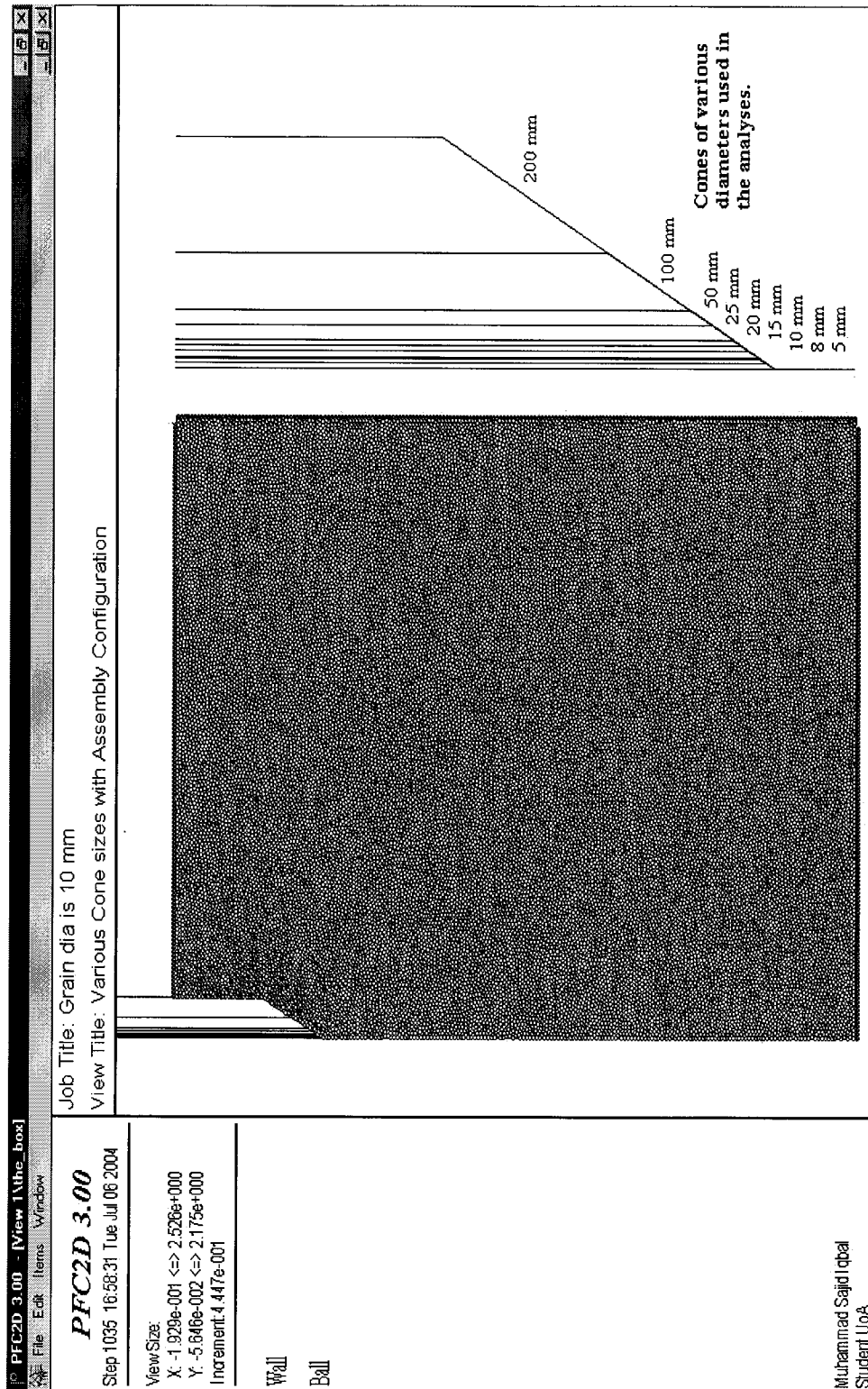


Figure 5.9: Full scale view of the chamber / numerical model with the location of the various cone tips at an arbitrary depth.

## 6 RESULTS AND DISCUSSION:

The standard cone (35.7 mm diameter) is generally used for sands, silts and clays. The grain sizes for these materials range from 0.001 mm to 2 mm. This gives a grain to cone diameter ratio of 0.00003 to 0.056. The results obtained using a standard cone with these grain to cone diameter ratios are well understood with the help of extensive field and laboratory data. However, when the standard cone is pushed into gravels, it is possible to meet **refusal** with very large measured tip resistance values. The medium gravel particle size generally ranges from 2 mm to 10 mm. This gives a grain to cone diameter ratio of 0.056 to 0.28. This range of grain to cone diameter ratio is the main focus of this research.

Large grain to cone diameter ratios can be achieved in PFC<sup>2D</sup> simulation in two ways: either (i) by keeping one cone size (i.e. 35.7 mm) and reducing the grain size, or (ii) by keeping a single grain size and reducing the cone diameter.

Although cones as small as 1 cm<sup>2</sup> (11.28 mm diameter) have been used in experimental research, they have only been used in fine grained soils. With numerical modeling such small size of cone with high stiffness can be modeled to penetrate into even gravel size particulate. Bending of cone rods is not a problem in numerical modeling and refusal in terms of rod deflection etc. will not be met if the cone can push into the particulate.

Previous calibration chamber testing / experimental studies done on sands such as Ticino sand have been carried out mostly with a chamber diameter of 1.2 m, cone diameter of 35.7 mm and with an average grain size ( $d_{50}$ ) of about 0.6 mm (Baldi et al. 1982, Lunne et al. 1997).

The three important ratios in term of chamber size, cone size and grain size for these studies were as follows:

- Chamber to cone diameter ratio = 33
- Chamber to grain diameter ratio = 2000
- Grain to cone diameter ratio = 0.016

These calibration chambers were of finite and often limited size due to cost and time limitations. Hence a specific size of sand along with chamber size and cone size were considered in these experimental studies. The effect of chamber dimensions on the cone tip resistance was studied by some researchers and corrections were proposed to get tip resistance for matching field values (Parkin and Lunne, 1982; Lunne and Christophersen, 1983; Jamiolkowski et al., 1985; Mayne and Kulhawy, 1992 and Salgado et al., 1998).

To study the effect of chamber size and boundary effects on CPT tip resistance in sand, a numerical study was carried out by Ahmadi (2004) with a 35.7 mm diameter cone with different chamber diameters from 1.2 m to 4 m in width. Ahmadi (2004) used a continuum approach and hence did not model a specific grain size. His results were independent of grain size. The three important ratios in term of chamber size, cone size and an assumed grain size of about 0.6 mm for the work done by Ahmadi (2004) were as follows:

- Chamber to cone diameter ratio = 33 to 112
- Chamber to grain diameter ratio = 2000 to 6666
- Grain to cone diameter ratio ~ 0.016 (approx.)

Ahmadi (2004) modeled four different boundary conditions as listed in Table 2.2. Ahmadi (2004) has shown that the effect of boundary conditions on measured cone resistance diminishes with increasing chamber to cone diameter ratio. Ahmadi (2004) modeled a vertical overburden stress of 70 kPa and horizontal stress of 35 kPa i.e.  $k_0 = 0.5$ . Ahmadi (2004) showed that for dense sand a chamber to cone diameter ratio should be more than about 110 to avoid boundary effects (Section 2.8; Figure 2.11).

During the initial phase of this study, to see if PFC<sup>2D</sup> could model the correct penetration mechanism and to achieve the above mentioned three ratios regarding chamber, cone and grain size, a 2 m diameter chamber, grain sizes of 10 mm, 7 mm, 5 mm and 2 mm and three different cone diameters 50 mm, 35.7 mm, 25 mm were modeled. The cone tip resistance was measured under a vertical overburden stress of 100 kPa and a zero horizontal strain at the lateral boundaries i.e. boundary condition (BC3). The values of two dimensional porosity (relative density in real world) were 0.20, 0.18, 0.16, 0.12 and 0.10. In this study, a porosity value of 0.20 was considered equivalent to about 50 % relative density whereas a value of 0.1 was regarded as 90 % relative density.

Figure 6.1 shows the cone tip resistance versus the grain to cone diameter ratio. In all cases it was observed that for a given grain size, smaller diameter cone gave higher cone resistance. This trend is shown by the solid lines drawn on Figure 6.1. This is synonymous to the case where a standard cone is used in gravels and gives high resistance measurements. These results are also in agreement with field work done by de Lima and Tumay (1991) as mentioned in Section 2.7. Also higher relative density produced higher cone resistance.

Yet, it was also observed that for a given cone size, when the grain size increased the cone tip resistance decreased as a general trend. This trend is shown by the broken (dashed) lines showing the range of cone tip resistance with increasing grain size for three different cone sizes in Figure 6.1. This appears to be an incorrect trend because the cone tip resistance should increase for a larger grain size when a single cone size is used. The various ratios regarding chamber, cone and grain size used were as follows:

- Chamber to cone diameter ratio = 40 to 80
- Chamber to grain diameter ratio = 200 to 1000
- Grain to cone diameter ratio = 0.04 to 0.4

The reason for this apparent incorrect trend was attributed to the chamber size effects as the chamber to cone diameter ratio was less than 110. As pointed out by

Ahmadi (2004) and the experimental chamber studies a chamber to cone diameter ratio of 110 or more is required to minimize the cone tip resistance being influenced by the chamber size for dense sands. To overcome this chamber size effects, a trial run was carried out to compare results with the work done by Ahmadi (2004).

The trial run was carried out with a grain diameter of 10 mm and chamber diameter of 3 m. This limited the chamber to grain diameter ratio to 300. This ratio is much less than the ratios used in the experimental studies and the numerical work by Ahmadi (2004) but this is considered to be also the least important ratio in terms of effect on cone tip resistance measurement. Also the grain size and chamber size were kept constant to limit the number of particles required and to acquire minimum possible time increments for the simulation (Section 5.1). The cone diameter was varied from 20 mm to 100 mm. The chamber to cone diameter ratio therefore varied between 150 and 30. The porosity of the sample was kept at 0.10 (~90 % relative density). Boundary conditions BC3 (constant vertical stress of 100 kPa and zero horizontal strain) and BC1 (constant vertical stress of 100 kPa and constant horizontal stress of 50 kPa, i.e.  $k_0 = 0.5$ ) were investigated. The forces applied on balls in the rafts were equivalent to approximately 2000 N per ball on top and bottom rafts and 1000 N per ball on the side raft.

Figure 6.2 shows the results obtained by this trial run for BC1 compared to results reported by Ahmadi (2004) for BC1. It was observed that the trend shown by the PFC<sup>2D</sup> under simulated boundary condition BC1 were in better agreement with the trend shown by Ahmadi (2004) for chamber to cone diameter ratios greater than about 110. However, the results did not match for chamber to cone diameter ratios less than about 110. Salgado et al. (1998) also refers to boundary condition BC1 as the one most suitable for numerical simulations to investigate chamber size effects.

Ahmadi (2004) validated his results with those of experimental chamber calibration testing. For Ticino sand with relative density of about 90 % ;  $k_0 = 0.45$ , normally consolidated and average effective overburden stress of 100 kPa, the cone tip resistance measured experimentally by calibration tests and afterwards corrected for

chamber effects is about 18 MPa (Baldi et al. 1986). The cone tip resistance (magnitude) measured in this trial run was slightly larger than 18 MPa when the chamber to cone diameter ratio was greater than 110. The trend for chamber to cone diameter ratios less than 110 was in general agreement to that of Ahmadi (2004). The trend shown by Ahmadi (2004) was extrapolated beyond chamber to cone diameter ratio of 110 and shows good agreement with the results of this study. Hence it was established that chamber size effects appear to diminish with a chamber to cone diameter ratio of 110 or more for dense granular assembly, using PFC<sup>2D</sup>.

The trend shown by results for BC3 in this study was not in general agreement to the trend presented by Ahmadi (2004) for BC3. Hence boundary condition BC3 was not considered for further analysis in this study and only the BC1 was adopted. The results for the trial run compared to results presented by Ahmadi (2004) for both BC1 and BC3 are shown in Appendix - C for reference.

The grain to cone diameter ratios modeled so far were in the range of 0.1 to 0.5. To further investigate the effect of coarser particle size on cone tip resistance, cones with even smaller size were modeled. Boundary condition BC1 with overburden stress of 100 kPa and horizontal stress of 50 kPa ( $k_o = 0.5$ ), chamber diameter of 3m and grain diameter of 10 mm remained unchanged. Cone diameters ranged from 200 mm down to 5 mm. This gave a chamber to grain diameter ratio of 300, chamber to cone diameter ratio of 15 to 600 and a grain to cone diameter ratio of 0.05 to 2.

Figure 6.3 shows the cone resistance versus chamber to cone diameter ratios as high as 600. It was observed that the cone tip resistance remained almost constant for chamber to cone diameter ratios from 110 to 150 but increased for chamber to cone diameter ratios greater than 150. This increase in cone tip resistance for chamber to cone diameter ratios greater than 150 is attributed to the grain size effect. In this range of chamber to cone diameter ratios the cone diameter was between 20 mm to 5 mm. Such small cone sizes if used in gravel in the field would be expected to encounter refusal. The maximum cone tip resistance for standard CPT used in very dense sands or sandy gravels

is about 100 MPa. The analysis up to this point did not give cone tip resistance as high as 100 MPa thus simulating essentially no reaching of refusal to penetration.

For all the analyses up to this point, the cone resistance has been calculated by taking the average vertical force on the cone tip for the last 100 cycles. For small grain to cone diameter ratios, this approach worked well, as larger number of particles under a cone means less difference between the high and low values (i.e. a more uniform cone resistance). But for larger grain to cone diameter ratios the number of particles decrease dramatically and there is a marked difference between the maximum and minimum vertical force on the cone tip (i.e., erratic cone resistance). Figures 6.4 and 6.5 show the vertical force versus depth for grain to cone diameter ratios of 0.05 and 2, respectively. The maximum vertical force is generated as peaks when individual large particles underneath the cone exert force on it. The cone can experience severe damage or prominent marks on the tip / surface as a result of these high instantaneous contact forces when penetrating coarse gravels. Appendix – D contains a few photographs of damaged cones that have penetrated gravelly sands (courtesy of ConeTec Limited).

The minimum vertical force occurs when particles move away from the cone tip to acquire new positions in the soil matrix. For large grain to cone diameter ratios, the cone tip can exist in a void with zero cone resistance, before touching the next grain. For grain to cone diameter ratios more than 1, the minimum vertical force measured on the cone came out as negative (Figure 6.5). This prompted the need to run a sensitivity analysis for the time step chosen for large grain to cone diameter ratios. The time step was reduced to one tenth of the original time step for this sensitivity analysis. Yet, minimum vertical force was still negative and the difference between vertical forces measured for reduced time step versus original time step was within 2 %.

The above discussion showed that the averaging approach does not show the real behavior of the “Refusal” mechanism that usual occurs in the field for cone penetration in coarser soils (gravel / sandy gravel). The remaining analyses thus include determination of maximum, average and minimum vertical force experienced by the cone during the



penetration mechanism. Figure 6.6 shows the same results as depicted in Figure 6.3 with the maximum, average and minimum cone resistance also plotted versus both the chamber to cone and the grain to cone diameter ratios.

It is evident by the near vertical maximum cone resistance trend (grain / cone diameter ratio more than 1), that the maximum cone resistance is the likely cause of “Refusal” observed in the field. It is this sharp peak resistance at an instant which determines that the cone is unable to penetrate into coarse grained soil.

Figure 6.7 shows the plot for the calculated maximum cone resistance versus the grain to cone diameter ratios for uniformly graded, dense (porosity = 0.1, relative density 90 %) and loose (porosity = 0.2, relative density 50 %) granular assembly. The marked drop in the initial phase of the cone resistance plot which is for large cone diameters (i.e. chamber to cone diameter ratios less than 110) is attributed to the chamber size effects on the measured cone resistance. Note that the cone is more capable of penetrating larger grain to cone diameter ratios for loose sand than dense sand.

A trial run was also carried out to see the effect of a well graded granular assembly on the measured cone resistance. This was achieved by changing the particle generation algorithm but keeping the other parameters identical. The grain size ranged from 5 mm to 15 mm. Figure 6.8 shows the configuration for both uniformly graded and a more well graded granular assembly. Fig. 6.9 shows the calculated maximum cone resistance plot with varying mean grain size at relative density 90 % along with the plots already shown in Figure 6.7. It is evident that a well graded granular assembly produces larger cone resistance than a uniformly graded granular assembly for a given grain to cone diameter ratio. *Figures 6.7 and 6.9 should be seen as a 3-D visualization. The plots have two axes on the horizontal and these plots represent 3-D spaces in a 2-D manner.*

The cone tip resistance for normally consolidated Ticino sand with  $k_o = 0.5$ , overburden stress of 100 kPa is around 18 MPa and 8 MPa for relative density of 90 % and 50 %, respectively (Baldi et al. 1986). The initial part of the plot in Figures 6.7 and

6.9 has thus been matched to the corrected cone tip resistance for granular assembly without any effect of chamber size. This suggested trend needs to be verified by further research.

Available literature suggests that “Refusal” is considered in the field to be when cones experience cone resistance in excess of 100 MPa. The latter part of the curve (vertical trend) reaches 100 MPa, which is due to the fact that large grains exert very large peak forces on the penetrating cone. It is suggested that this region of the plot is affected by the grain size. Chamber size only affects the cone resistance when the chamber to cone diameter ratio is less than 110.

This research has indicated that refusal for cone penetration can be expected when the grain to cone diameter ratio is around 1.0 or more. Also the measured cone tip resistance will start to be influenced by the grain size when the grain to cone diameter ratio reaches about 0.3. A grain to cone diameter ratio more than 0.3 can be used to provide a rough estimate of when the measured cone resistance in the field may require a correction due for the grain size effects.

## **6.1 Implications of Results:**

The results obtained from this two dimensional study are dependent on certain assumptions and limitations. The simulations were carried out with the following assumptions;

- granular particles are clean and non-compressible
- granular assembly is normally consolidated (NC)
- no cementation, and,
- rounded shape particles.

In general, most natural sand and gravel deposits contain some fine particles which can influence the response of the sand. This response is a function of the plasticity

of the fines. Also many sand and gravel deposits can have a stress history that can influence the horizontal stress state.

Naturally cemented granular deposits can occur throughout many parts of the world. Data and evidence suggest that even the cleanest natural sand deposits may be very weakly cemented, (Mitchell and Solymar, 1984). Cementation tends to increase the cone tip resistance in granular soils.

The particle shape simulated in this research has been limited to circular (2D analysis). The coefficient of contact friction between cone and particle was considered equal to zero in this study. Grain angularity can have an important role in determining the strength of a soil deposit. Soils composed of angular particles tend to have a higher friction angle and hence higher cone tip resistance.

In PFC<sup>2D</sup> modeling, the out-of-plane force component and the two in-plane moment components are not accounted for in the equations of motion or via the force-displacement laws. This limits the analysis as there is no stress and / or strain transfer in the 3<sup>rd</sup> dimension (PFC<sup>2D</sup> manual, 2002). The Poisson's ratio effect is also not considered. The possible impact is that the cone resistance obtained under such force and moment conditions is greater. Three dimensional modeling is required to evaluate the importance of this limitation. The calculated average cone resistance using PFC<sup>2D</sup> in this study was generally slightly larger than that observed experimentally in Ticino sand. However, the calculated values were within about 20 % of the experimental / field observed values.

The critical time step selected in the analyses should be such that the granular assembly remains stable. During this simulation study, several trial runs were carried out at different time steps (Sections 3.2.6 and 3.3.1). These trial runs indicated that larger time step than the critical value makes the system unstable and produces higher cone resistance due to the non-dissipation of potential energy stored in the particles. Hence for

any numerical analysis to be performed on granular assembly, whether 2-D or 3-D, should be carried out after determination of critical time step.

This research has shown that refusal of penetration can be expected when the grain to cone diameter ratio is around 1.0. Also the measured cone tip resistance will start to be influenced by the grain size when the grain to cone diameter ratio reaches about 0.3. A grain to cone diameter ratio more than 0.3 thus can be used to provide a rough estimate of when the measured cone resistance in the field may require a correction due to the grain size effects. Further study is needed to clarify this effect on the measured cone resistance.

ConeTec Investigations Limited kindly provided example CPT profiles that include sections through gravel. These example profiles are presented in Appendix - E. In these example profiles, the corrected cone tip resistance recorded in sandy gravel / gravel range from 300 bars (approx. 30 MPa) to 500 bars (approx. 50 MPa) and show rapid variations from very large values to low values over very short distances. This highly erratic cone profile is typical for cone testing through gravel deposits. The high values can ultimately result in refusal of the cone. The observed erratic cone profiles are consistent with the calculated variation of cone resistance in this study for high grain to cone diameter ratios.

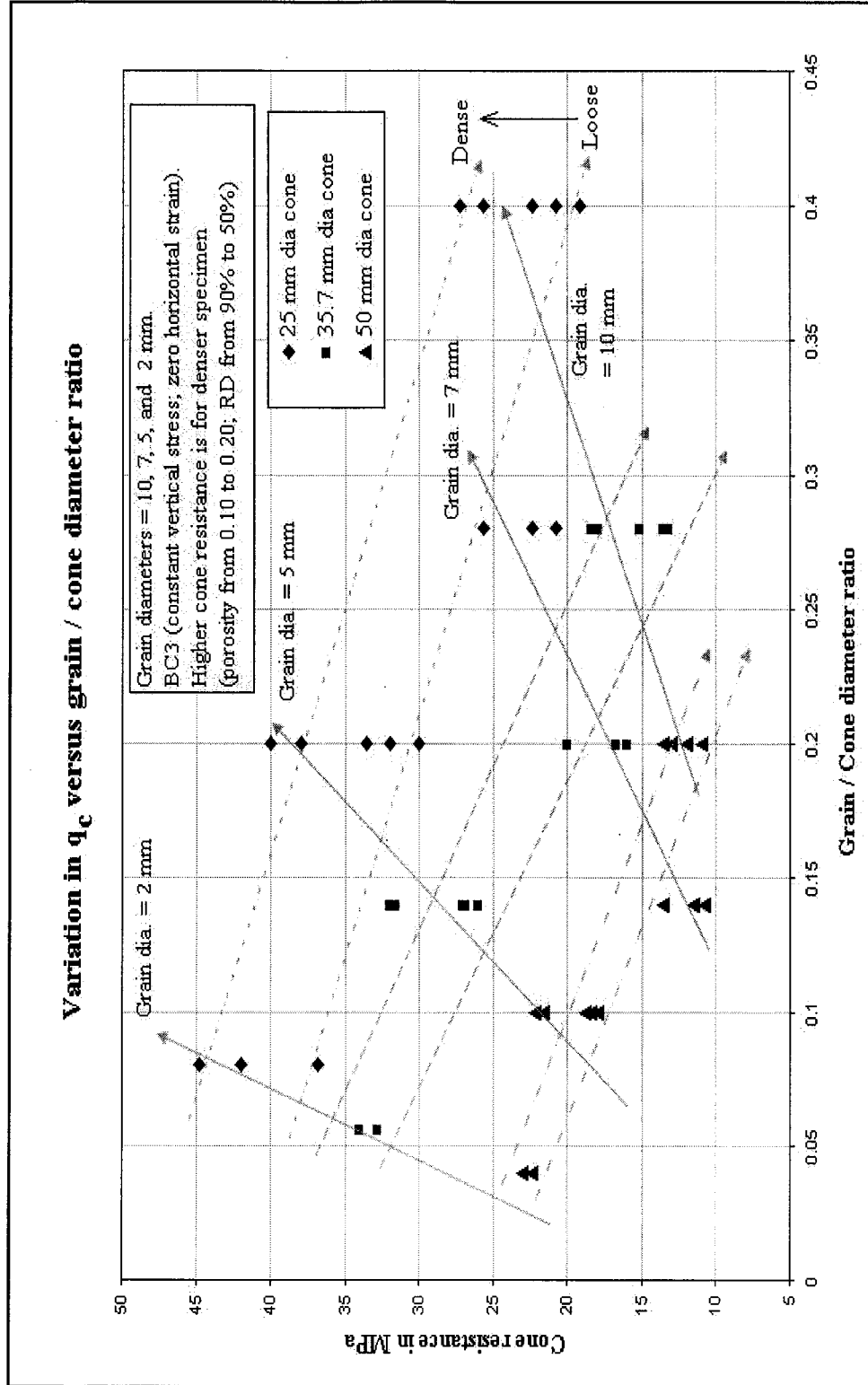


Figure 6.1: Plot of cone tip resistance versus the grain to cone diameter ratio at varying porosity values.

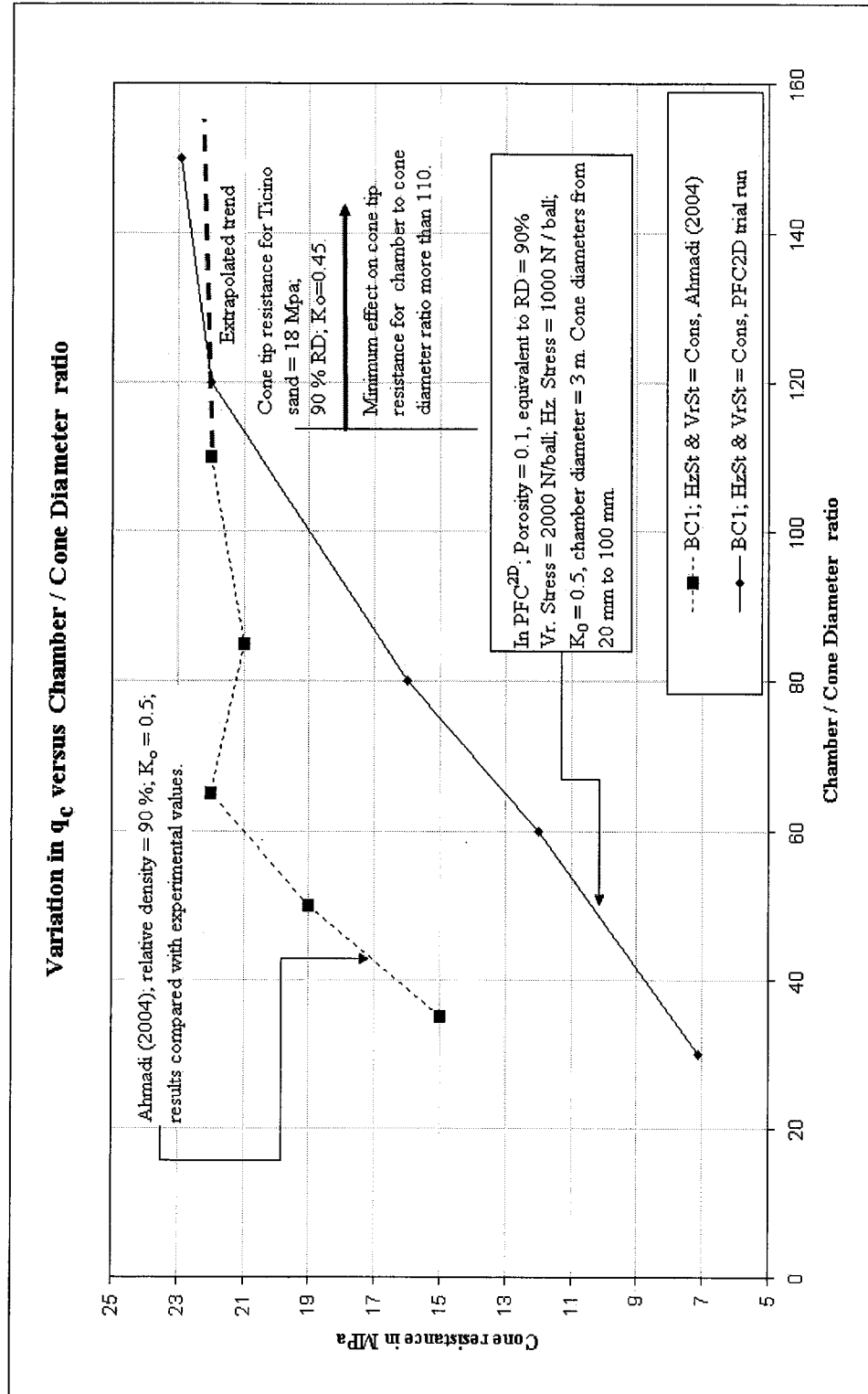


Figure 6.2: Plot of cone tip resistance versus chamber / cone diameter ratio. Trial run Results.

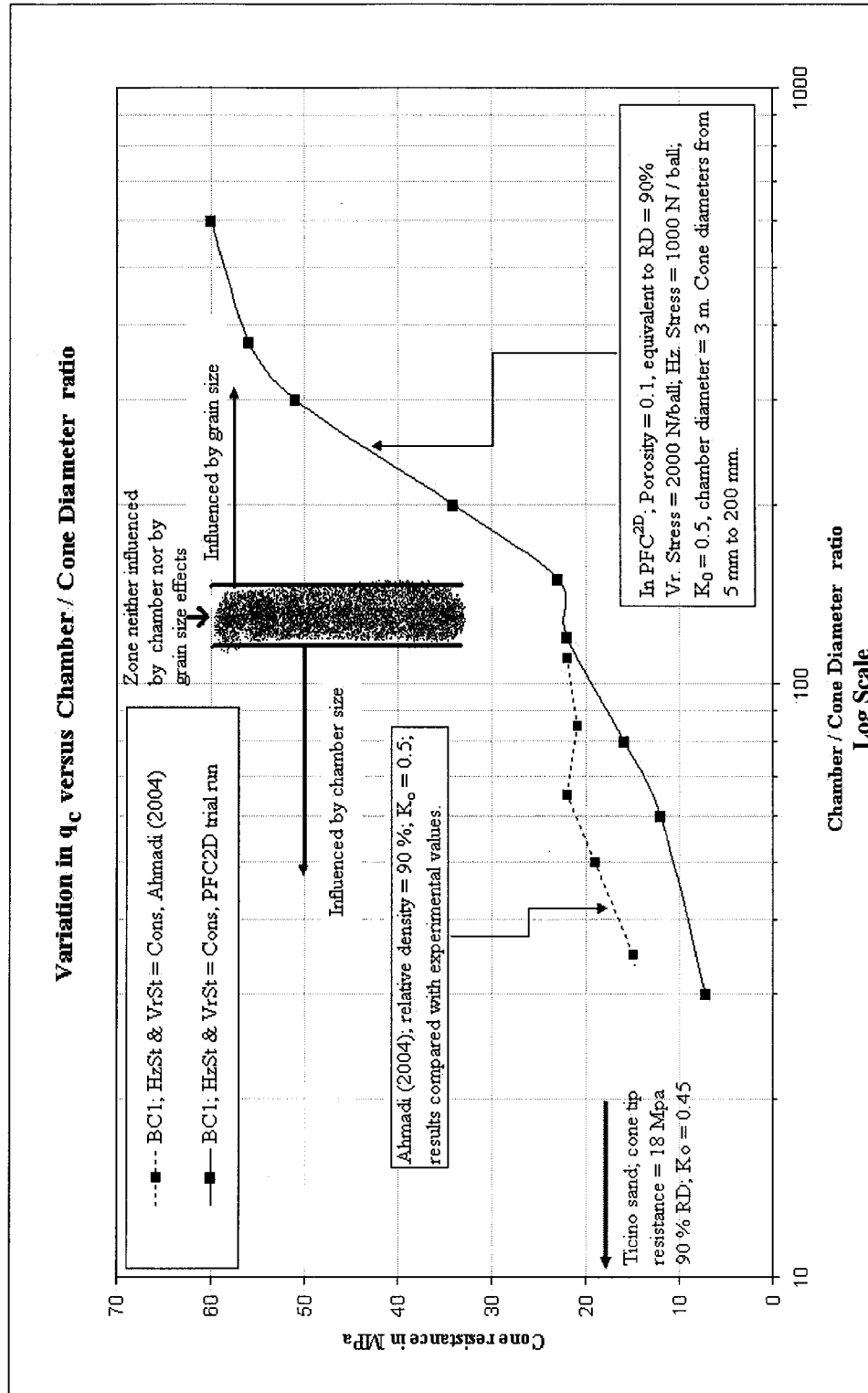


Figure 6.3: Plot of average cone tip resistance versus chamber to cone diameter ratio. Extended for chamber/cone diameter ratio up to 600 (cone diameter = 5 mm).

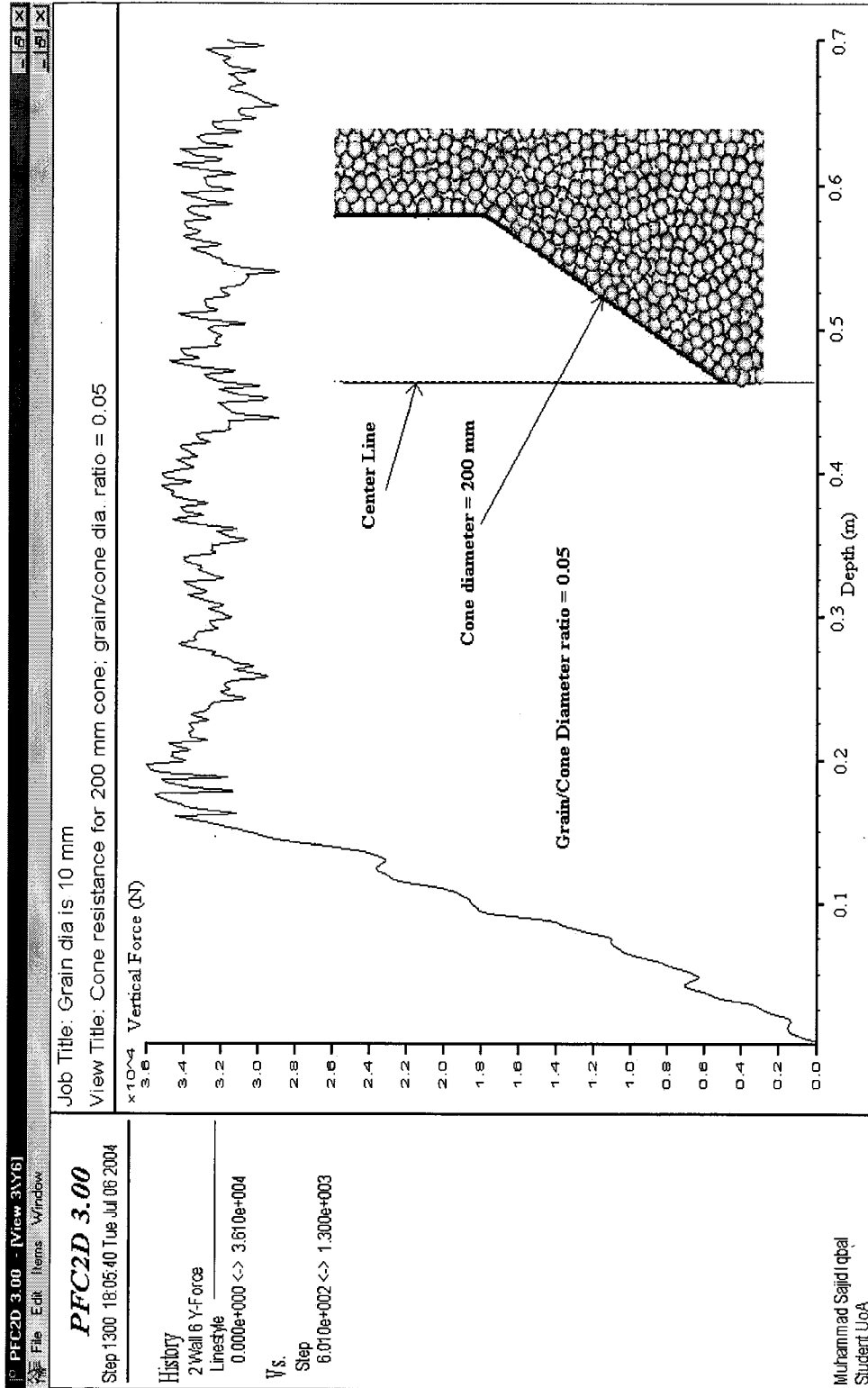


Figure 6.4: Plot showing the vertical force versus depth for a grain/cone diameter ratio of 0.05.



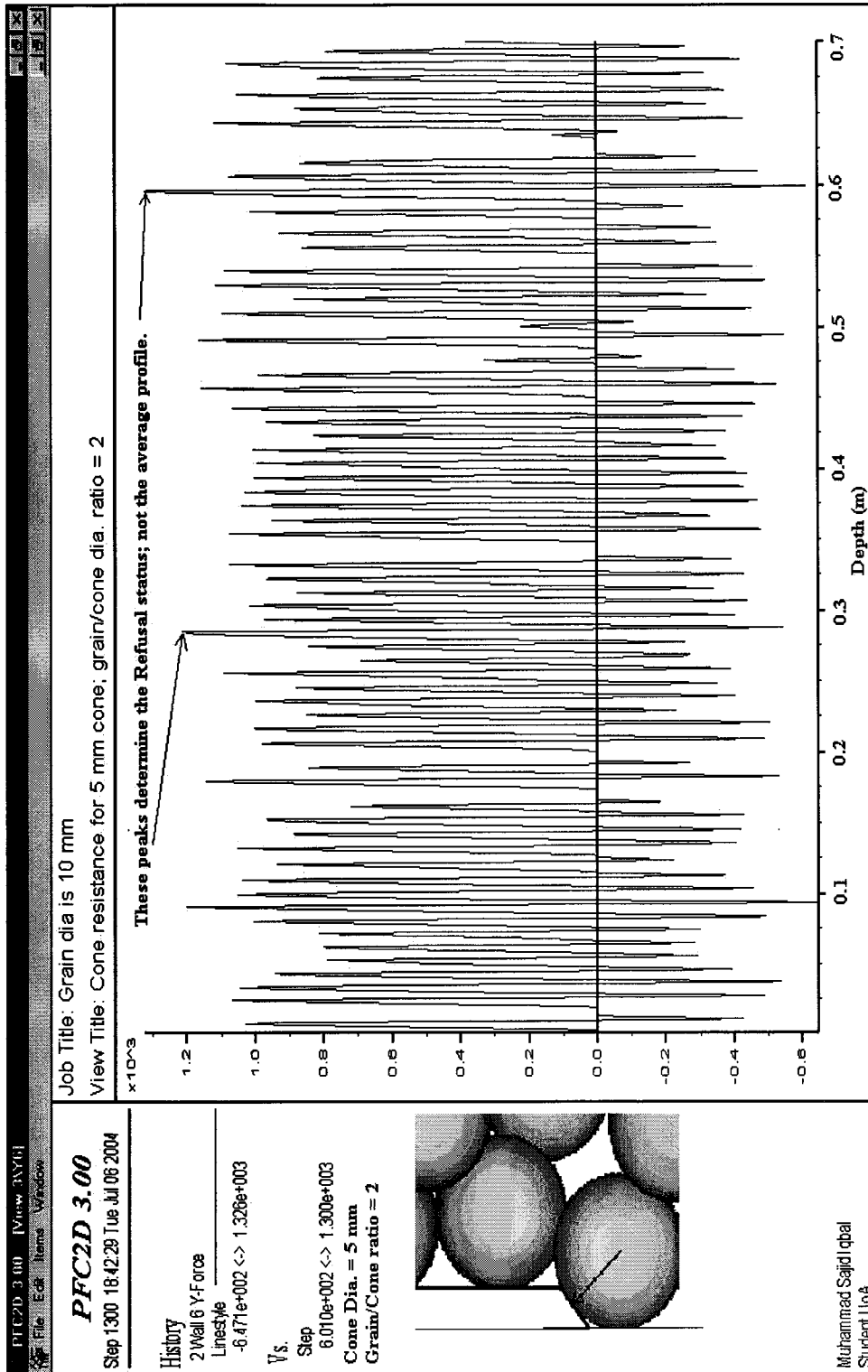


Figure 6.5: Plot showing the vertical force versus depth for a grain to cone diameter ratio of 2.0.

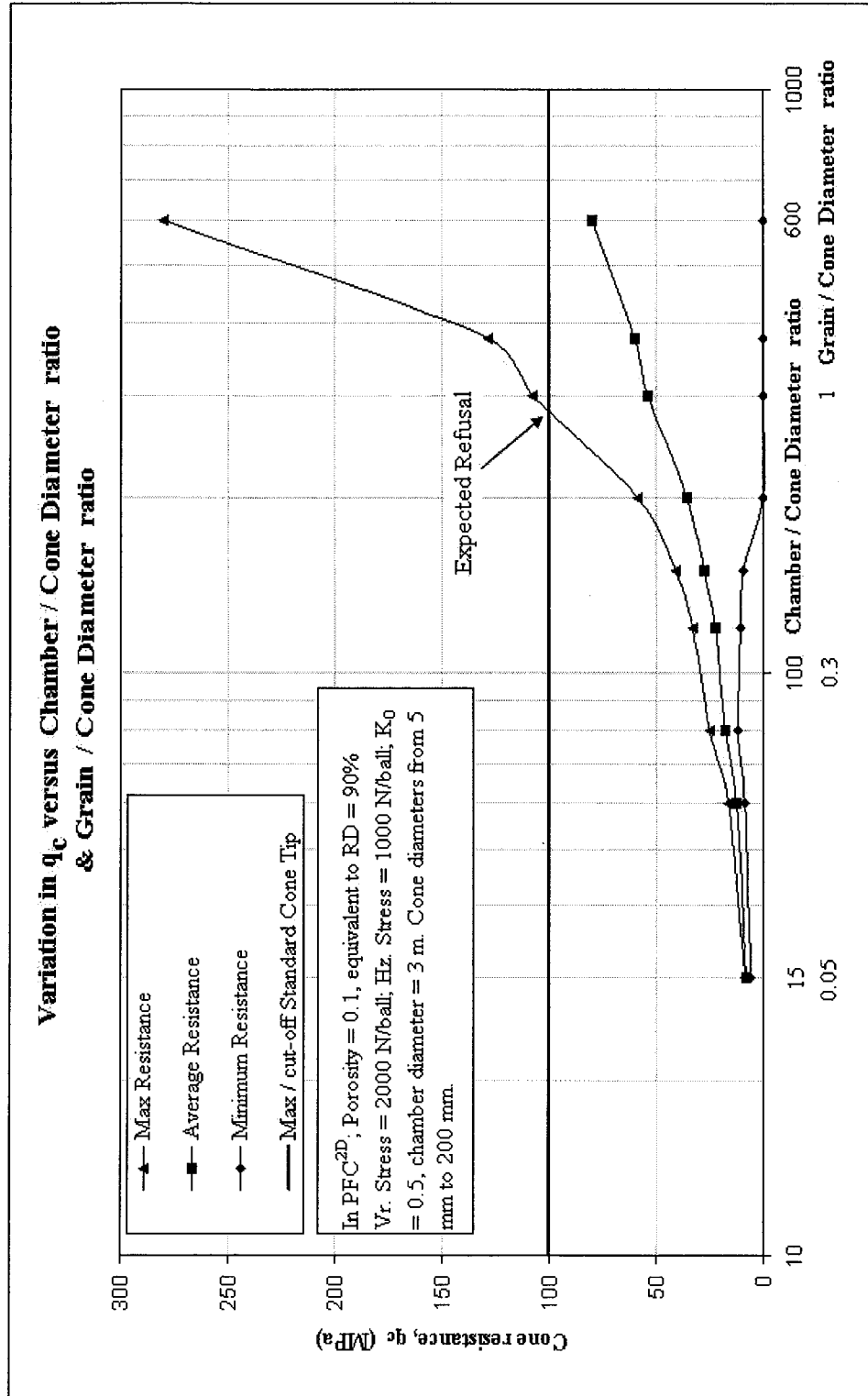


Figure 6.6: Plot showing the maximum, average and minimum cone tip resistance versus the chamber / cone diameter ratio and grain / cone diameter ratio. (refer to Figure 6.3 for comparison).

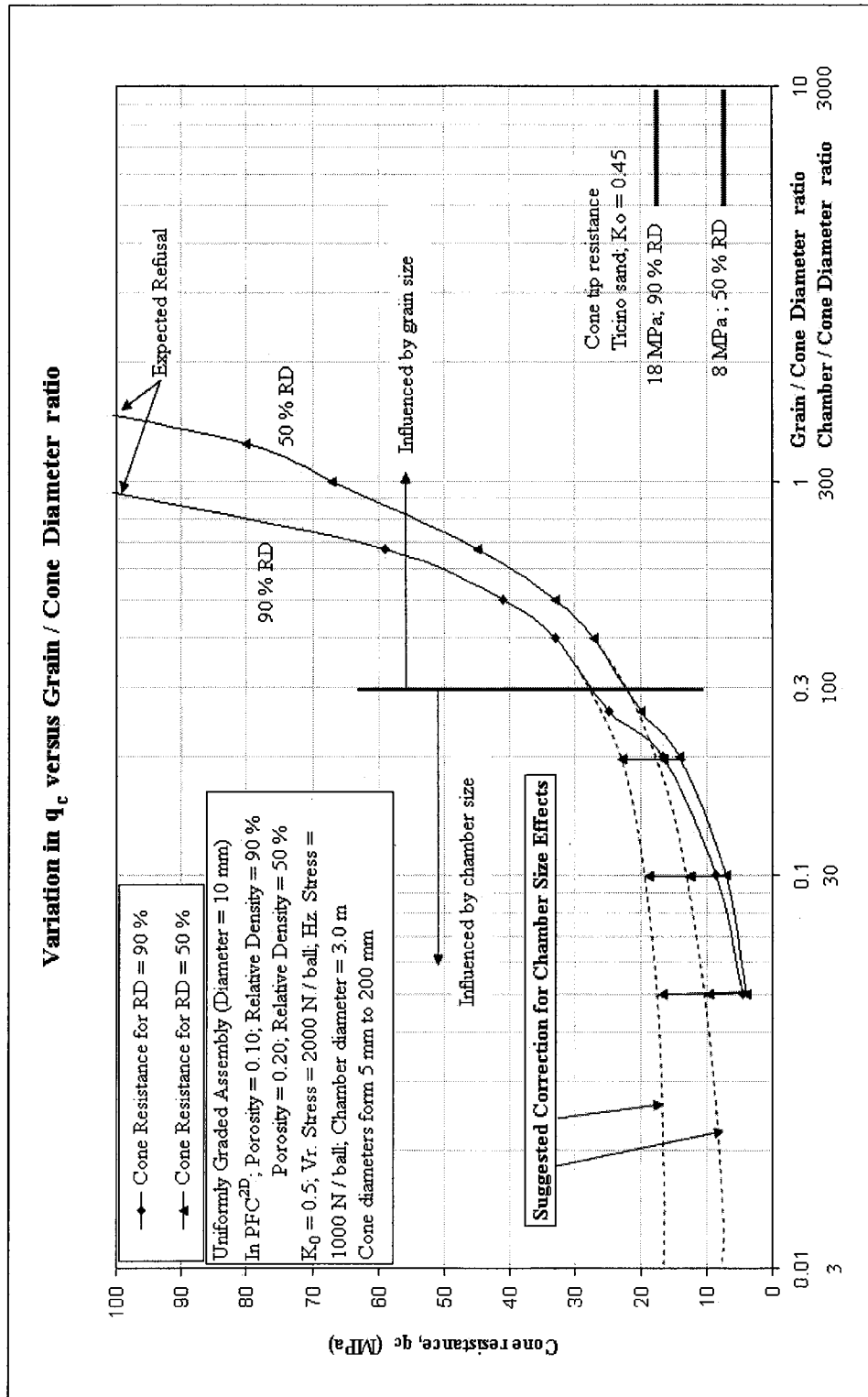


Figure 6.7: Plot for maximum cone tip resistance versus grain / cone diameter ratio.

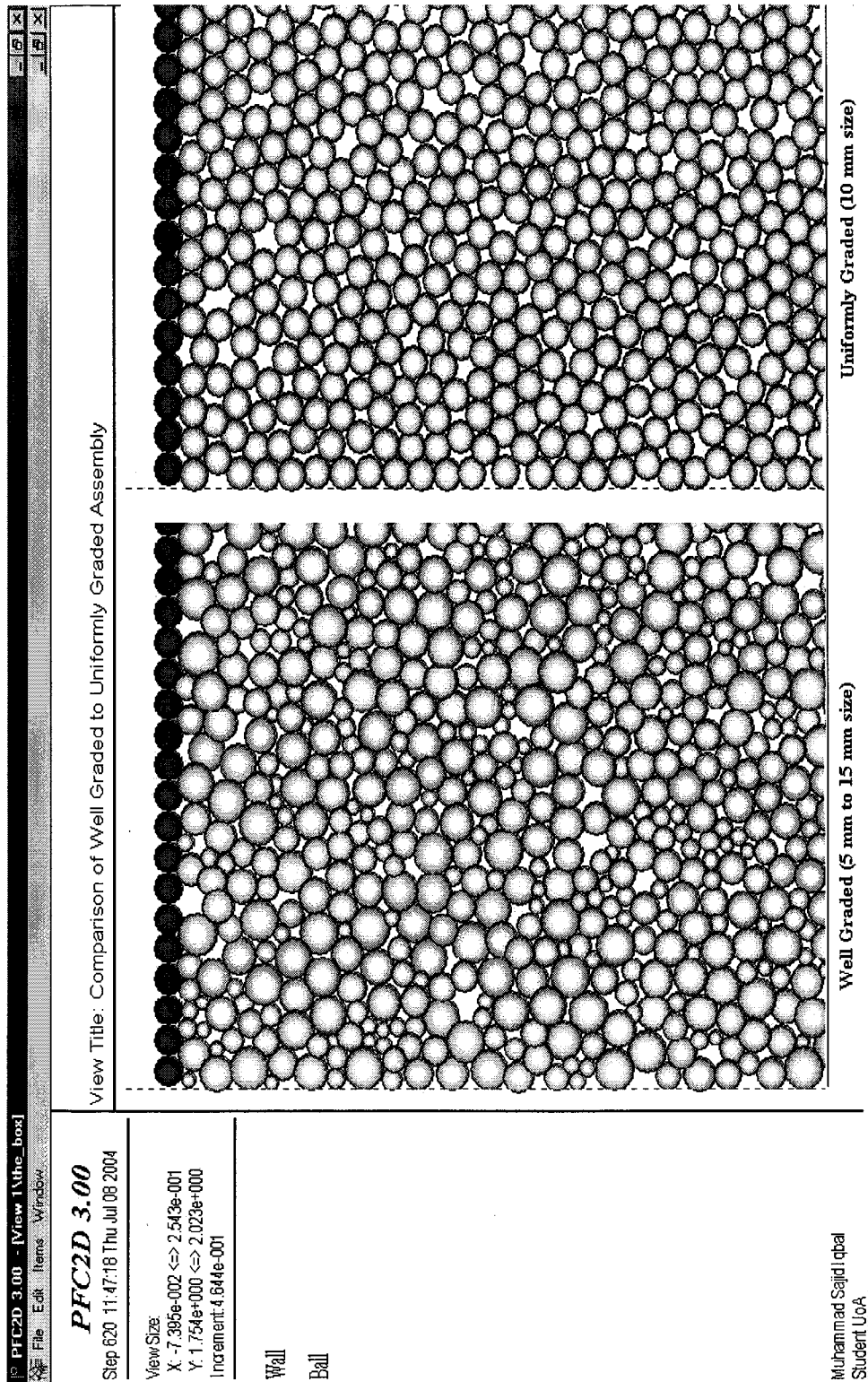


Figure 6.8: Configuration of a well graded and a uniformly graded assembly.

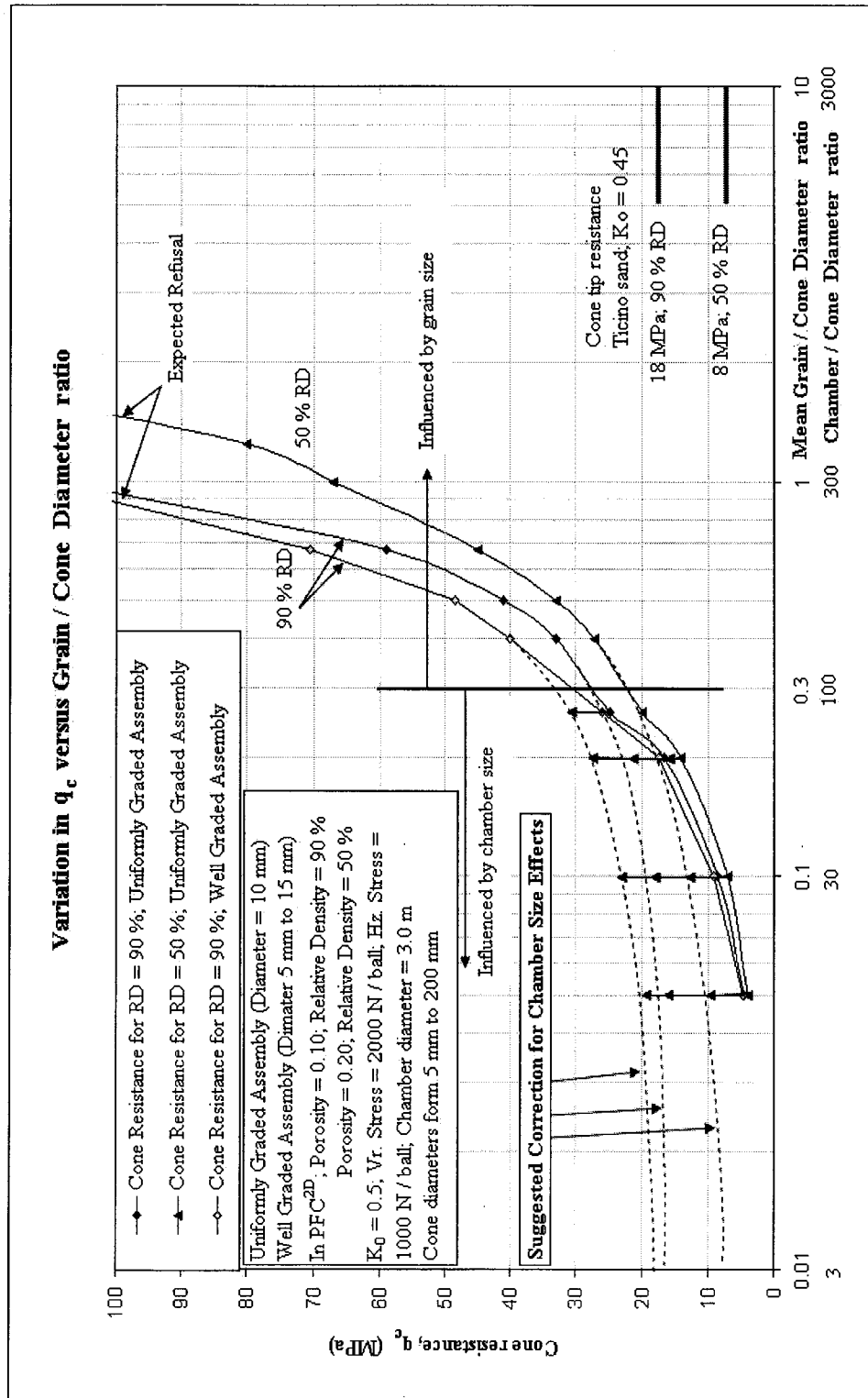


Figure 6.9: Plot for maximum cone tip resistance versus mean grain / cone diameter ratio (well & uniformly graded assemblies).

## 7. CONCLUSIONS AND RECOMMENDATIONS:

A coarse granular / particulate assembly comprised of circular, uniformly and well-graded, clean, non-cemented, normally consolidated and non-compressible (rigid) particles was modeled for cone penetration testing. A computer software program Particle Flow Code in 2-dimensions (PFC<sup>2D</sup>) was used which is based on discontinuum approach employing a Discrete Element Method (DEM). The computer code was written in FISH programming language assuming certain limitations and assumptions.

The granular assembly was assigned mechanical / physical / strength properties and *in-situ* stress conditions were applied using well defined boundary conditions. The cone penetration mechanism was modeled using a cone with a rigid 60° apex angle. Velocity was applied to the cone in the downward direction to simulate the penetration mechanism. Since the explicit numerical scheme is used to obtain a solution in DEM, a critical time step was determined and applied to keep the system stable. The simulations were carried out with an in-plane symmetrical section option, an out of plane unit width (2-D), a finite height, a single grain size, finite chamber / model dimensions and varying cone sizes.

Results were in good agreement to those obtained by Ahmadi (2004), in that the chamber size and boundary conditions influence the measured cone tip resistance for chamber to cone diameter ratios less than 110. Grain / particle size influenced the predicted cone tip resistance when the grain to cone diameter ratio was greater than about 0.3. When the grain to cone diameter ratio was greater than about 1.0, the maximum cone tip resistance developed, due to individual peaks in the force generated by large particles, reached very high values which result in refusal of the penetration process. This phenomenon was verified by field data and with observed damage on cone tips used in field test after penetration through gravels.

Other observations include confirmation that denser assemblies give higher cone tip resistance and also well graded assembly gives higher cone tip resistance.

Finally, recommendations for further research follow from the current research. The followings areas are recommended for further research:

- The development of 3-D simulation model using PFC<sup>3D</sup>
- Development of larger chamber size and greater number of individual particles
- Laboratory testing to compare with simulations
- Simulation of cementation between particles
- Consideration of the coefficient of contact friction between cone (polished and smooth steel surface) and particle (silica sand)
- Application of locked-in stresses (stresses applied within the assembly instead of at the boundaries) to compare with results obtained in this study
- Simulation of particles with clump logic to generate shapes other than circular to compare its effect
- Measurement of porosity changes within the vicinity of cone i.e. determination of the behavior of particle assembly (contraction or dilation)

Nevertheless, the results obtained in this study provide a practical approach towards developing an approximate guide for the size of a cone to be used in coarse granular deposits. As computing power increases and more RAM becomes available, larger chambers / models with more granular particles can be simulated and any effects related to these parameters can be studied in greater depth. Three dimensional modeling should be considered as the next step in this area because limitations regarding two dimensional aspects have been the biggest hurdle in this study. PFC<sup>3D</sup> should thus be used in modeling this research topic further.

## 8. REFERENCES:

- Ahmadi M. M. (2000): "Analysis of cone tip resistance in sand", PhD thesis, University of British Columbia, Vancouver, Canada.
- Ahmadi M. M. and Robertson P. K. (2002): "Calibration chamber size and boundary effects for CPT  $q_c$  measurements", 2<sup>nd</sup> International Conference on Site Characterization, ISC, 02, Porto.
- Ahmadi M. M. and Robertson P. K. (2004): "A numerical study of chamber size and boundary effects on CPT tip resistance ( $q_c$ ) in sand", accepted for publication in the Canadian Geotechnical Journal.
- Antony, S. J. (2000): "Evolution of force distribution in three-dimensional granular media", Physical Review, vol. 63, 011302.
- Baldi, S. and Bellotti, R. (1982): "Design parameters for sands from CPT", *Proc. 2<sup>nd</sup> European symposium on penetration testing*, Amsterdam, 425 – 432.
- Baldi, G., Bellotti, R., Crippa, V., Fretti, C., Ghionna, V. N., Jamiolkowski, M., Pasqualini, E., Pedroni, S. and Ostricati, D. (1985): "Laboratory Validation of In-situ Tests", AGI Jubilee Volume – IX ICSMFE, San Fransisco.
- Baldi, G., Bellotti, R., Ghionna, V.N., Jamiolkowski, M. and Pasqualini, E. (1986): "Interprtation of CPT's and CPTU's", 2<sup>nd</sup> part: "Drained penetration of sands", *Proc. IV Int. Geotech. Sem.*, Singapore, 143 - 156.
- Baligh, M. M., Azzouz, A. S., Wissa, A. Z. E., Matyin, R. T. and Morrison, M. H. (1981): "The piezocone Penetrometer", Cone Penetration Testing and Experience", Proceedings of the ASCE National Convention, St. Louis, 247 – 263.
- Bayne, J. M. and Tjelta, T. I. (1987): "Advanced cone penetrometer development for in-situ testing at Gullfaks C", Offshore Technology Conference, Richardson, Texas, paper No. 5420.
- Been, K., Jefferies, M. G., Crooks, J. H. A. and Rothenburb, L. (1987): "The cone penetration test in sands: General inference of state", *Geotechnique*, 37(3), 285 – 299.
- Been, K., Crooks, J. H. A., and Rothenburb, L. (1988): "A critical appraisal of CPT calibration chamber tests", *Proc. International Symposium on Penetration Testing, ISOPT –I*, Orlando, 2, 651 – 660, Balkema Pub., Rotterdam.
- Begemann, H. K. S. Ph. (1953): "Improved method of determining resistance to adhesion by sounding through a loose sleeve placed behind the cone", Proceedings of the 3<sup>rd</sup>



International Conference on Soil Mechanics and Foundation Engineering, Zurich, 1, 213 – 217.

Begemann, H. K. S. Ph. (1965): “The friction jacket cone as an aid in determining the soil profile”, Proceedings of the 6<sup>th</sup> International Conference on Soil Mechanics and Foundation Engineering, Montreal, 1, 17 – 20.

Begemann, H. K. S. Ph. (1969): “The Dutch Static Penetration Test with the adhesion jacket cone”, LGM Mededelingen, 12(4), 69 - 100.

Bellotti, R., Bizzi, G. and Ghionna, V. (1982): “Design, construction and use of a calibration chamber”, *Proc. 2<sup>nd</sup> European Symposium on Penetration Testing, ESOPT – II*, Amsterdam, 2, 439 – 446, Balkema Pub., Rotterdam.

Bellotti, R., Crippa, V., Pedroni, S. and Ghionna, V. N. (1988): “Saturation of sand specimen for calibration tests”, *Proc. International Symposium on Penetration Testing, ISOPT – I*, Orlando, 2, 661 – 672, Balkema Pub., Rotterdam.

Broms, B. B. and Foldin, N. (1988): “History of soil penetration testing”, Proceedings of the International Symposium on Penetration Testing, ISOPT-1, Orlando, 1, 157 – 220, Balkema Pub., Rotterdam.

Brand, E. W. and Phillipson, H. B. (1985): “Review of international practice for the sampling and testing of residual soils”, *Sampling and Testing of Residual Soils: a Review of International Practice*, 7 – 21, Scorpion Press, Hong Kong.

Campanella, R. G. and Robertson, P. K. (1981): “Applied cone research”, Proceedings of the ASCE National Convention: Cone Penetration Testing and Experience”, St. Louis, 343 – 362, American Society of Engineers (ASCE).

CANLEX Project (1998): “Summary and Conclusions”, Canadian Geotechnical Journal.

Chang, M. F. (1988): “In-situ testing of residual soils in Singapore”, Proceedings of the 2<sup>nd</sup> International Conference on Geomechanics in Tropical Soils, Singapore, 2, 97 – 108, Balkema Pub., Rotterdam.

Chang, C. S., and Misra, A. (1989): “Computer simulation and modeling of mechanical properties of particulates”, *Computers and Geotechnics*, vol. 7, 269 - 287.

Cleary, P. W., Metcalfe, G., and Liffman, K. (1998): “How well do discrete element granular flow models capture the essentials of mixing processes?”, *Applied Mathematical Modeling*, vol. 22, 995 - 1008.

Cundall, P. A. (1971): “A Computer Model for Simulating Progressive Large Scale Movements in Blocky Rock Systems,” Proceedings of the Symposium of the International Society for Rock Mechanics, Nancy, France, Vol. 1, Paper No. II - 8.

- Cundall, P. A. and Strack, O. D. L. (1979): "A discrete numerical model for granular assemblies", *Geotechnique*, vol. **29**, 47 – 65.
- Cundall, P. A. (1988): "Formulation of a three-dimensional model, Part -1, A scheme to detect and represent contacts in a system composed of many polyhedral blocks", *International Journal of Rock Mechanics, Mining Sciences and Geomechanics*, vol. 25, No. 3, 107 – 116.
- Cundall, P. A. and Hart, R. D. (1992): "Numerical modeling of discontinua", *Engineering Computations*, vol. **9**, 101 – 113.
- de Graaf, H. C. van and Vermeiden, J. (1988): "Half a century of static cone penetration techniques". LGM Mededelingen, Part XXII (95).
- de Lima, D. C. and Tumay, M. T. (1991): "Scale effects in cone penetration tests", *Proceedings of the Geotechnical Engineering Congress 1991*, ASCE, Boulder, Colorado, 1, 38 – 51.
- de Ruiter, J. (1971): "Electrical penetrometers for site investigations", *Journal of Soil Mechanics and Foundation Division*, ASCE, 97, SM2, 457 – 472.
- de Ruiter, J. (1981): "Current Penetrometer Practice; Cone Penetration Testing and Experience", *Proceedings of the ASCE National Convention*, St. Louis, 1 – 48.
- Douglas, B. J. and Olsen, R. S. (1981): "Soil classification using electric cone penetrometer", *Proceedings of the ASCE National Convention: Cone Penetration Testing and Experience*, St. Louis, 209 – 227, American Society of Engineers (ASCE).
- Ghionna, V. N. and Jamiolkowski, M. (1992): "A critical appraisal of calibration chamber testing of sands", *Proceedings of the International Symposium on Calibration Chamber testing*, Potsdam, New York, 1991, 13 -40, Balkema Pub., Rotterdam.
- Gillespie, D. G. (1990): "Evaluating velocity and pore pressure data from the cone penetration test", Ph.D. thesis, Department of Civil Engineering, University of British Columbia, Vancouver, BC.
- Gourves, R., Oudjehane, F. and Zhou, S. (1997): "The in-situ characterization of mechanical properties of granular media with the help of penetrometers", *Powders and Grains* 97, 57 - 60.
- Heijnen, W. J. (1973): "The Dutch Cone Test; study of the shape of the electrical cone", *Proceedings of the 8<sup>th</sup> International Conference on Soil Mechanics and Foundation Engineering*, Moscow, 1, 181 – 184.

- Hart, R., Cundall, P. A. and Lemos, J. (1988): "Formulation of a three-dimensional distinct element model, Part - II, Mechanical calculations for motion and interaction of a system composed of many polyhedral blocks", *International Journal of Rock Mechanics, Mining Sciences and Geomechanics*, vol. 25, No. 3, 117 – 125.
- Holden, J. C. (1971): "Laboratory research on static cone penetrometers", University of Florida, Gainesville, Department of Civil Engineering, Internal Report CE – SM – 71 – 1.
- Holden, J. C. (1992): "History of the first six CRB calibration chambers", *Proceedings of the International Symposium on Calibration Chamber Testing*, Potsdam, New York, 1991, 1 -12.
- Hopkins, M. A. (1992): "Numerical simulation of systems of multitudinous polugonal blocks", *CRREL Report 92 -122*.
- ISSMFE (1989) Appendix A: "International Reference Test Procedure for Cone Penetration Test (CPT)". Report of the ISSMFE Technical Committee on Penetration Testing of Soils – TC 16, with Reference to Test Procedures, Swedish Geotechnical Institute, Linkoping, Information, 7, 6 – 16.
- Itasca Consulting Group, Inc. (2002): "PFC<sup>2D</sup> (Particle Flow Code in 2 Dimensions) Manual, Version 3.0, ICG, Minneapolis, Minnesota.
- Jamiolkowski, M., Ladd, C. C., Germain, J. T. and Lancellota, R. (1985): "New developments in field and laboratory testing of soils", *State of the Art Report, 9<sup>th</sup> Inter. Conf. on Soil Mech. And Found. Engrg.*, San Francisco, CA, 57 – 153.
- Jamiolkowski, M., Ghionna, V. N., Lancellota, R. and Pasqualini, E. (1988): "New correlations of penetration tests for design practice", *Proc. ISOPT - I*, Orlando, Florida, 263 – 296.
- Janbu, N. and Senneset, K. (1974): "Effective stress interpretation of in-situ static penetration tests", *Proceedings of the European Symposium on Penetration Testing, ESOPT*, Stockholm, 2.2, 181 – 193.
- Jensen, R. P., Bosscher, P. J., Plesha, M. E. and Edil, T. B. (1999): "DEM simulations of granular media – structure interface: effects of surface roughness and particles shape", *Int. J. Numer. Anal. Meth. Geomech.*, **23**, 531 – 547.
- Jones, G. A., Van Zyl, D. and Rust, E. (1981): "Mine tailings characterization by piezometer cone", *Proceedings of the ASCE National Convention: Cone Penetration Testing and Experience*, St. Louis, 303 – 324, American Society of Engineers (ASCE).
- Lorig, E., Gibson, W., Alvial, J. and Caevias, J. (1995): "Gravity flow simulations with the Particle Flow Code (PFC)", *ISRM News J.*, 3(1), 18 – 24.

- Lunne, T., and Christophersen, H. P. (1983): "Interpretation of cone penetrometer data for offshore sands", Proceedings of Offshore technology Conference, Richardson, Texas, paper No. 4464.
- Lunne, T., Eidmoen, T., Powell, J. J. M. and Quaterman, R. S. T. (1986): "Piezocone testing in overconsolidated clays", Proceedings of the 39<sup>th</sup> Canadian Geotechnical Conference, Ottawa, Preprint Volume, 209 – 218, Canadian Geotechnical Society.
- Lunne, T. and Powell, J. J. M. (1992): "Recent developments in in-situ testing in offshore soil investigations", Proceedings of the Symposium: From Theory to Practice in Deep Foundations, Porto Allegre, Brazil, Oct 1985, Published in : Norwegian Geotechnical Institute, Oslo, Publication, 169.
- Lunne, T., Robertson, P. K. and Powell, J. J. M. (1997): "Cone Penetration Testing in Geotechnical Practice", Blackie Academic & Professional, UK.
- Mayne, P. W. and kulhawy, F. H. (1992): "Calibration chamber database and boundary effects correction for CPT data", Proceedings of the International Symposium on Calibration Chamber Testing, Potsdam, New York, 1991, 257 – 264, Elsevier.
- Minchinton, A., and Lynch, P. M. (1996): "Fragmentation and heave modeling using a coupled discrete element gas flow code." Rock Fragmentation by Blasting, Mohanty Ed., 1 - 80.
- Mitchell, A. K. and Solymar, Z. V. (1984): "Time dependent strength gain in freshly deposited or densified sands", J. Geotech. Engr. ASCE, 110(11), 1559 - 1576.
- Muhs, H. (1978): "50 years of deep sounding with static penetrometers", Berlin Universitat, Deutsche Forschungsgesellschaft fur Boden-Mechanik (Degebo). Mitteilungen (34), 45 – 50.
- Munjiza, A. and Andrews, K. R. F. (1998): "NBS contact detection algorithm for bodies, similar size", International Journal for Numerical Methods in Engineering 43, 131 - 149.
- Muromachi, T. (1981): "Cone penetration testing in Japan", Proceedings of the ASCE National Convention: Cone Penetration Testing and Experience", St. Louis, 49 - 75.
- Ng, T. T. (1999): "Fabric study of granular materials after compaction", Journal of Engineering Mechanics, vol. 125, no. 12, 1390 – 1394.
- Olsen, R. S. and Farr, J. V. (1986): "Site characterization using the cone penetration test", Proceedings of the ASCE Specialty Conference In-situ' 86: Use of In-situ Tests in Geotechnical Engineering, Blacksburg, 854 – 868, American Society of Engineers (ASCE).

- Parkin, A. K. and Lunne, T. (1982): "Boundary effects in the laboratory calibration of a cone penetrometer in sand", *Proc. 2<sup>nd</sup> European symposium on penetration testing, ESOPT –II*, Amsterdam, 2, 761 – 768, Balkema Pub., Rotterdam.
- Perkins, E. and Williams, J. R. (2001): "A fast contact detection algorithm insensitive to object sizes", *Engineering Computations*, Vol. 18, No. 1/2, 48 - 61.
- Peuchen, J. et al. (1995): "New concepts for CPT standardization in the Netherlands", *Proceedings of the International Symposium on Cone Penetration testing, CPT' 95*, Sweden, 2, 67- 72, Swedish Geotechnical Society.
- Plantema, G. (1948): "Construction and method of operating a new deep sounding apparatus", *Proceedings of the 2<sup>nd</sup> International Conference on Soil Mechanics and Foundation Engineering*, Rotterdam, 1, 277 – 279.
- Potyondi, D. O., Cundall, P. A. and Lee, C. A. (1996): "Modeling rock using bonded assemblies of circular particles", *Rock Mechanics*, 1937 – 1944.
- Powel, J. J. M., Quarterman, R. S. T. and Lunne. T. (1988): "Interpretation and use of the piezocone test in UK clays", *proceedings of the Geotechnology Conference: Penetration testing in the UK*, Birmingham, 151 – 156, Thomas Telford, London.
- Powel, J. J. M., Clarke, B. G. and Shields, C. H. (1995): "CPT' 95 – National Report on UK Practice", *Proceedings of the International Symposium on Cone Penetration Testing*, Linkoping, Sweden, 2, 253 – 262, Swedish Geotechnical Society.
- Power, P. and Geise, J. (1995): "Seascount mini CPT system", *Proceedings of the International Symposium on Cone Penetration Testing, CPT' 95*, Linkoping, Sweden, 2, 79 – 84, Swedish Geotechnical Society.
- Robertson, P. K. and Campanella, R. G. (1983a): "Interpretation of cone penetration test: Part I: Sand", *Can. Geotech. J.*, Ottawa, Canada, 20(4), 718 – 733.
- Robertson, P. K. and Campanella, R. G. (1983b): "Interpretation of cone penetration test: Part I: Clay", *Can. Geotech. J.*, Ottawa, Canada, 20(4), 734 – 745.
- Robertson, P. K. and Campanella, R. G., Gillespie, D. and Greig, J. (1986): "Use of piezometer cone data", *Proceedings of the ASCE Specialty Conference In-situ' 86: Use of In-situ Tests in Geotechnical Engineering*, Blacksburg, 1263 – 1280, American Society of Engineers (ASCE).
- Robertson, P. K. (1990): "Soil classification using the cone penetration test", *Canadian Geotechnical Journal*, 27(1), 151 – 158.

Rothenburg, L., and Bathurst, R. J. (1991): "Numerical simulation of idealized granular assemblies with plane elliptical particles", *Computers and Geotechnics*, vol. 11, 315 – 329.

Sanglerat, G. (1972): "The penetrometer and soil exploration", Elsevier, Amsterdam, 464 pp.

Salgado, R., Mitchell, J. K. and Jamiolkowski, M. (1998): "Calibration chamber size effects on penetration resistance in sand, *J. Geotech. And Geoenviron. Engrg.*, ASCE, 124, No. 9, 878 – 888.

Schmertmann, J. H. (1974): "Penetration pore pressure effects on quasi-static cone bearing,  $q_c$ ", *Proceedings of the European Symposium on Penetration Testing, ESOPT*, Stockholm, 2.2, 345 – 351.

Schmertmann, J. H. (1975): "Measurement of in-situ shear strength", *Proceedings of the ASCE Specialty Conference on In-situ Measurement of Soil properties*, Raleigh, North Carolina, 2, 57 -138, American Society of Engineers (ASCE).

Schmertmann, J. H. (1976): "An updated Correlation Between Relative Density,  $D_r$ , and Fugro-type Electric Cone Bearing,  $q_c$ ", Contract Report DACW 39 – 76 M 6646, Waterways Experiment Station, Vicksburg, Miss., 1976.

Schmertmann, J. H. (1978): "Guidelines for cone penetration test; performance and design", FHWA – TS - 209, FHWA, Washington, DC.

Sowers, G. F. (1985): "Residual soils in the United States", *Sampling and Testing of Residual Soils: a Review of International Practice*, 183 - 191, Scorpion Press, Hong Kong.

Taylor, L. M., and Preece, D. S. (1992): "Simulation of blasting induced rock motion using spherical element models", *Engineering Computations*, vol. 9, 243 - 252.

Thallak, S., L. Rothenburg and Dusseault, M. (1990): "Hydraulic fracture (parting) simulation in granular assemblies using the discrete element method", *AOSTRA Journal of Research*, Vol. 6, 141 - 153.

Ting, J. M., Meachum, L. R. and Rowell, J. D. (1995): "Effects of particle shape on the strength and deformation mechanisms of ellipse-shaped granular assemblage", *Engineering Computation*, vol. 12, 99 - 108.

Torstensson, B. A. (1975): "Pore pressure sounding instrument" *Proceedings of the ASCE Specialty Conference on In-situ Measurement of Soil Properties*, Raleigh, North Carolina, 2, 48 – 54, American Society of Engineers (ASCE).

Trent, B. C., and Margolin, L. a. (1994): "Modeling fracture in cemented granular materials", ASCE, Fracture mechanics applied to geotechnical engineering, 54 - 69.

Tumay, M. T., Bogges, R. L. and Acar, Y. (1981): "Subsurface Investigation with piezocone penetrometer", Proceedings of the ASCE National Convention: Cone Penetration Testing and Experience", St. Louis, 325 – 342, American Society of Engineers (ASCE).

Veismanis, A. (1975): "Laboratory investigation of electrical friction cone penetrometers in sands", Proceedings of the European Symposium on Penetration Testing, Stockholm, June 1974, 2.2, 407 -419.

Vermeiden, J. (1948): "Improved sounding apparatus as developed in Holland since 1936". Proceedings of the 2<sup>nd</sup> International Conference on Soil Mechanics and Foundation Engineering, Rotterdam, 1, 280 – 287.

Vinogradov, O. (1992): "Explicit equations of motion of discrete system of disks in two dimensions", Journal of Engineering Mechanics, vol. 118, No. 9, 1850 – 1858.

Vinogradov, O. (1993): "Dynamic equations for system of irregularly shaped plane bodies", Journal of Engineering Mechanics, vol. 119, No. 11, 2226 – 2237.

Vinogradov, O. (1997): "Scalar form of dynamic equations for a cluster of bodies", Structural Engineering and Mechanics, vol. 5, no. 2, 209 - 220.

Vinogradov, O., and Sun, Y. (1997): "Multibody approach in granular dynamics simulations", Computational Mechanics, vol. 19, 287 - 296.

Vlasblom, A. (1985): "The electrical penetrometer; a historical account of its development", LGM Mededekingen, Part XXII, 92 pp.

Wissa, A. E. Z., Martin, R. T. and Garlanger, J. E., (1975): "The piezometer probe", Proceedings of the ASCE Specialty Conference on In-situ Measurement of Soil Properties, Raleigh, North Carolina, 1, 536 – 545, American Society of Engineers (ASCE).

Zuidberg, H. M., Ten Hoope, J. and Geise, J. M. (1987): "Advances in in-situ measurements", Proceedings of the 2<sup>nd</sup> International Symposium on Field Measurements in Geomechanics, Kobe, 1, 279 – 291, Balkema Pub., Rotterdam.

## **APPENDIX – A**

**Letter of permission from Itasca Consulting Group, Inc.**




July 12, 2004

Muhammad Sajid Iqbal  
University of Alberta  
Department of Civil & Environmental Engineering  
Room No. 107, CEB, Geotechnical Group  
Alberta, Canada T6G 2E1

Dear Muhammad,

You have our permission to incorporate portions of our PFC manual into your thesis, with a reference and acknowledgement to the use of our software. Also, we ask that you provide us with a copy of your thesis when your work is finished.

Regards,



Roger D. Hart, Ph.D., P.E.  
Director, Software Services

ref: 5907

rh/rih

## **APPENDIX – B**

### **Random Generated Assemblies in PFC<sup>2D</sup>**

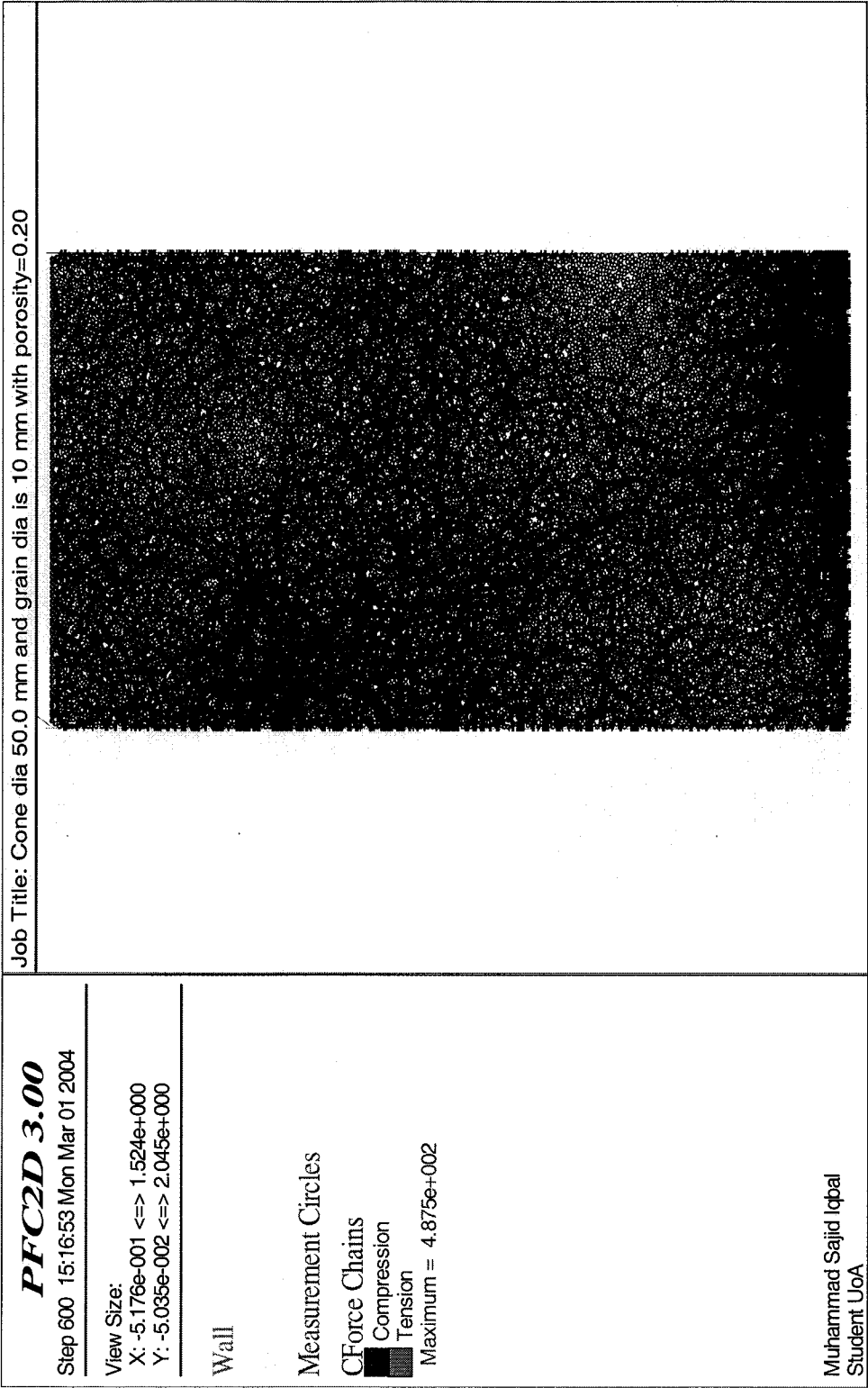


Figure B.1: Example of random generated assembly configuration.



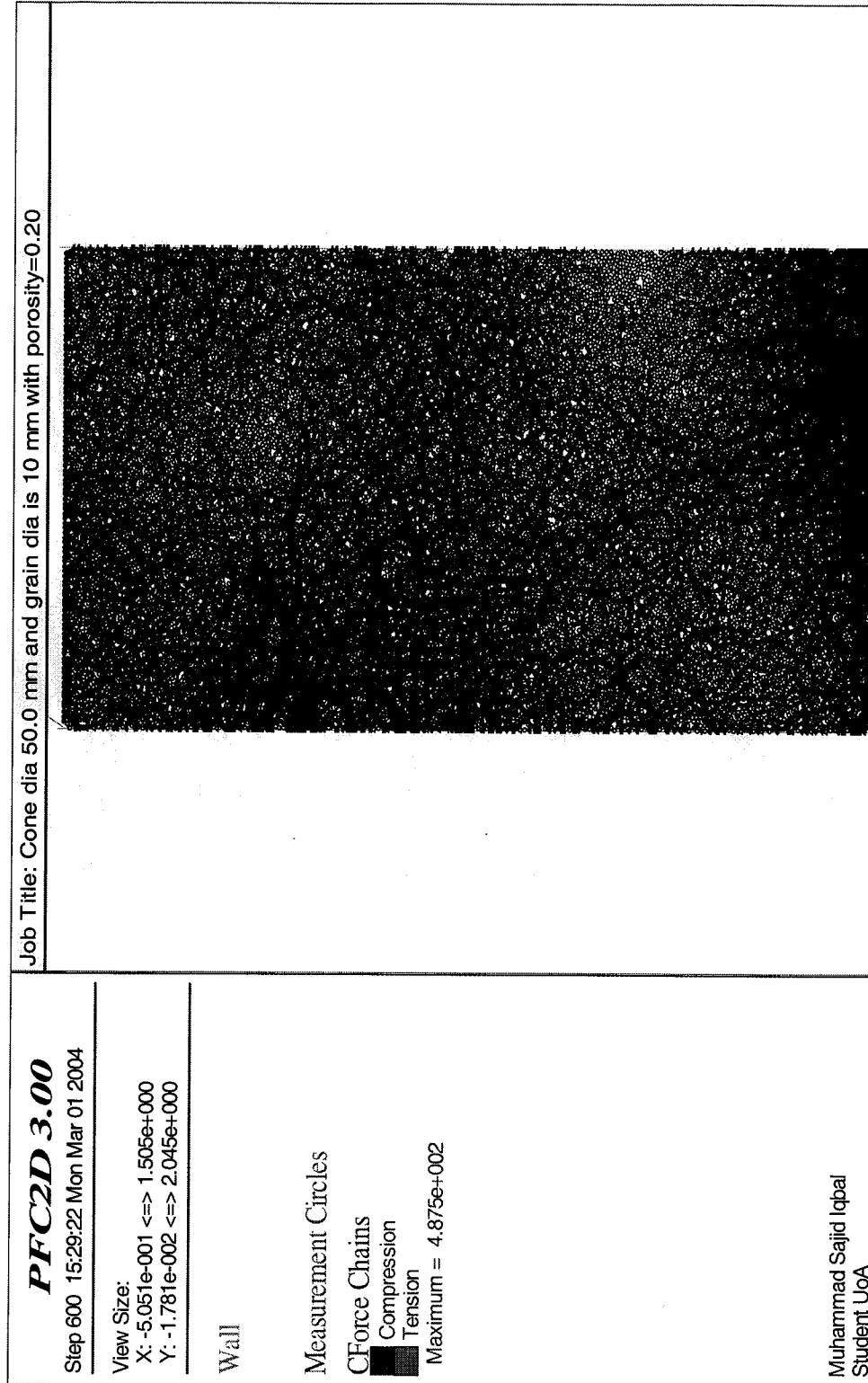


Figure B.3: Example of random generated assembly configuration.

## **APPENDIX – C**

**Trial run results in comparison to Ahmadi (2004)  
for both BC1 and BC3**

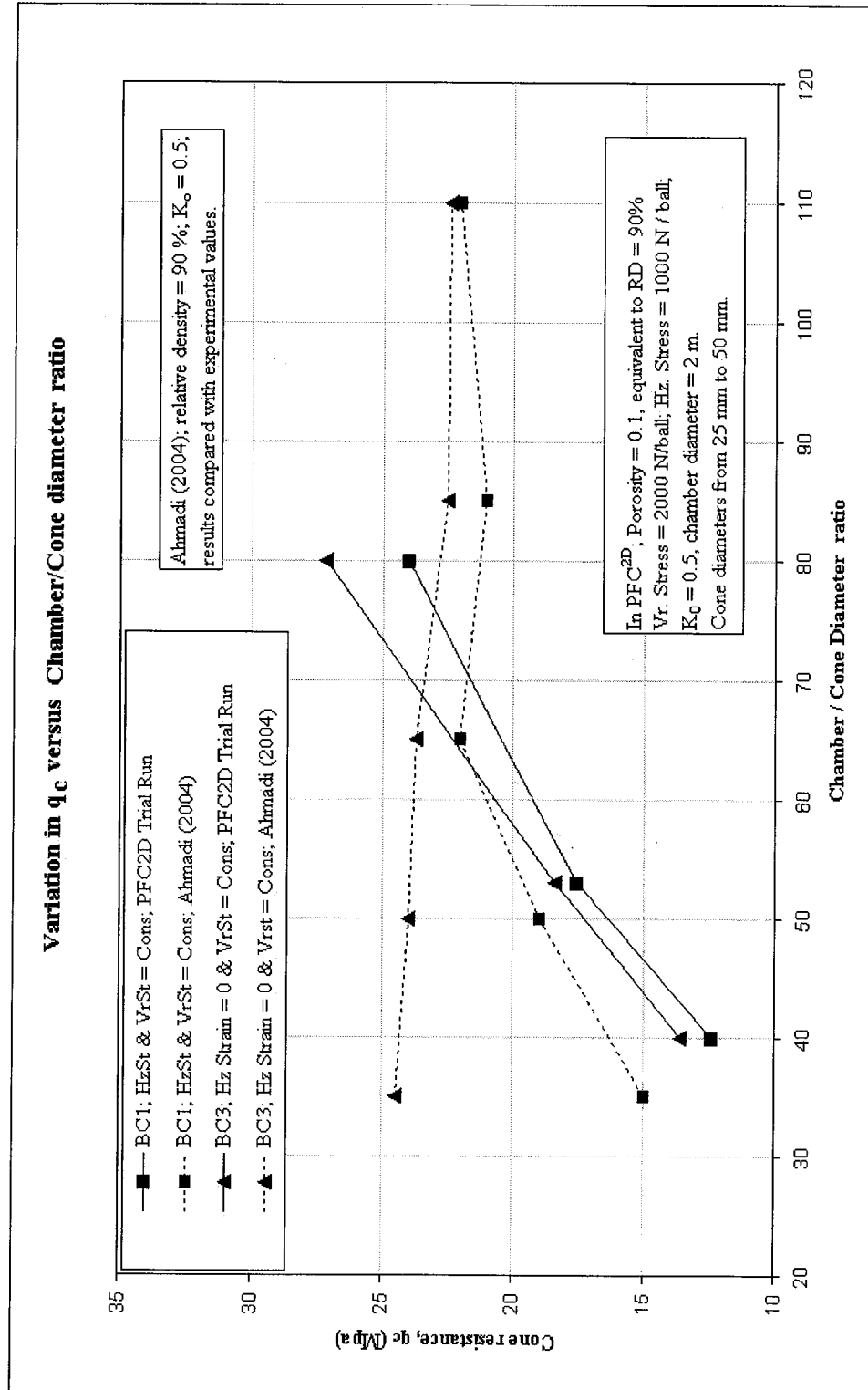


Figure C.1: Plot of cone tip resistance versus chamber / cone diameter ratio. Trial run results.

## **APPENDIX – D**

**Photographs of damaged cones that have penetrated gravelly sands  
(Courtesy of ConeTec Limited).**



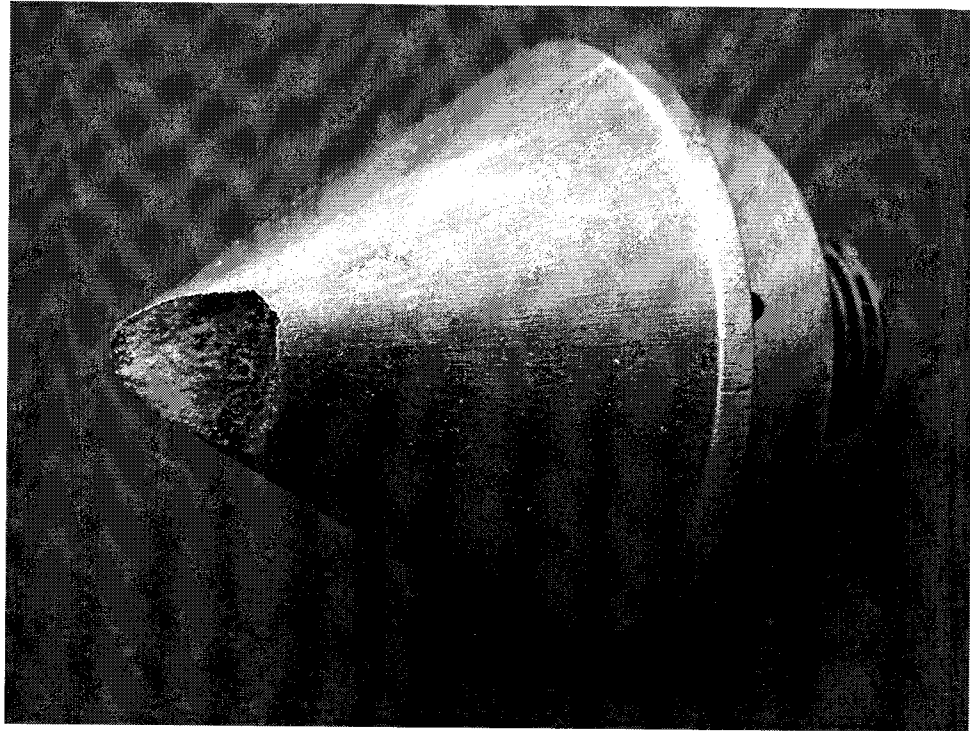


Figure D.1: A damaged cone with a broken tip.

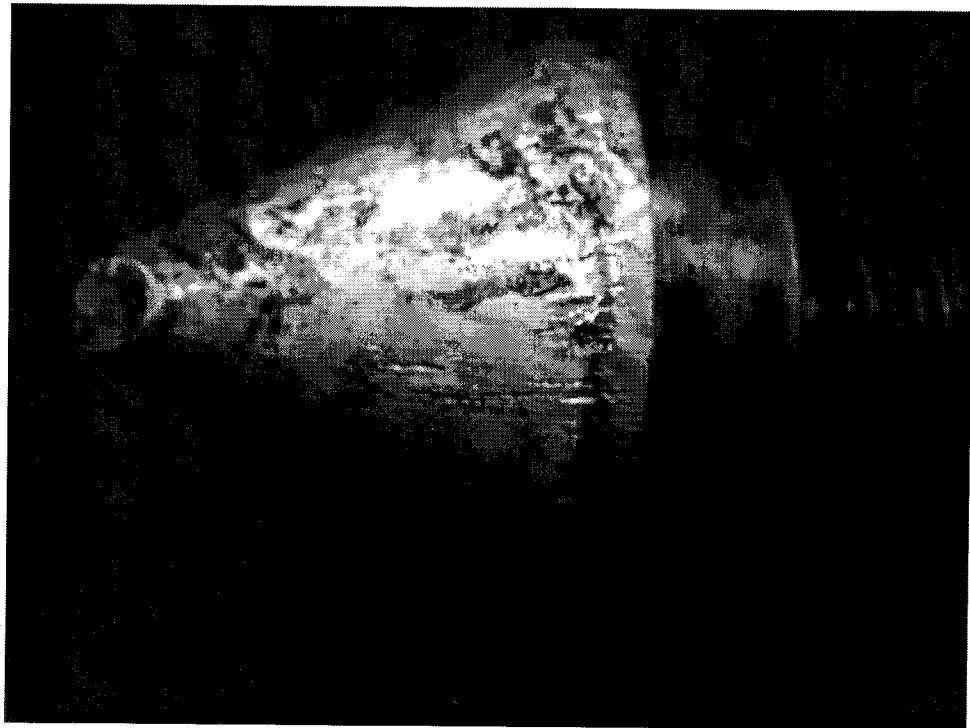


Figure D.2: A damaged cone with prominent scratch marks.

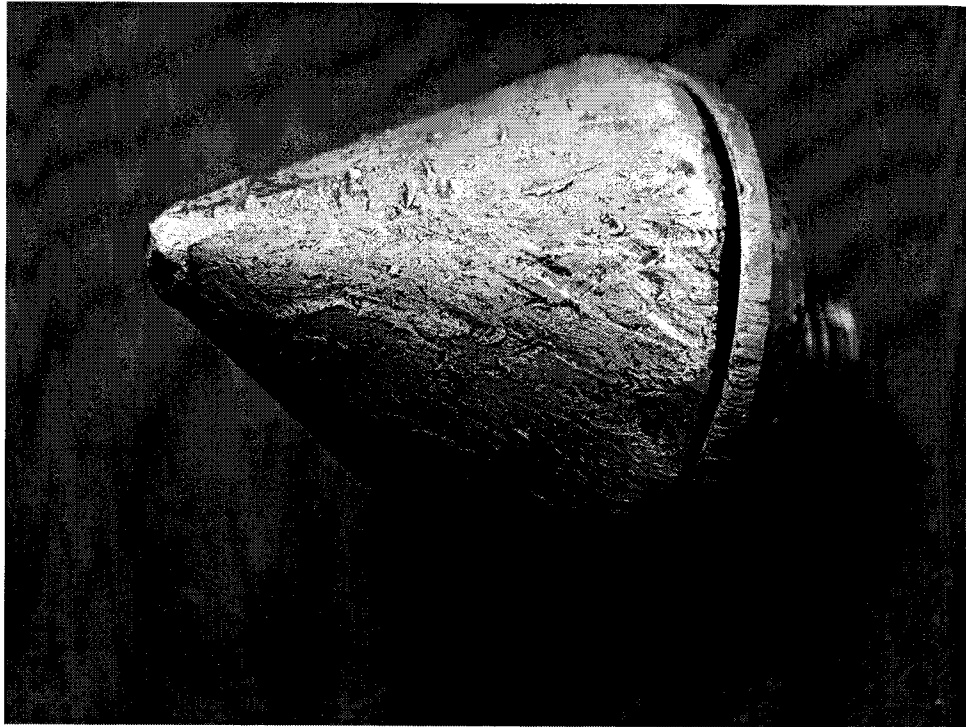


Figure D.3: A damaged cone with prominent scratch marks.

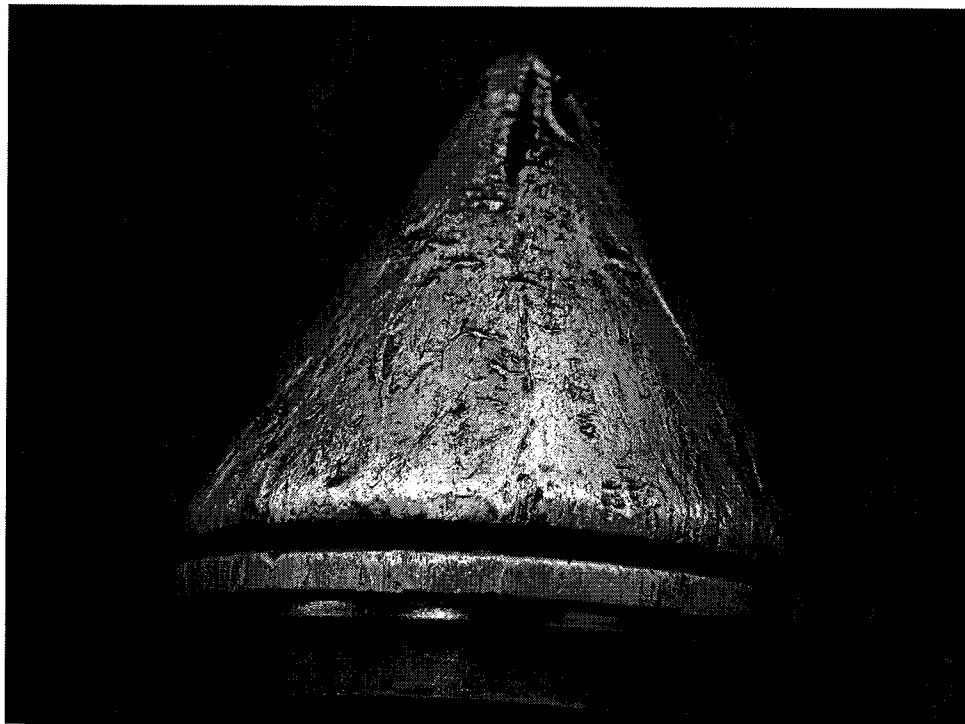


Figure D.4: A damaged cone with prominent scratch marks.

## **APPENDIX – E**

**Example CPT profiles (Including sections through gravel).  
(Courtesy of ConeTec Limited).**

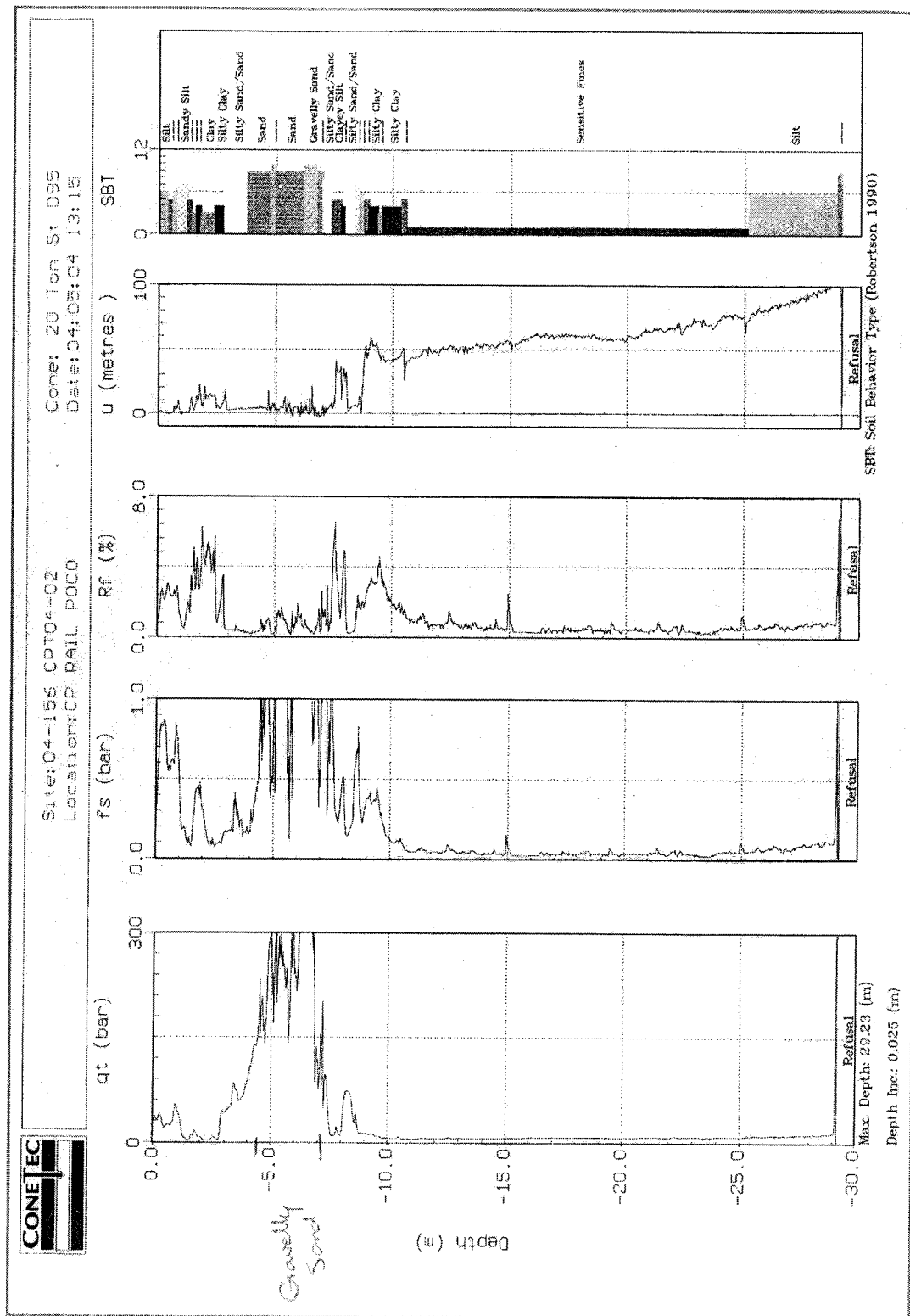


Figure E.1: CPT Profile at CP Rail Poco location. Site: 04 - 156; CPT04 - 02.

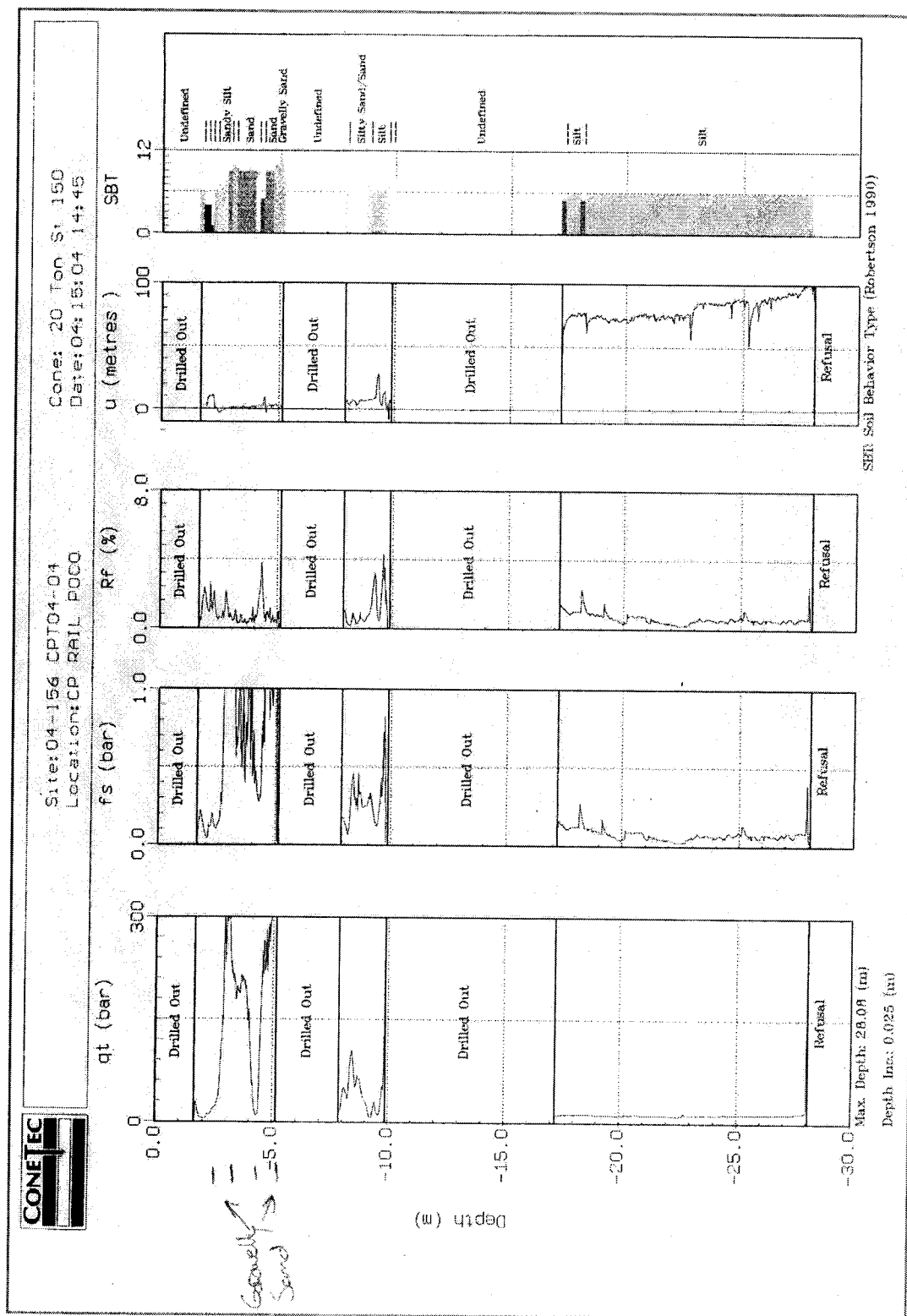


Figure E.2: CPT Profile at CP Rail Poco location. Site: 04 – 156; CPT04 - 04.

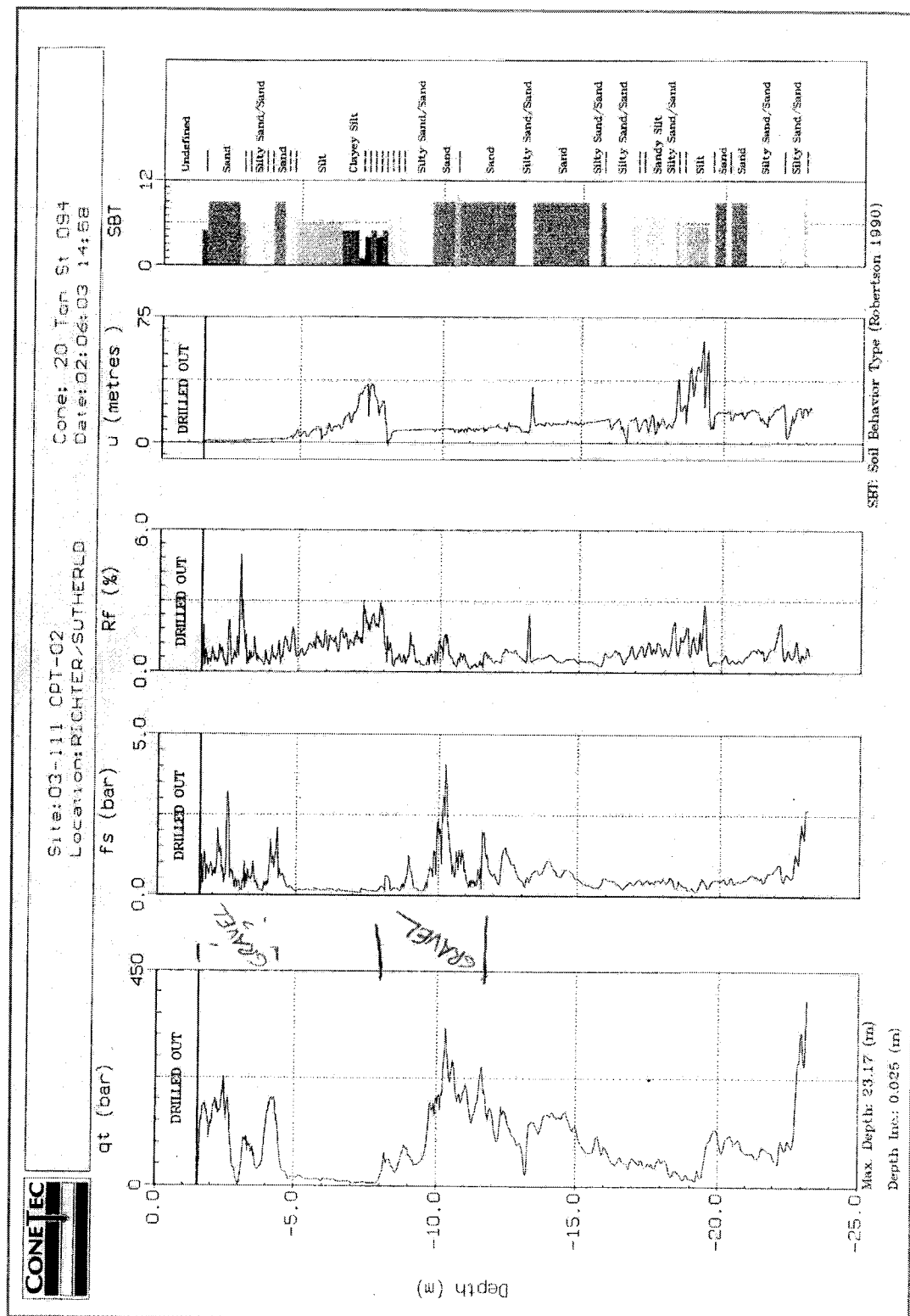
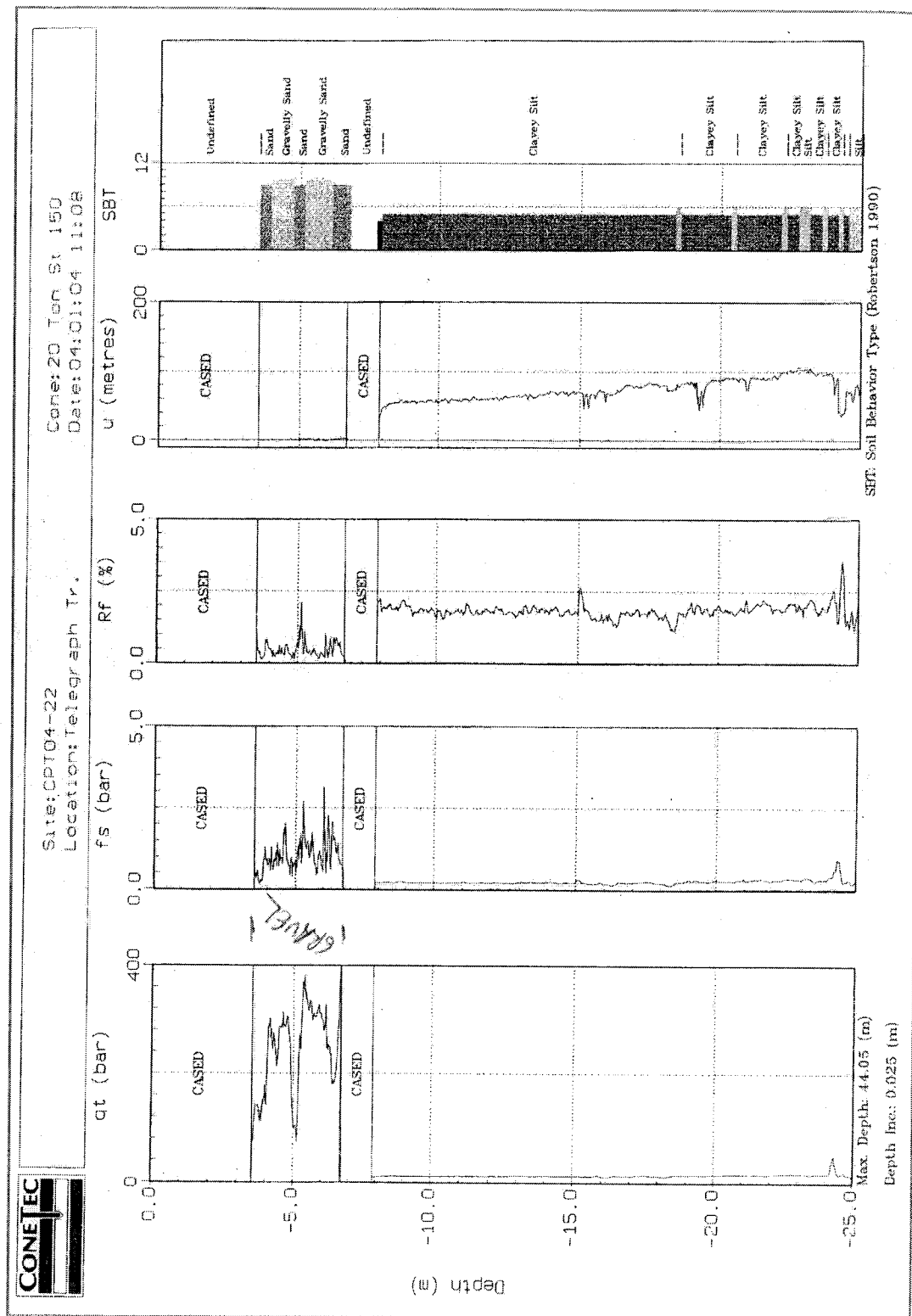


Figure E.3: CPT Profile at Richter / Sutherland location. Site: 03 – 111; CPT - 02.



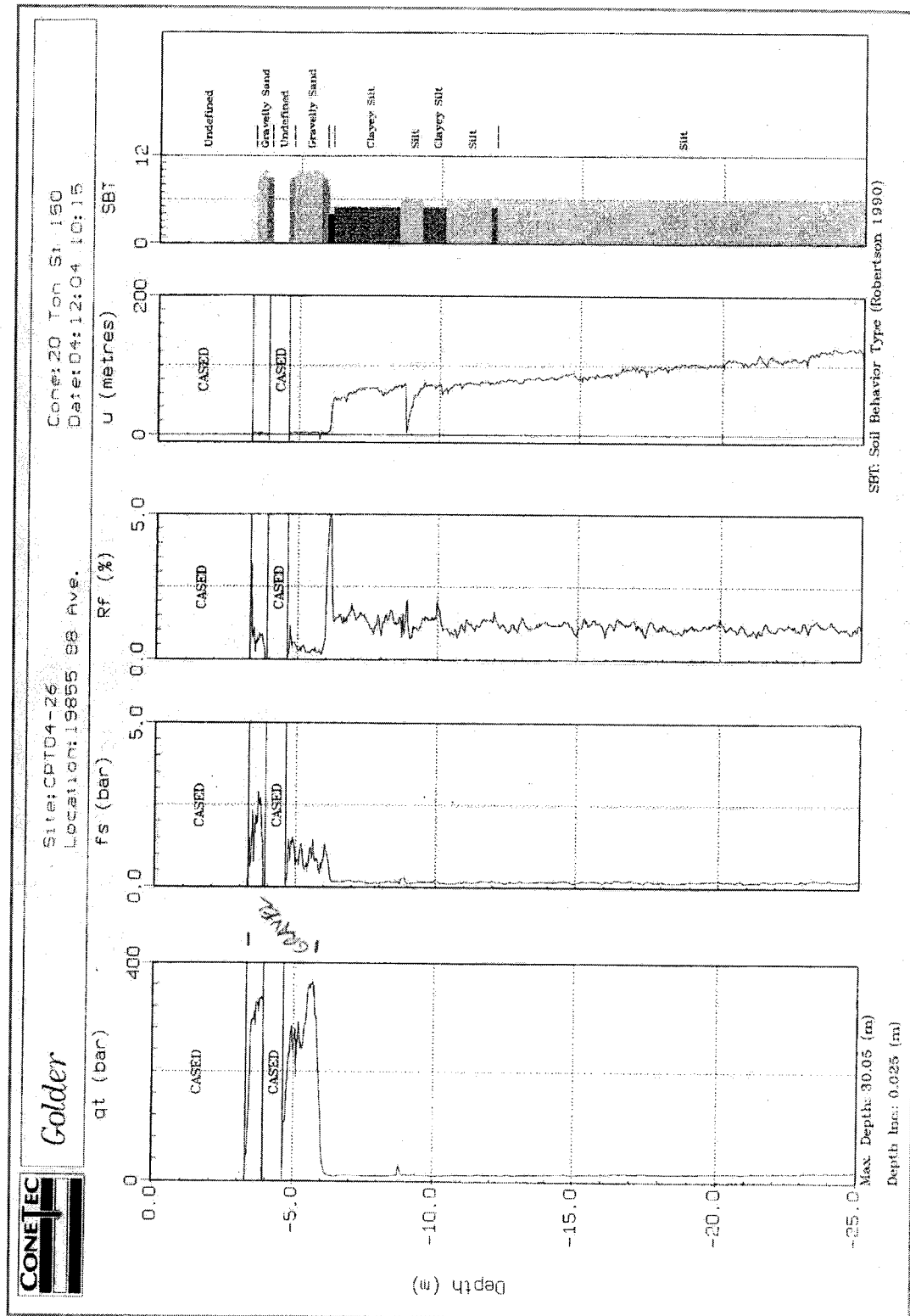
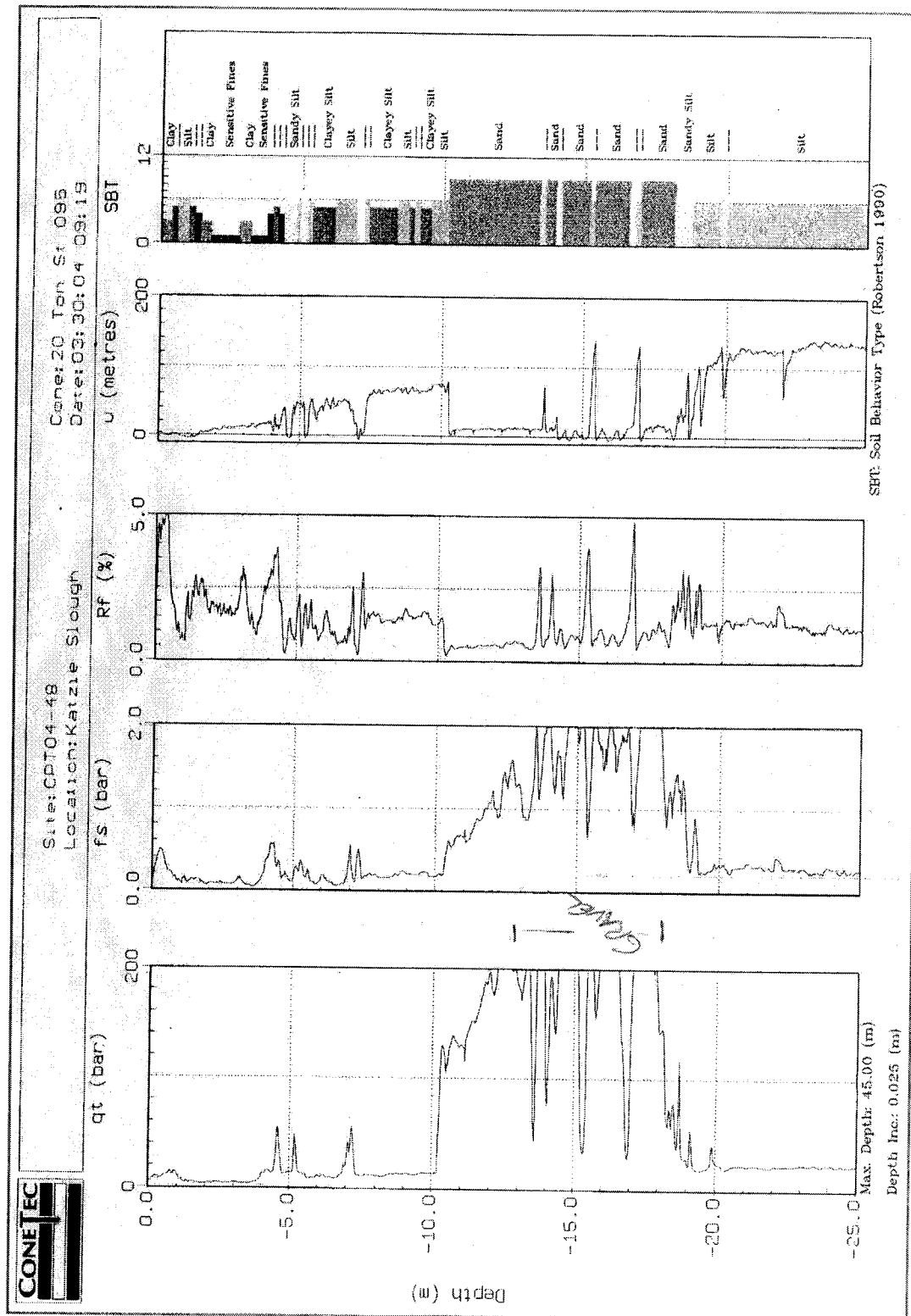


Figure E.5: CPT Profile at 19855 98 Ave. location. Site: CPT04 - 26.







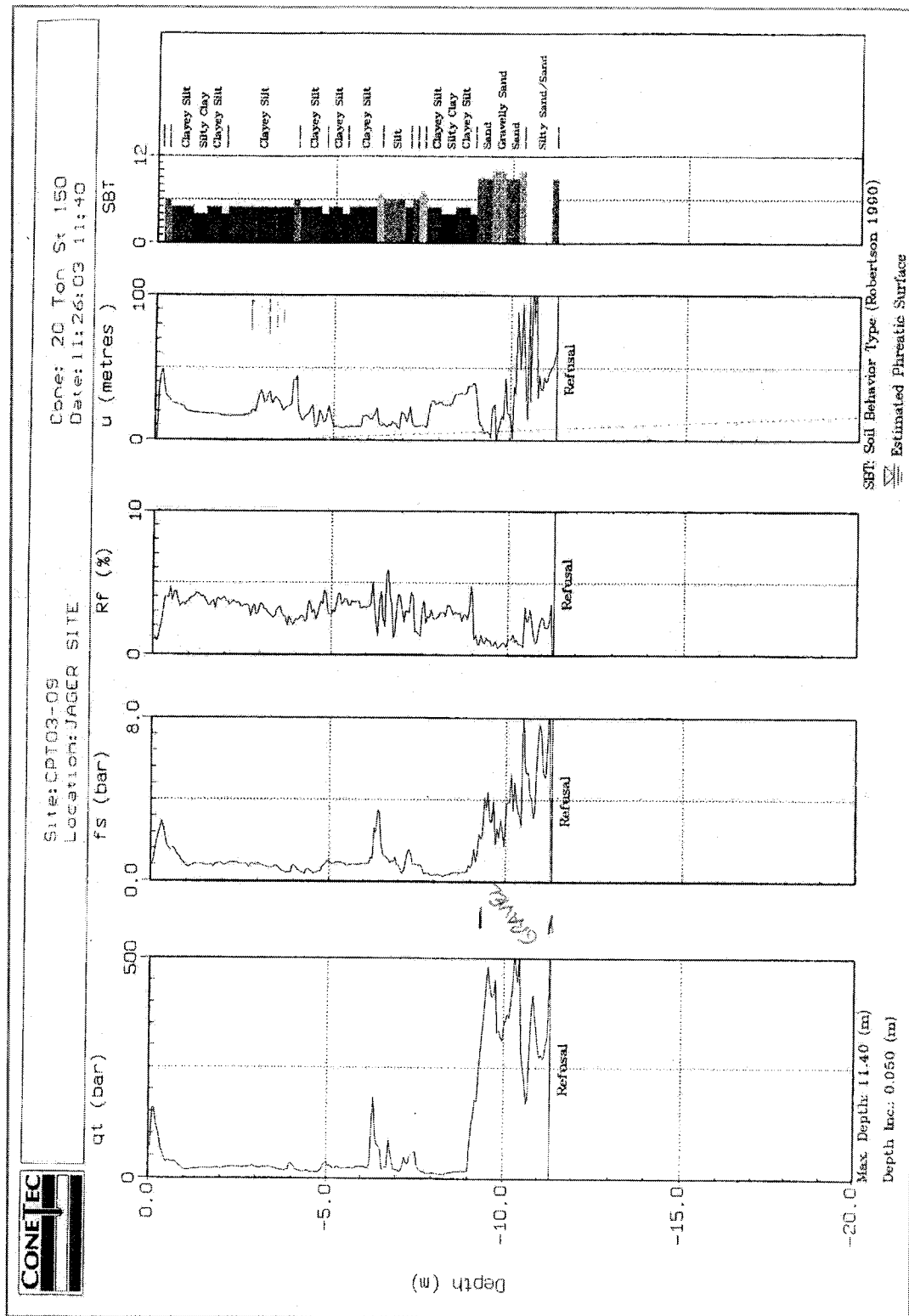


Figure E.8: CPT Profile at Jager Site location. Site: CPT03 - 09.

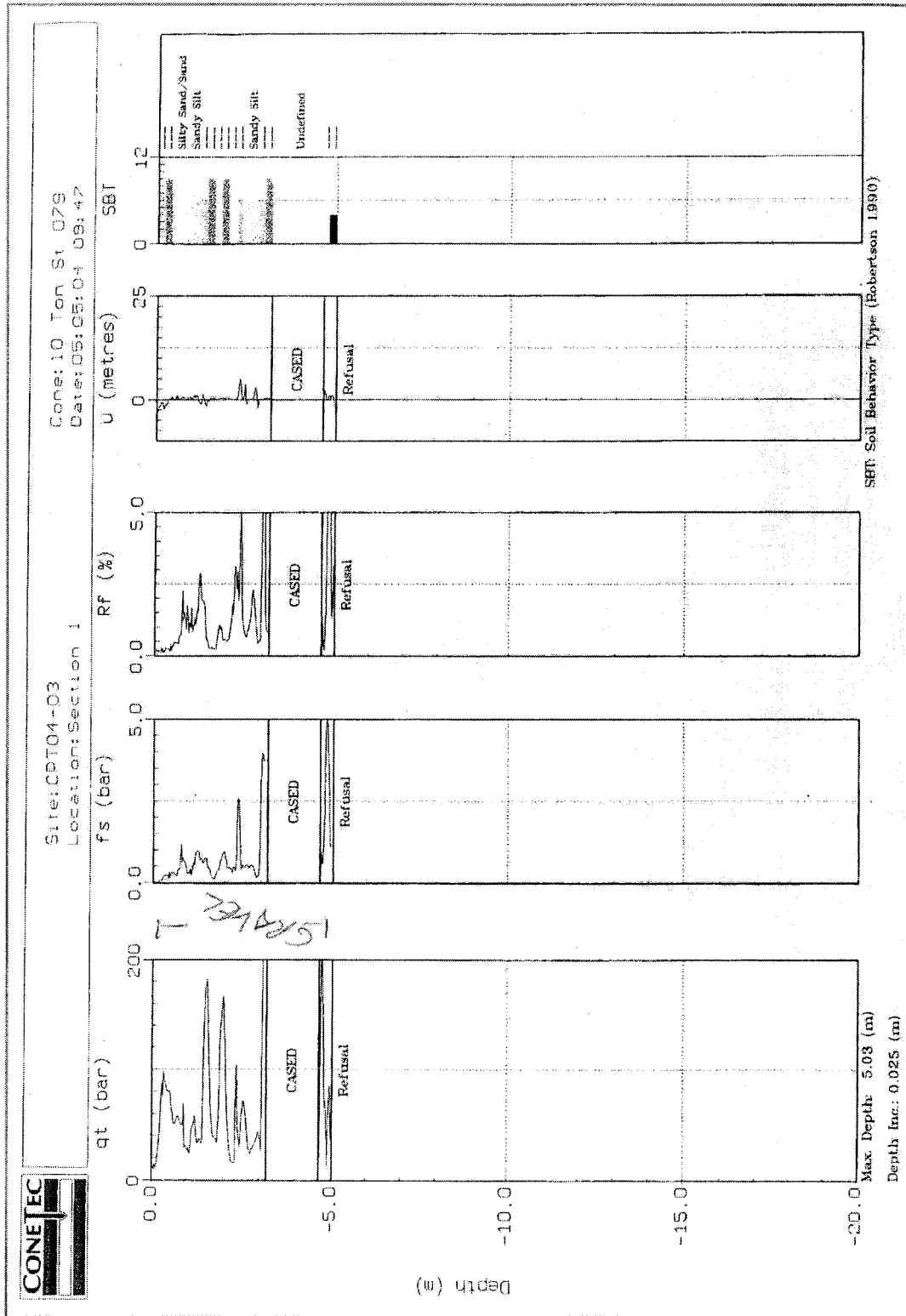


Figure E.9: CPT Profile at Section 1 location. Site: CPT04 - 03.